MERCURY -ARC CONVERTORS and COGNATE PROBLEMS.

THESIS

for

DEGREE Ph. D.

Submitted to the University of Glasgow

by

ERIC S. FAIRLEY, B.Sc., A.R.T.C.

THE ROYAL TECHNICAL COLLEGE, GLASGOW.

MARCH, 1939.

ProQuest Number: 13905615

All rights reserved

INFORMATION TO ALL USERS
The quality of this reproduction is dependent upon the quality of the copy submitted.

In the unlikely event that the author did not send a complete manuscript
and there are missing pages, these will be noted. Also, if material had to be removed,
a note will indicate the deletion.

ProQuest 13905615

Published by ProQuest LLC (2019). Copyright of the Dissertation is held by the Author.

All rights reserved.
This work is protected against unauthorized copying under Title 17, United States Code
Microform Edition © ProQuest LLC.

ProQuest LLC.
789 East Eisenhower Parkway
P.O. Box 1346
Ann Arbor, MI 48106 – 1346

PREFACE

This thesis comprises four papers grouped under the general title of mercury-arc convertors.

In Paper I the results of load tests carried out on a 6-kW grid-controlled, mercury-arc convertor are given and the writer shows how these results may be accurately predicted from the characteristics of the several components. Problems arising in the course of the tests are discussed.

Though the greater part of the paper is of a general nature and deals with efficiency, voltage regulation, and power factor, originality is claimed for two sections - the estimation of the efficiency from no-load and short-circuit tests, and the explan:ation of the discontinuities in the voltage regulation characteristics under certain conditions. The work on the distortion, displacement, and power factors, including the effect of overlap between anodes, was developed independently by the writer but it has since been found that some of this work had already been done by Dr. Ing. R. Feinberg[15] and Dr. C. Dannatt.[14]

Paper II discusses the conditions causing short-circuit in mercury-arc invertors. A diagram is given from which the load on an invertor may be rapidly pre:determined for various values of ignition angle, alternating and direct voltage. The results are confirmed by experiment. The diagram is original, but the short-circuit conditions were derived previously by H. Keller.[7]

The object of Paper III is to justify the assumption that the resistance of the transformer windings may be neglected when determining the overlap between anodes. This is done by developing an expression for overlap by taking the resistance into consideration, and showing that the error incurred by neglecting it does not exceed three per cent in practice An experimental method of measuring overlap by using a stroboscope is described, and curves derived by each of the three methods are plotted together for comparison Originality is claimed for the entire work in this paper.

Paper IV is devoted exclusively to the performance and design of interphase transformers for grid-controlled convertors. Hitherto this component has been designed largely by trial and error, and as far as the writer is aware no attempt has been made to estimate the losses occurring in it. The writer gives a complete theory of the action of the interphase transformer and develops a simple method of designing this component. Relevant oscillograms are given, and a complete design is worked through to illustrate the application of the method. The work in this paper also is entirely original.

During the development of the research work it became increasingly evident that no fundamental difference existed between rectification (A.C. to D.C.)

and inversion (D.C. to A.C.), hence one general theory was sufficient to cover both operations. The distinction between the two processes is actually the algebraic sign of the direct voltage. This method of treatment has been adopted throughout the work, and the equations obtained can be interpreted for any stage intermediate between rectification up to the maximum value of the direct voltage and inversion up to short-circuit.

In compiling these papers, a knowledge of the operation of grid-controlled rectifiers is assumed, the subject being one that has been extensively dealt with in recent years.

The writer wishes to take this opportunity of expressing his sincere gratitude to Professor S. Parker-Smith for granting him facilities to carry out this research work, and for the kindly interest which he has taken in its progress.

CONTENTS

page

Preface IV

Notation VIII

Paper I - Efficiency, power factor and voltage regulation characteristics of mercury-arc convertors... ... ... 1.

Paper II - A no-load and short-circuit diagram for mercury-arc invertors ... ... 28.

Paper III - The duration of overlap in mercury-arc convertors ... ... 34.

Paper IV - The design of interphase transformers for mercury-arc convertors ... ... 43.

Appendix ... ... 55.

Bibliography... XIV

NOTATION.

A_1, A_2, A_3	Coefficients of the cosine terms in a Fourier series.
A_i	Interphase transformer core area, $cm.^2$
A_w	Interphase transformer window area, $cm.^2$
(AT)	The resultant ampere-turns on the interphase transformer at any instant.
a	The cross-sectional area of the conductor comprising the winding of the interphase transformer, $mm.^2$
$a_1\, a_2\, a_3$	The instantaneous values of the anode current, amperes.
$at_{\hat{B}}$	The ampere-turns per $cm.$ required to produce a flux density of $\hat{B}$
B	The value of the flux density in the core of the interphase transformer at any instant, lines per $cm.^2$
$\hat{B}$	The maximum value of the flux density in the interphase transformer core, lines per $cm.^2$
$B_1\, B_2\, B_3$	Coefficients of the sine terms in any Fourier series.
$\cos\phi$	The displacement factor (see page 8).
d	The length of the mean path of the flux in the interphase transformer, $cm.$
$\hat{e}$	The amplitude of the e.m.f. induced in any secondary phase of the main transformer.

Notation.

$e_1 e_2 e_3$	The instantaneous values of the e.m.f.s induced in the secondary phases of the main transformer.
e_i	The instantaneous value of the e.m.f. induced in the interphase transformer winding.
f	The frequency of the a.c. main supplying the convertor, cycles per second.
$f(N, \alpha, u)$	A function of N, α and u , see expression 5 ~~page~~
$f(N_6, \alpha, u_{30})$	$f(N \alpha u)$ when $N = 6$ and $u = 30°$
I	The r.m.s. value of the alternating current in any circuit.
I_{crit}	The value of the direct current at the critical load.
I_d	The direct current.
I_h	The r.m.s. value of the harmonics in any current wave.
$I_R \; I_Y \; I_B$	The r.m.s. values of the currents in the R, Y and B lines.
I_{sc}	The value of the direct current when the convertor is about to short-circuit.
I_1	The r.m.s. value of the fundamental of I
$i_a \; i_b$	Instantaneous values of the currents in the neutrals of phase groups a and b Fig. 50
$i_R \; i_Y \; i_B$	Instantaneous values of the currents in the R, Y and B lines.

Notation.

$i_1\ i_2\ i_3$	Instantaneous values of the currents in the secondary phases of the main transformer.
k	Twice the maximum value of expression 18 times $\frac{\omega l}{E}$, between the limits $\omega t = 0$ and $\omega t = \frac{2\pi}{N}$
$k'\ k''$	Constants.
k_s	Window space factor.
K	Constant.
$l\ l_0$ ...	Leakage inductance per phase of the main transformer referred to the secondary side with 4-wire primary and with 3-wire primary, henries.
L' ...	Inductance of the smoothing reactor, henries.
L ...	The inductance of the interphase transformer winding, henries.
N ...	The number of phases on the secondary of the main transformer.
n ...	The order of the harmonic under consideration.
P_e ...	The total eddy-current loss in the core
P_H ...	The total hysterises loss in the core
r ...	The equivalent resistance per phase of the main transformer referred to the secondary side, ohms.
R ...	The internal resistance of the d.c. circuit, ohms.
t ...	Time, seconds.
$t_0\ t_1$ ...	See Fig. 33
T ...	The total number of turns on the interphase transformer winding.

Notation.

T_1 T_2	The number of turns on each primary, and each secondary phase of the main transformer.
u	The overlap angle, radians or degrees.
V	The r.m.s. value of the alternating voltage in a circuit.
V_d	The mean value of the direct voltage at the terminals of the convertor.
V_0	The mean value of the direct voltage when the direct current is infinitely small.
V_{sc}	The mean value of the direct voltage when the convertor is on the point of short-circuiting.
v	The instantaneous value of the voltage across the interphase transformer.
v_d	The instantaneous value of the direct voltage between the secondary neutral and the cathode.
v_R v_Y v_B	The instantaneous values of the voltages in the R, Y and B phases.
W_1 W_2 W_3	Power in any circuit, ~~in~~ or wattmeter readings.
Z	The total losses in a convertor.

Notation.

α . . .	The ignition angle, Fig. 59
β . . .	The instantaneous value of the fundamental of the flux density in the core of the interphase transformer, lines per cm^2
$\hat{\beta}$ . . .	The maximum value of β
δ . . .	The current density in the winding of the interphase transformer, A per mm^2
Σ . . .	Pertaining to stroboscope measurements, see page 41
ϵ . . .	The amplitude of the fundamental of the voltage across the interphase transfomer.
θ' . . .	Angular error in stroboscope.
θ . . .	Pertaining to condition when the direct current is discontinuous.
λ . . .	The arc drop, volts.
μ . . .	The distortion factor.
Φ . . .	The instantaneous value of the flux in the core of the interphase transformer.
Φ_e . . .	The eddy-current loss which would occur in a volume of iron if only the fundamental of a particular flux wave were present.
Φ_H . . .	The hysterises loss which would occur in a volume of iron if only the fundamental of a particular flux wave were present.
Φ_o	Leakage flux, see Fig. 30

Notation.

φ ... The phase angle between the voltage and the fundamental of the current.

ϕ_x ... Leakage flux, see Fig. 30

ψ ... The power factor.

ω ... $2\pi f$

PAPER I

Efficiency, power factor and voltage regulation characteristics of mercury-arc convertors.

INTRODUCTION

In this paper in addition to certain novel investigations the efficiency, power factor and voltage regulation of mercury-arc convertors are discussed and test results on a 6-kW set are given. These standard results are needed for reference, etc.

In practice many different rectifier circuits are employed, some of which operate in a complicated manner. Such circuits are avoided in the first part of this paper and the performance of one of the simplest arrangements is dealt with. Later some of the more complicated circuits are discussed.

Testing arrangements.

The 6-kW convertor on which all the practical work was carried out is fully described in the appendix ~~page~~.
Fig. 9 ~~page~~ shows the connections used for all the load tests. The d.c. busbars were supplied from a 35-kW, 500-V motor-generator set. Variable voltage and reversible polarity were obtained by separately exciting the generator field through a centre-tapped potentiometer in the manner shown. This potentiometer was mounted on the bench beside the instruments, where it proved to be a very convenient method of adjusting the load on the convertor.

Instruments.

Moving-coil and dynamometer-type instruments were used on the d.c. and on the a.c. side respectively. The former type records the mean value, and the latter the root-mean-square value of the quantity being measured. Where the readings are used to calculate power factors it is essential that dynamometer instruments should be used to measure a.c. quantities which are not sinusoidal. The a.c. power was measured on either two or three wattmeters depending on whether a three-wire or a four-wire input was used. Wave forms of current and voltage were recorded, using the cathode-ray oscillograph described in the appendix ~~page~~. Fig. 10 ~~page~~ shows the convertor circuit used in the first series of tests. A mesh-connected primary winding might have been used equally well and indeed is much more widely used in practice owing to the improved wave form of the a.c. line current obtained. In the present case the primary of the transformer used in the tests was rated at 250 volts per phase and the 440-V supply mains were employed, which of course necessitated a star-connected primary winding. The neutral connection was required, otherwise the suppression of the triplen harmonics in the line current would have complicated the performance of the convertor, as explained on page 23. Normally the excitation and the grid-control circuits were in continuous operation and were supplied from auxiliary windings on the main transformer.

EFFICIENCY.

The efficiency of a mercury-arc convertor is defined as $V_d I_d / \Sigma W$ when the power is being transmitted from the a.c. to the d.c. busbars and as

$\Sigma W / V_d I_d$ when the transference of power is in the opposite direction. The former process is called rectification, the latter inversion. ΣW denotes the a.c. power, which is usually read on two or more wattmeters connected in the a.c. leads; while V_d and I_d are the mean values of the direct voltage and current respectively. For certain values of ignition angle a transition stage between rectification and inversion occurs, during which the losses in the convertor are supplied from both a.c. and d.c. busbars. Within this range the efficiency has of course no practical significance.

Determination of efficiency by Load Tests.

Fig. 9 ~~page~~ shows the connection diagram which has already been fully explained on page 2.

Constant ignition angle tests: The ignition angle was kept constant at a given value and the load on the convertor was varied by adjusting the voltage on the d.c. busbars. Readings of a.c. and d.c. power were taken for values of direct current between no-load and 25 per cent overload.

A similar test was run at a second value of ignition angle.

The results are shown in Figs. 12, 13 ~~and pages~~

Constant-current test: The direct current was adjusted to 75 per cent of full-load value and the a.c. and d.c. powers were measured over a wide range of ignition angle. The efficiency curve obtained is shown in Fig. 14 ~~page~~.

Determination of efficiency by summation of losses.

The losses occurring in a convertor comprise (a)

losses in the transformer core, excitation and grid circuits. These are dependent on the a.c. voltage and frequency but are independent of the ignition angle and of the load on the convertor. (b) Losses in the transformer windings, smoothing reactor and bulb. These depend on the load current and to a minor extent on the applied voltage, but are practically independent of the ignition angle.
Denoting the former losses by K and the latter by $f(I_a)$ the efficiency of the convertor is

$$1 - \frac{K + f(I_d)}{V_d I_d + K + f(I_d)} \qquad \text{--------} \qquad (1)$$

when the set is rectifying, and

$$1 - \frac{K + f(I_d)}{V_d I_d} \qquad \text{---------} \qquad (2)$$

when the set is inverting.

We are now able to put forward a simple method of measuring efficiency. Since both groups of losses are independent of the ignition angle, the losses occurring in the convertor when the ignition angle has such a value that V_d is zero will be the same as those occurring at any other value of ignition angle. This fact permitted the losses to be measured in the following simple manner: as can be seen from equation ~~(1) page~~ 31 setting the ignition angle to 150 degrees made V_d equal to zero and thus permitted the d.c. terminals to be short-circuited through a moving-coil ammeter. The direct current was varied between zero and 25 per cent overload by adjusting the ignition angle. For each value of direct current the input power was read from wattmeters connected in the a.c. input leads.
Fig. 15 ~~page~~ shows the curve of total losses which

was obtained. The separation of the no-load losses was carried out by removing first the grid-circuit fuses and then the excitation-circuit fuses, the wattmeters being read in each case.

If we assume that λ, the voltage drop in the bulb, is constant then the total losses, z may be expressed as $K + \lambda I_d + \beta I_d^2$ where K, λ and β are all constants.

Differentiating this expression we have that

$$\frac{dz}{dI_d} = 0 + \lambda + \beta I_d$$

from which it can be seen that

$$\lambda = \frac{dz}{dI_d} \quad \text{when} \quad I_d = 0$$

Now $\frac{dz}{dI_d}$ is the gradient of the tangent to the curve of total losses drawn on a base of I_d, hence λ is given by the gradient of the tangent to the curve at the vertical axis. This tangent has been drawn in Fig. 15 ~~page~~ and a value of 20·75 volts was obtained for λ. This compares favourably with the figure of 22 volts which was obtained using direct current. A description of the latter method is given on page 18 .

The efficiency at any load and direct voltage may be obtained by substituting the appropriate value of the losses in either equation (~~9~~ 1) or (~~10~~ 2) depending on whether the set is rectifying or inverting. Curves of efficiency calculated in this manner are plotted in Fig. 16 ~~page~~ . A good agreement with the values obtained from the load tests will be observed.

Reasons ~~for~~ contributing to the slight differences are: (a) due to variation in overlap the copper loss in the transformer is not completely independent of the ignition angle; (b) the direct voltage was assumed constant for a constant value of ignition angle.

If necessary this slight error could be eliminated by calculating V_d from equation ~~(4)~~ 31, ~~page~~ for each different value of direct current. This procedure would destroy the simplicity of the method.

POWER FACTOR.

Generally the term power factor and cosine ϕ are regarded, somewhat loosely, as different names for the same quantity. Where current and voltage vary sinusoidally both terms have the same value, but when the current or the voltage, or both, are nonsinusoidal this is no longer the case. The B.S.I. defines the power factor of a single-phase load as the ratio of the watts to the volt-amperes, and of an unbalanced polyphase load as the ratio of the total watts to the total equivalent volt-amperes. What is meant by the equivalent volt-amperes is rather vaguely expressed and involves a term $\cos\phi$ which obviously limits the definition to circuits in which the current varies sinusoidally.

In mercury-arc convertors the single-phase load taken by the excitation and grid-control circuits may produce a small degree of out of balance in the total load.

No definite method of measuring power factor has been standardised by B.S.I. for a case such as this where the load is unbalanced and non-sinusoidal, and various methods are in use at the present time. Three of these are mentioned below and are discussed in detail later in the paper.

(a) By using a power factor meter.

(b) By dividing the watts by the volt-amperes in one phase.

(c) By dividing the total power input by the arithmetical sum of the volt-amperes in the several phases.

Power factor tests on a 6-kW convertor.

Using the circuit shown in Fig. 9 three tests were run, two with constant ignition angle and varying direct current and one with constant direct current and varying ignition angle. The tests were conducted in a similar manner to the efficiency tests described previously on page 4 . The values of the power factor were determined by method (c) above. Figs. 12, 13 and 14 show the results.

Distortion and displacement factors.

The problem of power factor has been receiving a good deal of attention in recent years* in connection with the metering of rectifier loads and in 1927 a considerable advance was made when Brynhildsen and Kern introduced two new quantities. The first of these they called the displacement factor and defined as the cosine of the angle of phase difference between the sinusoidal applied voltage and the fundamental of the current wave. The second was called the distortion factor and was defined as the ratio of the r.m.s. value of the fundamental of the current wave to the r.m.s. value of the entire current wave. Certain relations between these new quantities and the power factor are established below.

---

* See bibliography.

By the difinition of power factor in a single-phase circuit

$$W = VI\psi$$

where W is the power, V the r.m.s. voltage, I the r.m.s. current and ψ the power factor. Where the harmonics in the current wave have no counterpart in the voltage wave, as in the convertor, the harmonic power is zero and in this case the power W is also given by

$$W = VI_1 \cos\phi$$

where I_1 is the r.m.s. value of the fundamental of the current and $\cos\phi$ is the displacement factor. Hence the distortion factor, μ is given by

$$\mu = \psi / \cos\phi$$

From the definition of r.m.s. values

$$I = \left[I_1^2 + I_h^2\right]^{\frac{1}{2}}$$

where I_h is the harmonic current

and also

$$\frac{I_h}{I} = (1-\mu^2)^{\frac{1}{2}}$$

Measurement of displacement and distortion factors. When two wattmeters are connected in the usual way to measure the a.c. power to a balanced 3-phase, 3-wire convertor the displacement factor is the same for each of the three phases and is given by[5]

$$\left[(W_1+W_2)^2 \Big/ \left\{(W_1+W_2)^2 + 3(W_1-W_2)^2\right\}\right]^{\frac{1}{2}}$$

Power factor.

Where a convertor constitutes an unbalanced load, the displacement factor must be determined for each phase separately. For this purpose the circuit shown in Fig. 11 was used by the writer. Representing the line-to-neutral voltages by $v_R = \hat{v}\sin\omega t$, $v_Y = \hat{v}\sin(\omega t - \frac{2\pi}{3})$ and $v_B = \hat{v}\sin(\omega t + \frac{2\pi}{3})$ the voltage across the wattmeter pressure coil is $v_R - v_Y = \sqrt{3}\,\hat{v}\cos(\omega t - \frac{\pi}{3})$ when the switch is in position 1 and the voltage is

$$v_R - v_B = -\sqrt{3}\,\hat{v}\cos(\omega t + \frac{\pi}{3})$$

when the switch is in position 2.

Let the current in the red line be expressed by

$$\hat{i}\sin(\omega t - \phi) + \sum_{m=3}^{m=\infty} \hat{i}_m \sin(m\omega t - \phi_m)$$

then with the switch in position 1 the wattmeter reading, W_1 is given by

$$W_1 = \frac{1}{2\pi}\int_{\omega t=0}^{\omega t=2\pi} \sqrt{3}\,\hat{v}\cos(\omega t - \frac{\pi}{3})\left\{\hat{i}\sin(\omega t - \phi) + \sum_{m=3}^{m=\infty}\hat{i}_m \sin(m\omega t - \phi_m)\right\} d\omega$$

$$= \sqrt{3}\,VI_1\sin(\phi - \frac{\pi}{3})$$

Similarly when the switch is in position 2

$$W_2 = -\sqrt{3}\,VI_1\sin(\phi + \frac{\pi}{3})$$

hence $$W_1 + W_2 = 3VI_1\cos\phi$$

and $$W_1 - W_2 = \sqrt{3}\,VI_1\sin\phi$$

from which $$\tan\phi = \sqrt{3}\,\frac{W_1 - W_2}{W_1 + W_2} \quad \text{or}$$

$$\cos\phi = \left[(W_1+W_2)^2 \Big/ \left\{(W_1+W_2)^2 + 3(W_1-W_2)^2\right\}\right]^{\frac{1}{2}}.$$

The power factor can be obtained from

$$\psi = \frac{W_1 + W_2}{3VI}.$$

Since the transformer magnetising current introduces harmonics not easily calculable and which would probably obscure the agreement which it was desired to bring out between the calculated and the test results, the writer decided to compare the theoretical and test results for the anode current, the shape of which is known fairly accurately. Up till now it has been tacitly assumed that the displacement and distortion factors have referred to the line current only, but obviously these factors can apply to the current in any circuit and can be measured by methods similar to those already outlined.

In the course of the following investigation one original and rather useful curve was derived. It is given in Fig. 20 and has definite practical value since the r.m.s. value of the anode current can be determined from it at any value of ignition angle. The method is given on page 14. Marti and Winograd have done similar work on the uncontrolled rectifier, but the above is on the controlled convertor and is apparently new.

Analytical derivation of the distortion and displacement factors of the anode current.

In order to simplify the work two assumptions will be made. The first, that the direct current does not contain harmonics - an assumption generally made in the treatment of rectifier problems; and the second, that the resistance of the main transformer windings has a negligible effect on commutation - this assumption is justified in Paper III of this thesis.

Fig. 17 shows the current in anode I, and the voltage between anode I and the secondary neutral point. For convenience, the axis $\omega t = 0$ has been taken in the position shown. In a similar way to that ~~already~~ described on page 56 it can be shown that the equation of the anode current between $\omega t = \alpha$ and $\omega t = \alpha + \mu$ is given by

$$i_1 = -\frac{\hat{e}\sin\frac{\pi}{N}}{l}\int\cos\left(\omega t + \frac{\pi}{N}\right)dt + k$$

Power factor.

$$= \frac{\hat{e}}{\omega l} \sin\frac{\pi}{N} \sin\left(\omega t + \frac{\pi}{N}\right) + k$$

Now $i_1 = 0$ when $\omega t = \alpha$, and inserting these limits we have that

$$i_1 = \frac{\hat{e}}{\omega l} \sin\frac{\pi}{N}\left[\sin\left(\alpha + \frac{\pi}{N}\right) - \sin\left(\omega t + \frac{\pi}{N}\right)\right] \text{------} (3)$$

from α to $\alpha + u$

Similarly

$$i_2 = \frac{\hat{e}}{\omega l} \sin\frac{\pi}{N}\left[\sin\left(\alpha + \frac{\pi}{N}\right) - \sin\left(\omega t - \frac{\pi}{N}\right)\right]$$

between $\alpha + \frac{2\pi}{N}$ and $\alpha + \frac{2\pi}{N} + u$

Again, since $i_1 + i_2 = I_d$

$$i_1 = I_d - \frac{\hat{e}}{\omega l} \sin\frac{\pi}{N}\left[\sin\left(\alpha + \frac{\pi}{N}\right) - \sin\left(\omega t - \frac{\pi}{N}\right)\right] \text{----} (4)$$

from $\alpha + \frac{2\pi}{N}$ to $\alpha + \frac{2\pi}{N} + u$

Between $\alpha + u$ and $\alpha + \frac{2\pi}{N}$, i_1 is of course equal to I_d.

The fundamental of the anode current.

Using Fourier's method of harmonic analysis, the r.m.s. value of the fundamental of the anode current is $(A_1^2 + B_1^2)^{\frac{1}{2}}/\sqrt{2}$ where

$$A_1 = \frac{1}{\pi}\int_{\alpha}^{\alpha + \frac{2\pi}{N} + u} i_1 \cos\omega t \; d(\omega t) \quad \text{and}$$

$$B_1 = \frac{1}{\pi}\int_{\alpha}^{\alpha + \frac{2\pi}{N} + u} i_1 \sin\omega t \; d(\omega t).$$

Inserting the appropriate values of i_1, from the above equations, integrating and simplifying, we have

$$A_1 = \frac{2I_d}{\pi} \sin\frac{\pi}{N}\left[\frac{\sin u \cos(2\alpha + u + 2\pi/N) + u}{4\cos(\alpha + \pi/N + u/2)\sin\frac{u}{2}}\right]^*$$

and

$$B_1 = \frac{2I_d}{\pi} \sin\frac{\pi}{N}\left[\sin(\alpha + \pi/N + u/2)\cos u/2\right]^*$$

Inserting these values for A_1 and B_1, the r.m.s. value of the fundamental becomes

$$\frac{\sqrt{2}\, I_d}{\pi} \sin\frac{\pi}{N}\left[\frac{\sin^2 u + u^2 + 2u \sin u \cos\left(2\alpha + u + \frac{2\pi}{N}\right)}{16\cos^2\left(\alpha + \frac{\pi}{N} + \frac{u}{2}\right)\sin^2\frac{u}{2}}\right]^{\frac{1}{2}}$$

Since u rarely exceeds 20° in practice, we may write

---

*See appendix, page 69

$2\sin\frac{u}{2}$ in place of u and unity in place of $\cos\frac{u}{2}$ without introducing any appreciable error; whence the above expression simplifies to

$$\frac{\sqrt{2}\,I_d}{\pi}\sin\frac{\pi}{N}$$

Thus the fundamental of the anode current is practically independent of u and α, and is directly proportional to the direct current.

The displacement factor, $\cos\phi = B_1/(A_1^2+B_1^2)^{\frac{1}{2}}$ which with the same approximations simplifies to

$$\cos\phi = \sin(\alpha+\frac{\pi}{N}+\frac{u}{2})$$

The r.m.s. value of the anode current: By definition the r.m.s. value of the anode current equals

$$\left[\frac{1}{2\pi}\int_{\alpha}^{\alpha+\frac{2\pi}{N}+u} i_1^2\,d(\omega t)\right]^{\frac{1}{2}}$$

After intigrating and simplifying this expression becomes equal to *

$$\frac{I_d}{\sqrt{N}}\left[1-\frac{N}{\pi}\left\{\frac{-\sin(\alpha+\frac{\pi}{N})u-2\sin(\alpha+\frac{\pi}{N}+\frac{u}{2})\sin\frac{u}{2}}{\sin(u+\alpha+\frac{\pi}{N})-\sin(\alpha+\frac{\pi}{N})}-\frac{\sin^2(\alpha+\frac{\pi}{N})u+\frac{u}{2}-4\sin(\alpha+\frac{\pi}{N})\sin(\alpha+\frac{\pi}{N}+u)\sin\frac{u}{2}-\frac{1}{2}\cos(2\alpha+\frac{2\pi}{N}+u)\sin u}{\{\sin(u+\alpha+\frac{\pi}{N})-\sin(\alpha+\frac{\pi}{N})\}^2}\right.\right]^{\frac{1}{2}}$$

This may be written as

$$\frac{I_d}{\sqrt{N}}\left[1-f(N,\mu,\alpha)\right]^{\frac{1}{2}} \quad ----------(5)$$

This expression is the general case of the one developed by Marti and Winograd for the uncontrolled rectifier.

Curves were drawn of $f(N,\alpha,u)$ ~~out~~ to a base of u for various fixed values of α. Two of these curves are reproduced in Fig. 19. In every case the curve approximated very closely to a straight line passing through the origin. This linear relationship

* See appendix, page 71

permits $f(N,u,\alpha)$ to be written as

$$\frac{u}{30} f(N,\alpha,u_{30})$$

where u is the overlap expressed in degrees and $f(N,\alpha,u_{30})$ is the value of $f(N\alpha u)$ when $u = 30^\circ$ A value of 30° is of course chosen quite arbitrarly. A curve of $f(N\alpha u)$ for $N=6$ and $u=30^\circ$ is drawn to a base of α in Fig. 20 . The method of using this curve is illustrated by the following example:

> Determine the r.m.s. value of the anode current of a 6-phase convertor given the following conditions; $\hat{e} = 371\ V$, $\omega L = 0{\cdot}462$ ohm, $\alpha = 210^\circ$ and $I_d = 40A$
>
> From equation ~~(3) page~~ 30 the overlap, equals 15°. Fig. 20 gives $f(N\alpha u)$ as $0{\cdot}133$ at $\alpha = 210^\circ$ when $N=6$ and $u = 30^\circ$
>
> Hence $f(N\alpha u)$ for $N=6$, $\alpha=210^\circ$ and $u = 15^\circ$
>
> $$= \frac{15}{30} \times 0{\cdot}133 = 0{\cdot}0665$$
>
> and from equation ~~(11) page~~ 5 the anode current equals
>
> $$\frac{40}{\sqrt{6}}\left(1 - 0{\cdot}0665\right)^{\frac{1}{2}} = 15{\cdot}8$$

We have now deduced equations which give both the r.m.s. value of the anode current and the r.m.s. value of the fundamental of the anode current. Hence curves of distortion, displacement and power factors may now be drawn. These are shown in Fig. 18 and 21

Distortion and Displacement factors of the Anode Current obtained from Experiment.

Fig. 22 shows the circuit used to check these results experimentally. The method has already been discussed on page 9 . Fig. 21 shows the results thus obtained experimentally, and it will be seen that the results derived analytically agree closely with them. The small differences are partly explained by the presence of harmonics in the direct current.

Conclusion.

Criticisms of the three methods of measuring power factor are now made, followed by a suggestion.

Method (a) - the use of the power factor meter: It is well known that the mean value of the force between two magnetic fields alternating at different frequences is zero, hence in a power factor meter the mean torque between the harmonics in the current wave and the sinusoidal voltage wave is zero. Therefore the indication of a power factor meter is independent of harmonics in the current wave - always assuming of course that the voltage wave is sinusoidal - and it depends on the phase angle between the voltage and the fundamental of the current. The reading indicated is therefore a displacement factor and not a power factor. In normal practice, however, the two are equal, and thus it has come about that the instrument has been incorrectly named a power factor meter.

Method (b) - watts divided by volt-amps for one phase only: This method could be extended to cover unbalanced load conditions by giving the value of the power factor for each phase.

Method (c) - The total watts divided by the arithmetic sum of the volt-amps: This is the most logical of the three and gives an empirical figure which could be employed as a basis for comparing the performance of different convertors.

A Suggestion: Reviewing this problem of the power factor of unbalanced polyphase loads, it appeared to the writer that the original conception of power factor had been lost sight of. In the writer's opinion, a more useful and a fundamentally more logical definition of the power factor of an unbalanced N-phase load supplied from a symmetrical N-phase system would be given by W/NVI where W is the total power taken, I is the largest of the line currents, and V is the phase voltage. It will be observed that this figure penalises out-of-balance as well as phase displacement between voltage and current. This fact appears to be justified because out-of-balance may be as undesirable as phase displacement. An alternative definition, which would penalise out-of-balance to a lesser degree would be the total power taken divided by the total power which could be taken for the same heating of the supply mains, or

$$\frac{W}{NV\left[\frac{1}{N}\left(I_1^2 + I_2^2 \ldots \; I_N^2\right)\right]^{1/2}}$$

where $I_1, I_2 \ldots$ etc. are the respective line currents. Either of these definitions applies equally well to single-phase loads, to 3-phase balanced loads, and to circuits in which the currents are neither balanced nor sinusoidal. In the former cases, i.e., single-phase and 3-phase balanced loads, no change in the present form of the power factor would occur. If necessary, the definition could be extended to cover the case of unbalanced and nonsinusoidal voltages also but as any further developement of this subject is intimately connected with tariffs and economics, the discussion will not be continued in this thesis.

VOLTAGE REGULATION.

A.c. and d.c. networks are often interconnected through convertors to permit an interchange of power. When this is the case the load on the convertors is fixed by the relative magnitudes of the a.c. and d.c. voltages. This relation between the terminal voltage and the direct current is termed the voltage regulation of the convertor. Only inherent voltage regulation, as distinct from the regulation of convertors fitted with automatic compounding devices, will be discussed here.

Voltage Regulation.

Determination of Voltage Regulation curves from Load Tests: Fig. 9 shows the circuit used. The a.c. voltage and the ignition angle were maintained constant and simultaneous readings of the direct voltage and current were taken. The test was repeated for one other value of ignition angle. The results obtained are shown in Figs. 12, 13 and 14

Calculation of Voltage Regulation: On page 57 it was shown that the direct voltage is given by

$$\hat{e}\frac{N}{\pi}\sin\frac{\pi}{N}\sin\left(\alpha+\frac{\pi}{N}\right)-\lambda-I_d\left(R+\frac{N}{2\pi}\omega l\right)$$

This equation can be used for predetermining the regulation of convertors by calculation, as all the quantities involved can be obtained from the design. In our case, however, $\hat{e}$, λ, R and ωl were measured in the laboratory.

Arc Drop, λ : For the present purpose, sufficiently accurate results were obtained by measuring the arc drop on direct current. Fig. 23 shows the circuit used. A value of 22 volts was obtained, no variation being apparent between 0 and 15 amperes. The temperature of the anode arm had considerable effect on the value obtained which was higher, and unsteady, when the limb was cold. 22 volts was the value obtained when the limb was at approximately normal working temperature. Currents exceeding 15 amps were not used because of possible damage to the anode seal through excessive heating.

Leakage Reactance, ωl : Referring to the derivation of equation 31 ~~page~~ , it will be seen that $2\omega l$ represents the reactance between any two consecutive anodes when the primary of the transformer is connected to the supply mains. Assuming the leakage reactance of the supply mains to be negligible, ωl will be the reactance between any anode and the star-point of the secondary when the primary is short-circuited. The measurement of ωl was made using three voltmeters and a standard resistance. A value of 0·462 ohm was obtained for the reactance at 50 cycles, the corresponding value of the equivalent resistance being 0·713 ohm.

The remaining quantities $N, \hat{e}$ and R are 6,371 volts and 0·52 ohm respectively. Substituting in equation 31 the direct voltage becomes equal to

$$354 \sin(\alpha + 30^\circ) - 22 - 0{\cdot}961\, I_d$$

Curves of V_d to a base of I_d for the same values of α as chosen in the load tests are given in Figs. 12 and 13. A comparison between the voltage regulation curves obtained from test results and those derived analytically is interesting. The outstanding difference is the sharp rise of voltage evident at light loads in the former curves. The reason is that the assumptions that the d.c. is free from harmonics - on which the derivation of equation 31 is based - breaks down at light load. The assumption of course implies that the d.c. is continuous; whereas oscillograph records show that the direct current contains a considerable a.c. component and actually becomes discontinous at a value depending on the ignition angle and the amount of inductance in the d.c. circuit. The oscillograms reproduced in Fig.7J,I were taken at values of direct current, respectively greater and less than the critical value at which the sharp rise in voltage commences. The discontinuity can be seen in the second case.

Voltage Regulation.

Voltage and Current Relations when the Direct Current is Discontinuous : Consider the instant when anode 1 is in operation, the d.c. circuit comprising an inductance L' and a voltage V_d. When conditions are such that the direct current is discontinuous, the current in effect becomes a series of transients, in the calculation of which no great error will be involved by neglecting the resistance of the d.c. circuit. Applying Kirchhoff's law to the closed circuit comprising the arc path, the secondary phase, the d.c. busbars and the inductance, we find that

$$e_1 - \lambda - L'\frac{di_1}{dt} - V_d = 0$$

hence
$$i_1 = \frac{1}{L'}\int \hat{e}\sin(\omega t+\alpha)\,dt - \frac{\lambda+V_d}{L'}dt + k$$

$$= \frac{\hat{e}}{\omega L'}\cos(\omega t+\alpha) - \frac{\lambda+V_d}{\omega L'}\omega t + k$$

Referring to Fig. 24 it will be seen that if the direct current is discontinuous $i_1 = i_d = 0$ when $\omega t = 0$

hence
$$k = \frac{\hat{e}}{\omega L'}\cos\alpha$$

and therefore

$$i_d = \frac{\hat{e}}{\omega L'}\left\{\cos\alpha - \cos(\omega t+\alpha)\right\} - \frac{\lambda+V_d}{\omega L'}\omega t$$

assuming that i_d again falls to zero when $\omega t = \theta$

then
$$\frac{\lambda+V_d}{\omega L'}\cdot\theta = \frac{\hat{e}}{\omega L'}\left\{\cos\alpha - \cos(\theta+\alpha)\right\} \text{ ------ } (6)$$

from which

$$i_d = \frac{\hat{e}}{\omega L'}\left[\cos\alpha - \cos(\omega t+\alpha) - \frac{\omega t}{\theta}\left\{\cos\alpha - \cos(\theta+\alpha)\right\}\right]$$

Now the mean value of the direct current is given by

$$I_d = \frac{N}{2\pi}\int_0^\theta i_d\, d(\omega t)$$

$$= \frac{N}{2\pi}\frac{\hat{e}}{\omega L'}\left[\theta\cos\alpha - \sin(\theta+\alpha) + \sin\alpha - \frac{\theta}{2}\left\{\cos\alpha - \cos(\theta+\alpha)\right\}\right]$$

which simplifies to

$$\frac{N}{2\pi}\frac{\hat{e}}{\omega L'}\cos\left(\alpha+\frac{\theta}{2}\right)\left\{\theta\cos\frac{\theta}{2} - 2\sin\frac{\theta}{2}\right\} \text{ ------ } (7)$$

from this equation it can be seen that the direct current is zero when θ is zero. From equation 6 ~~page~~ we have that

$$V_d+\lambda = \frac{2\hat{e}}{\theta}\sin\left(\alpha+\frac{\theta}{2}\right)\sin\frac{\theta}{2} \text{ ---------- } (8)$$

hence when the direct current equals zero, i.e., when θ equals zero

$$V_d+\lambda = \hat{e}\sin\alpha$$

It is obvious that the discontinuity of the direct current must cease when θ equals $\frac{2\pi}{N}$, hence the critical value of I_d at the break in the V_d/I_d characteristic is got by putting θ equal to $\frac{2\pi}{N}$ in equation 7 ~~page~~ Denoting this value of I_d by I_d' we have that

$$I_d' = \frac{N}{2\pi}\frac{\hat{e}}{\omega L'}\cos\left(\alpha+\frac{\pi}{N}\right)\left\{\frac{2\pi}{N}\cos\frac{\pi}{N} - 2\sin\frac{\pi}{N}\right\}$$

Fig. 26 shows curves of V_d to a base of I_d constructed from equation 8 ~~page~~ and equation 7 ~~page~~ . The usual values of $N, \hat{e}, \omega L'$ etc. were taken. Good agreement is obtained with the test results which are given on the same sheet.

The Variation of Direct Voltage with Ignition Angle:

From equation 31 ~~page~~ it can be seen that if we maintain the direct current and the alternating voltage constant while varying the ignition angle, we may write the direct voltage as

$$V_d = k\sin(\alpha+a) - k'$$

where k, a and k' are all constants. This equation shows that a sinusoidal relation exists between V_d and α A load test was run on the convertor under these conditions and the curve of V_d against α which was obtained is shown in Fig. 14 On the same diagram a similar curve is drawn by substituting for $N, \hat{e}, \lambda,$ and ωL in equation 31 ~~page~~ . The curves compare very favourably and do not call for special comment.

The use of grid-controlled rectifiers for battery charging: There are on the market at the present time small grid-controlled rectifiers which have been specially designed for battery charging. The output voltage and the charging current are controlled by a regulator which operates by varying the ignition angle. In order to reduce the harmonics in the output which would otherwise cause considerable heating in the batteries, a cathode choke is fitted. Unfortunately, the charging current/ignition angle characteristic of these rectifiers is very poor, having the form shown in Fig. 27 This curve was obtained by using the convertor to charge a 78-V battery. Oscillograph records show that the break in the characteristic is due to the direct current becoming discontinuous on light load. This effect was fully discussed on page 20 and the equation derived then can also be used here. By substituting the usual values for $N, \hat{e}, \lambda$ and putting $R = 0{\cdot}52$ ohm, $L' = 11{\cdot}2$ mH and $V_d = 78$ V in equation 7 ~~page~~ and equation 8 ~~page~~ the second curve in Fig. 27 was drawn. In order to avoid the variation of inductance with current which occurs with most iron-cored reactors, an air-cored inductance, of which details are given in the appendix ~~page~~, was used.

This type of characteristic is inherent in the arrangement described, and the only practical method of improving the performance of such battery chargers would be to include large reactors in the anode or input leads.

MISCELLANEOUS

Notes on Some Special Transformer Connections.

The performance of a convertor can be modified considerably according to the arrangements of connections for the main transformer. Each such arrangement is treated as a separate problem.

Case I Primary:- 3-wire, 3-phase star; Secondary:- 6-phase star. Using the connections shown in Fig. 9 a load test was run on the convertor, from which the curves shown in Fig. 29 were obtained. The test was run at one value of ignition only, viz., 170 degrees, at which angle the interchange of power was from the d.c. to the a.c. busbars. During the test the cathode-ray oscillograph was connected to record the anode current. While the load was increasing from zero, the following points were observed: On light load each anode was in operation for $\frac{\pi}{3}$ radians. As the load was increased, the overlap between consecutive anodes increased rapidly until finally each anode was burning for $\frac{2\pi}{3}$ radians. This overlap occurred at the same value of the direct current as the discontinuities in the gradient of the voltage-regulation and power-factor curves. Beyond this point no increase in the burning time of the anodes was apparent as the load was increased further. These facts indicated that the leakage reactance between consecutive anodes was much greater than between alternate anodes, for the following reason:- Assuming that commutation from anode 1 to anode 2 commences when $\omega t = \frac{\pi}{3}$ and finishes when $\omega t = \frac{\pi}{3} + u$ where u is the overlap angle, then the period during which anode 1 is operating is $\frac{\pi}{3} + u$. Equation 30 ~~page~~ shows that depends on the reactance between anodes and on the magnitude of the direct current, hence as the direct current increases u increases until ultimately $u = \frac{\pi}{3}$ If any further increase in the direct current takes place anode 3 will have ignited before anode 1 is extinguished and commutation between anode 1 and anode 3 will begin. If the leakage reactance between anodes 1 and 3 is small, commutation will now be completed rapidly, and the overlap between these anodes will be small.

A similar performance is obtained with circuits including interphase transformers, which ~~is~~ are employed to increase artificially the reactance between consecutive anodes, while maintaining that between alternate anodes at its original low value.

In order to demonstrate the truth of this argument, the transformer reactances were measured in the manner described below.

Short-Circuit Tests on the Main Transformer.

With the three primary leads short-circuited and no connection to the neutral, the reactances between terminals 1 and 2, Fig. 30, and between terminals 1 and 3, were determined in the manner described on page 18. Check readings were made between other consecutive and alternate pairs of terminals. Denoting the leakage reactance between consecutive phases by $2\omega l_0$ and between alternate phases by $2\omega l$ the following average figures were obtained $\omega l = 0{\cdot}462$ ohm and $\omega l_0 = 10{\cdot}2$ ohms. Since ωl_0 is thus known, the particular value of direct current at which the breaks in the characteristics occur can be calculated. It has been seen that these breaks occurred when the overlap between adjacent anodes had increased to $\frac{\pi}{3}$ hence by substituting $\alpha = 170$ degrees, $N = 6$, $\hat{e} = 371$ V and

ωl_0 = 10·2 ohms in equation 30 ~~page~~ , the critical value of the direct current is found to be:-

$$I_d' = \frac{371 \sin\frac{\pi}{6}}{10\cdot 2}\left\{\sin 200 - \sin 260\right\} = 11{\cdot}7\ A$$

This value agrees fairly well with the test results given in Fig. 29

Analytical Investigation of Reactances ωl and ωl_0.

From Fig. 30 it is seen why two different values of reactance exist. Assuming a one-to-one turn ratio, Fig. 30 shows that

$$i_R - i_2 = i_Y + i_2 = i_B + 0 = \frac{m}{T}$$

or

$$\frac{3m}{T} = i_R + i_Y + i_B - i_2 + i_2 = 0$$

hence

$$m = 0$$

This shows that the resultant M.M.F. on each of the limbs is zero; therefore the reactance between 1 and 3 is due to the leakage flux ϕ_x , which is normally small.

In the second case, Fig. 30

$$i_R - i_2 = i_Y + 0 = i_B - i_2 = \frac{m}{T}$$

or

$$\frac{3m}{T} = i_R + i_Y + i_B - 2i_2 = -2i_2$$

hence

$$m = -\frac{2}{3}Ti_2$$

This indicates that a residual M.M.F. which is proportional to i_2 , exists on each limb. This M.M.F. produces the flux Φ_0 which is considerably greater than the normal leakage flux ϕ_x due to the higher permeance of its path. Both primary and secondary windings are linked by the flux Φ_0 and consequently the reactance ωl_0 is considerably greater than the normal leakage reactance which occurs between alternate phases.

Relations between Line and Anode Currents: Adopting the same nomenclature and method to that used in deriving the line current with a 4-wire, 3-phase, star-connected primary, we have

$$m = T_1 i_R + T_2(a_1 - a_4) = T_1 i_Y + T_2(a_3 - a_6) = T_1 i_B + T_2(a_5 - a_2)$$

also $i_R + i_Y + i_B = 0$

therefore $m = \frac{1}{3} T_2 (a_1 + a_3 + a_5 - a_2 - a_4 - a_6)$

and $i_R = \frac{1}{3} \frac{T_2}{T_1} (a_1 + a_3 + a_5 - a_2 - a_4 - a_6) - \frac{T_2}{T_1}(a_1 - a_4)$

Similar expressions can be obtained for i_Y and i_B From these equations the line current wave form is built up in Figs. 31 and 32

Case II. Primary; 4-wire, 3-phase star: Secondary; Double 3-phase star with Interphase Transformer.

The connection diagram is shown in Fig. 9 and the results of a load test run at constant ignition angle, in Fig. 28 . As the fourth paper of this thesis is devoted entirely to an investigation into the operation of interphase transformers, little need be said at this point regarding the matter. The oscillograph showed that on load, each anode burned for $\frac{2\pi}{3}$ and that the wave-form of the line current was similar to that shown in Fig. 32

Case III. Primary; 3-wire, 3-phase star: Secondary; Double 3-phase star with Interphase Transformer.

The only alteration from the previous case is the disconnection of the primary neutral. Neglecting secondary effects such as overlap and the magnetising current taken by the interphase transformer, the full-load primary line current can be represented as shown in Fig. 25 Choosing the time axis, $\omega t = 0$ in the position shown and analysing the wave by Fourier's method, we find that the amplitude of the $n^{\underline{d}}$ harmonic is

$$A_n = \frac{3}{\pi}\int_{-\frac{\pi}{3}}^{+\frac{\pi}{3}} I_d \cos n(\omega t)\, d(\omega t)$$

$$= \frac{3 I_d}{n\pi} \sin n\omega t \Big|_{-\pi/3}^{+\pi/3}$$

From this expression, it can be seen that $A_n = 0$, when $n = 3$ or any multiple of 3, hence no triplen harmonics are present in the line current in case II. Therefore, it follows that the current in the neutral must be zero and that the performance of the convertor will be the same whether or not the neutral connection is made. To check this conclusion the convertor was loaded and the neutral was alternately connected and disconnected. No change was evident on any of the instruments in circuit, and no current flowed to the neutral. Minor alterations in the wave-form of the line currents were shown on the oscillograph.

PAPER II

A No-load and Short-Circuit Diagram for Mercury-Arc Invertors.

Short-Circuit Diagram for Mercury-Arc Invertors.

In the course of investigations on the inverted operation of mercury-arc rectifiers the writer found it desirable to have a rapid method of predetermining the performance of the invertor under various conditions. Several methods were tried, but in practice the diagram described in this paper proved to be the simplest and the most useful.

Conditions causing Short-Circuit of an Invertor:

In order that the arc will commutate correctly from anode to anode in a mercury-arc rectifier the anode to which the arc is transferring must be maintained at a higher potential than the one which it is leaving. This condition must exist until commutation is complete.

In Fig. 33 e_1 and e_2 represent the voltages of anodes 1 and 2 respectively and i_1 represents the current in anode 1 for any particular value of the ignition angle, α During the interval, u assume that the arc is commutating from anode 1 to anode 2. If α is such that i_1 reaches zero before the instant, t_0 Fig. 33, then e_2 is positive to e_1 and commutation takes place correctly. If, however, a larger value of α is taken, such that the current in anode 1 is finite when the instant t_0 is reached commutation ceases because the commutating voltage $e_2 - e_1$ is now zero. After t_0 commutation is reversed since $e_2 - e_1$ becomes negative and all the current in anode 2 is transferred to anode 1. When this happens, none of the other anodes can take the load since they are either blocked out by the negatively biassed control grids or are negative to anode 1, which consequently continues to operate until the instant t_1 In Fig. 34 the polarities of the voltages at the instant t_1 are indicated. It will be noticed that the voltages of the d.c. busbars and of phase 1, instead of opposing each other, as is normally the case, are additive. This constitutes a severe short-circuit.

The results of the preceding argument may be summarised briefly by saying that short-circuit will not occur provided commutation is complete before the commutating voltage is reduced to zero.

This statement may be expressed mathematically by writing $\alpha + u + \frac{\pi}{N} = \frac{3\pi}{2}$ This equation gives the relation between α, u and N when the invertor is on the threshold of short-circuit. The usual equation giving the overlap angle as deduced in the appendix is:-

$$\sin\left(\alpha + u + \frac{\pi}{N}\right) = \sin\left(\alpha + \frac{\pi}{N}\right) - \omega L I_d / \hat{e} \sin\frac{\pi}{N}$$

If the direct current under those short-circuit conditions is denoted by I_{sc} then from the preceding equation

$$I_{sc} = \frac{\hat{e}}{\omega L} \sin\frac{\pi}{N}\left[1 + \sin\left(\alpha + \frac{\pi}{N}\right)\right] \text{ ---------- } (9)$$

The agreement between theory and practice was investigated at this point, by running a test on a 6 kw. invertor. In the set available $N = 6$, $\hat{e} = 371$ and $\omega L = 0{\cdot}462$ Substituting these values in equation 9 ~~(1)~~, then $I_{sc} = 401\left[1 + \sin\left(\alpha + \frac{\pi}{6}\right)\right]$ and from this function a graph on a base of α is drawn in Fig. 35

During these laboratory tests the circuit shown in Fig. 9 was used and adequate protection of the bulb and transformer was ensured by having fuses on the a.c. side and a high-speed circuit breaker on the d.c. side. This arrangement operated satisfactorily on the severe short-circuits to which the equipment was subjected.. The test was carried out by setting the ignition angle at a suitable value and gradually increasing the direct voltage until a short-circuit occurred. The value of the direct current, read on a robust moving-coil ammeter connected in the cathode lead, immediately prior to the short-circuit, was taken as the experimental value of for the particular setting of ignition angle on the regulator. The test was repeated for other values of ignition angle. From these results the second curve in Fig. 35 is drawn. It will be seen that in practice short-circuit occurs at lower values of direct current than are derived from theory. The explanation of this probably lies in the fact, that after the current has fallen to zero in any anode, a finite though very brief interval of time must elapse before the negative charge on the grid effectually prevents the anode reigniting should its potential rise again. When current is flowing in any anode limb, the effect of the negative charge on the grid is neutralized by a cloud of positive ions which settles round the grid. When the load current ceases, this space charge is absorbed into the grid circuit, an operation which is completed in between 10 to 100 microseconds. Only when this space charge has been dissipated can the anode be effectually "blocked out." This interval is known as the time of deconization.

The Construction of a No-Load and Short-Circuit Diagram for the Invertor:- The voltage at the input terminals of an invertor is given by

$$\frac{N}{\pi}\hat{e}\sin\frac{\pi}{N}\sin\left(\alpha+\frac{\pi}{N}\right)-\lambda-I_d\left(R+\frac{N}{2\pi}\omega L\right)$$

where, in addition to the usual symbols, R denotes the resistance of the d.c. circuit. On no-load the direct current is zero and the direct voltage is given by

$$V_0 = \frac{N}{\pi}\hat{e}\sin\frac{\pi}{N}\sin\left(\alpha+\frac{\pi}{N}\right)-\lambda \quad \text{--------} \quad (10)$$

Also, if the direct voltage on short-circuit is denoted by V_{sc} , then

$$V_{sc} = \frac{N}{\pi}\hat{e}\sin\frac{\pi}{N}\sin(\alpha+\frac{\pi}{N}) - \lambda - I_{sc}(R+\frac{2\pi}{N}\omega l$$

Substituting for I_{sc} from equation ~~(1)~~.9

$$V_{sc} = \frac{N}{\pi}\hat{e}\sin\frac{\pi}{N}\sin(\alpha+\frac{\pi}{N}) - \lambda - (R+\frac{N}{2\pi}\omega l)\Big[1+\sin(\alpha+\frac{\pi}{N})\Big]\frac{\hat{e}}{\omega l}\sin\frac{\pi}{N} \cdots (11$$

The simplest way to use equations (2) and (3) in practice is in graphical form, but since the direct voltage, the alternating voltage, and the ignition angle are all independent variables, it would appear that a three dimensional diagram was necessary. Fortunately, this can be avoided by combining two of the variables and writing both equations in the form $\frac{V_d+\lambda}{\hat{e}} = f(\alpha)$

In Fig.36 $\frac{V_0+\lambda}{\hat{e}}$ and $\frac{V_{sc}+\lambda}{\hat{e}}$ are plotted against α for $N = 6$, $R = 0{\cdot}52$ ohms and $\omega l = 0{\cdot}462$ ohms.

Consider an invertor operating with constant alternating voltage and ignition angle and assume that the direct voltage is gradually increased from zero. The invertor will be on no-load until $\frac{V_d+\lambda}{\hat{e}}$ becomes equal to $\frac{V_0+\lambda}{\hat{e}}$, thereafter the direct current will increase with further rise of voltage until finally $\frac{V_d+\lambda}{\hat{e}}$ becomes equal to $\frac{V_{sc}+\lambda}{\hat{e}}$ at which point short-circuit will occur. On higher values of direct voltage the invertor continues to short-circuit.

The current scale may be fixed for the load area from equations ~~(2)~~ 10 and ~~(3)~~ 11 by putting $V_d = V_0 + I_d(R+\frac{N}{2\pi}\omega l)$ hence

$$I_d = \frac{\hat{e}}{R+N\omega l/2\pi}\left[\frac{V_d - V_0}{\hat{e}}\right] = \frac{\hat{e}}{R+N\omega l/2\pi}\cdot x$$

where x is the distance measured in $\frac{V_d+\lambda}{\hat{e}}$ units from the no-load boundary line to any point, say P, which is fixed by the ignition angle and the values of the direct and alternating voltages under consideration.

Example:-

V_d = 330 volts, λ = 22 volts, $\hat{e}$ = 371 volts and α = 210° corresponds to the point P on Fig. 36 The point is within the load area, and, by measurement, $x = 0 \cdot 10$, giving $I_d = 39 \cdot 5\,A$ On test, a value of $36A$ was obtained.

Conclusions:- The diagram shown in Fig. 36 is drawn for the experimental invertor on which the tests were carried out, but the no-load and short-circuit equations from which it is constructed are quite general. The limits of α and $\frac{V_d+\lambda}{\hat{e}}$ may, of course, be extended if desired.

PAPER III

The Duration of Overlap in Mercury-arc Convertors.

PART I

Since the duration of the commutating period has a considerable effect on the performance of a convertor, accurate calculation of this quantity is necessary. The purpose of this paper is to examine the usual method of calculation and to describe a new laboratory method of measuring the overlap angle.

Standard Method:

The generally accepted equation giving the overlap angle is

$$\sin\left(u+\alpha+\frac{\pi}{N}\right) = \sin\left(\alpha+\frac{\pi}{N}\right) - \frac{\omega l I_d}{\hat{e}\sin \pi/N}$$

This equation is developed in the appendix ~~page~~ and a curve of u to a base of α for a constant value of I_d. is given in Fig. 38 Curves of u to a base of I_d for several constant values of α are given at a in Figs. 39 and 40 These curves are obtained by substituting in the above equation $N = 6$, $\omega l = 0{\cdot}462$ ohm and $\hat{e} = 371$ V, the values from the test convertor, in order that a comparison with measured results could be made later. This - the common - method of calculating u neglects the resistance of the transformer windings.

Influence of Resistance of Transformer Windings:

We shall now derive an equation containing terms involving the resistance of the transformer windings. Fig. 41 shows commutation taking place from anode N to anode 1. During this interval we can equate to zero the sum of the voltages round the closed circuit formed by the two arcs and the transformer phases.

Hence $$-l\frac{di_N}{dt} - ri_N + e_N - \lambda + \lambda + ri_1 + l\frac{di_1}{dt} - e_1 = 0$$

Overlap calculation.

Since two anodes are operating in parallel

$$i_1 + i_N = I_d$$

and assuming that the direct current has no alternating component

$$\frac{di_1}{dt} = -\frac{di_N}{dt}$$

therefore

$$2l\frac{di_1}{dt} + 2ri_1 - rI_d = -2\hat{e}\cos\left(\omega t + \alpha + \frac{\pi}{N}\right)\sin\frac{\pi}{N}$$

The solution of this equation has the form

$$i_1 = ke^{-\frac{rt}{l}} + \frac{1}{2}I_d - \frac{\hat{e}}{Z}\sin\frac{\pi}{N}\cos\left(\omega t + \frac{\pi}{N} + \alpha - \phi\right)$$

where $\phi = \tan^{-1}\frac{\omega l}{r}$ and $Z = (r^2 + \omega^2 l^2)^{\frac{1}{2}}$

As shown on page 56 $i_1 = 0$ when $\omega t = 0$

hence $k = \frac{\hat{e}}{Z}\sin\frac{\pi}{N}\cos\left(\frac{\pi}{N} + \alpha - \phi\right) - \frac{1}{2}I_d$

Furthermore $i_1 = I_d$ when $\omega t = u$ and therefore

$$\cos\left(u + \alpha + \frac{\pi}{N} - \phi\right) = \cos\left(\alpha + \frac{\pi}{N} - \phi\right)e^{-\frac{ru}{\omega l}} - \frac{Z I_d}{\hat{e}\sin\frac{\pi}{N}} \cdot \frac{e^{-\frac{ru}{\omega l}} + 1}{2} \text{-----} (12)$$

It will be noticed that when $r = 0$ this equation is identical with equation 30 ~~page~~

Putting $r =$ 0·713 ohm and using the same values for N, ωl and $\hat{e}$ as previously, curves of u are calculated from the above equation and drawn at b in Figs. 39 and 40 The close agreement between the curves a and b is remarkable and fully justifies the common practice of neglecting r .

We will now investigate within what limits of the ratio $r/\omega l$ the error introduced by neglecting r remains small. Taking values for $N, \omega l, I_d, \hat{e}$ and α of 6, 0·462 ohm, 20 amps, 371 volts and $\frac{2\pi}{6}$ (the case of the uncontrolled 6-phase rectifier) $r/\omega l$ is varied between 0 and 10 and the corresponding values of u calculated by each method. Fig. 43 shows the curves obtained. In view of the nature of equation 12 ~~page~~

a graphical solution was employed, the method being as follows:-

Equation 12 ~~page~~ can be rewritten thus

$$\frac{\omega l I_d \{(r/\omega l)^2+1\}^{1/2}}{2\hat{e}\sin \pi/N} = \frac{\cos(\alpha+\frac{\pi}{N}-\phi) - \cos(u+\alpha+\frac{\pi}{N}-\phi)e^{\frac{ru}{\omega l}}}{1+e^{\frac{ru}{\omega l}}}$$

Call the right-hand side $f(u)$ For any particular value of the $r/\omega l$ ratio, say 2, the left-hand side may be evaluated. For example, using the same values of $N, \hat{e}, \omega l$ and I_d as were given previously, the left-hand side evaluates to 0·0557. Now by giving u a series of values a graph of $f(u)$ to a base of u can be drawn. This curve is shown in Fig. 44 The solution of equation 12 ~~page~~ for $r/\omega l = 2$ is therefore given by the value of u when $f(u) = 0{\cdot}0557$. This procedure is repeated for each point on the $u, r/\omega l$ graph. Only one auxiliary graph, Fig. 44 , is reproduced here. In practice, the $r/\omega l$ ratio rarely exceeds 2 and it will be seen from Fig. 43 that the error involved is less than three per cent.

PART II

The following method has been evolved by the writer for confirming the preceding work by experiment.

Outline of Method: The method utilises the principle of the stroboscope. The convertor bulb is viewed through a slotted disc running synchronously with the a.c. mains supplying the rectifier. The bulb is thus exposed to the eye at the same instant in every cycle, i.e., when the rotating slot is in line with the bulb and the observer's eye. The synchronous motor driving the disc is fed through a phase-shifting transformer which enables the phase of the disc, in relation to the sequence of operations taking place inside the bulb, to be altered as desired. In this manner, any particular instant, say the ignition of an anode, may be observed. Further, by arranging suitable equipment to measure the phase-shift of the disc, e.g., between the ignition and the extinction of an anode, the time during which the anode is burning may be calculated. The phase-shift of the disc is measured on an a.c. potentiometer. Precautions are taken to prevent errors due to the lateral movement of the observer, and a correction is made for the finite width of the slots.

Description of the Apparatus Employed:

Synchronous Stroboscope: A press-board disc, 40 cm. in diameter and 0·9 mm. thick was mounted on the shaft of a 110-V, ¼-h.p., 1-phase, 50-cycle, 3000-r.p.m., synchronous motor. At the outer edge of the disc one slot was cut 3 cm. radially by 0·3 cm. wide. This assembly was solidly mounted on a base board. In front of the disc a piece of

1·6 mm. bakelite, in which a similar slot had been cut, was mounted vertically so that the slot in the disc was for one position of its travel in alignment with the fixed slot. Errors due to the lateral movement of the observer were practically eliminated by the addition of this fixed slot. The axial distance between the slots was about 5 cm. All bright parts were given several coats of a matt black paint. In this way the light reflected from the stroboscope, which would have had a dazzling effect on the eye, was reduced to a minimum, and consequently the arc could be seen with the greatest definition possible. A photograph of the stroboscope is shown in Fig. 2A.

Phase-shifting Transformer: A 15-kVA, 3-phase, 50-cycle, 0-440-V induction regulator was adapted for use as a phase-shifting transformer by reconnecting it as shown in Fig. 45 . The stroboscope motor was supplied from one phase of the rotor. When the regulator handle was rotated the phase of the voltage across the stroboscope was advanced or retarded by a certain phase angle. This produced an equal angular advancement or retardation of the stroboscope disc since the load on the synchronous motor remained unaltered. The phase of the voltage applied to the motor was read on an a.c. potentiometer.

A.C. Potentiometer: The model used was of the rectangular co-ordinate type patented by D.C. Gall and made by Messrs H. Tinsley & Co. The auxiliary supply to the instrument was taken from one phase of the mains supplying the convertor. A fraction of the voltage across the stroboscope motor was applied to the test terminals and this voltage was read from the instrument in the form

$a+jb$ with reference to the axes of the potentiometer. a and b are the "in phase" and "in quadrature" readings under balance conditions. Since only the phase difference between successive test voltages was required, no definite setting of the potentiometer axes was required. It was necessary, however, that the phase of the axes should not alter during a test.

Mercury-arc Convertor: The convertor on which the tests were carried out has been mentioned in previous papers and is fully described in the appendix ~~page~~ The transformer connections used are those shown in Fig. 10

Assembly of components: This is shown in Fig. 47 The stroboscope is mounted about six feet from the bulb.

Test Procedure.

With the convertor on load and the stroboscope running the bulb was viewed through the rotating disc. The phase-shifter was adjusted until a convenient anode, say number 1, was seen to be on the point of taking load. This was the instant at which commutation of the arc from anode 6 to anode 1 was starting. The direct current, the ignition angle, and the phase angle of stroboscope – $\tan^{-1} b/a$ – which was read on the a.c. potentiometer, were all noted. This test was repeated for other values of direct current up to full-load, the ignition angle being maintained constant. From the results graph d shown in Fig. 46 was drawn. The phase-shifter was now adjusted until the glow round anode 6 had just disappeared. This was the instant at which commutation of the arc was complete. Readings were again taken over the complete load range in the manner described previously, and from the results graph e in Fig. 46 was drawn. The angle intercepted between graphs d and e for any particular value of load current equals the overlap angle plus the angular error due to the finite width of the slots and the finite sensitivity of the observer's eye. The latter errors were considered jointly and denoted by θ . θ was found by exterpolation in the following manner; from Fig. 46 it is evident that $u = \Sigma - \theta$ where Σ is the angle between the ignition of one anode and the extinction of the preceding one as measured on the stroboscope. Now when I_d equals zero it is clear that u must also equal zero hence θ is given by the intercept between the two curves d and e on the $\tan^{-1} b/a$ axis. Since θ is independent of I_d , u can now be calculated for all values of I_d . The test was repeated for other values of ignition angle. Curves of direct current to a base of overlap angle for various values of ignition angle are given in Fig. 39 and 40 Photographs of the arc during commutation were taken through the stroboscope and are shown in Fig. 8 A and B

Conclusions.

This paper shows conclusively that the equivalent resistance of the transformer affects commutation in a minor degree and can be neglected in practice. The difference between the calculated and the experimental curves is partly due to the assumption that $\frac{dI_d}{d\tau} = 0$ ~~is zero~~ - an assumption which is not strictly true in practice. A second error is introduced by neglecting the short-circuit reactance of the mains in all the calculations.

The laboratory test described in Part II of this paper has been used successfully as a demonstration experiment. For this purpose the synchronous stroboscope motor was replaced by an induction motor. The operation of the bulb could then be viewed at slip frequency. The effect on the behaviour of the arc, of connecting the main transformer in different ways was very clearly shown.

Many other applications of the synchronous stroboscope described in this paper can be found outside the sphere of rectifier work altogether.

PAPER IV

Design of Interphase-Transformers for Mercury-Arc Convertors.

THEORY AND DESIGN.

In order to simplify the work as far as possible the following assumptions will be made during the development of the theory:- (1) the resistance of all windings is negligible, (2) the leakage reactance of the windings of the main transformer is negligible, (3) the direct current is free from harmonics, (4) the arc drop is independent of the current. The good agreement between the theoretical waveforms of current and voltage drawn out in Fig. 48, 49 and the oscillograms reproduced in Fig. 5, 4 shows that these assumptions are permissable. i/

Consider the case when the main transformer has N secondary phases divided into two symmetrical star-connected groups of $\frac{N}{2}$ phases each, the two neutral points of which are connected to an interphase transformer in the manner shown in Fig. 50

Let the e.m.f.s. induced in the secondary phases of the main transformer be $e_1\, e_2\, e_3 \ldots\ldots e_N$ where

$$e_1 = \hat{e} \sin(\omega t + \alpha)$$
$$e_2 = \hat{e} \sin\left(\omega t + \alpha - \frac{2\pi}{N}\right)$$
$$\cdots\cdots$$
$$\cdots\cdots$$
$$e_N = \hat{e} \sin\left(\omega t + \alpha + \frac{2\pi}{N}\right)$$

In Fig. 51 these waves are drawn for $N = 6$ corresponding to Fig. 50 Referring to Fig. 50 again, it will be seen that when the direct current I_d is sufficiently large to allow the two groups of phases to run in parallel continuously, the difference of the voltage between two consecutive secondary phases operating in parallel will be the voltage v across the interphase transformer. This voltage is equal and opposite to e_i the back e.m.f. of the winding which is $-\frac{L}{2}\frac{d(i_a - i_b)}{dt}$ where L is the inductance of the interphase transformer winding and i_a and i_b are the currents to phase groups a and b respectively (Fig. 50).

Since $i_a + i_b = I_d$ which has been assumed constant

$$\therefore \; v = \frac{L}{2}\frac{d}{dt}(2i_a + I_d) = L\frac{di_a}{dt}$$

$$\text{or} \quad i_a = \frac{1}{L}\int v\,dt + K$$

From Fig. 51 it is seen that for values of ωt between 0 and $\frac{2\pi}{N}$

$$v = e - e_N = -2\hat{e}\sin\frac{\pi}{N}\cos\left(\omega t + \alpha + \frac{\pi}{N}\right) \text{ - - - - - - - (13)}$$

so that within these limits the current i_1 in phase 1 is given by

$$i_1 = -\frac{2\hat{e}}{\omega L}\sin\frac{\pi}{N}\sin\left(\omega t + \alpha + \frac{\pi}{N}\right) + K_1 \text{ - - - - - - - (14)}$$

Similarly for values of ωt between $\frac{2\pi}{N}$ and $\frac{4\pi}{N}$

$$v = e_1 - e_2$$

from which

$$i_1 = \frac{2\hat{e}}{\omega L}\sin\frac{\pi}{N}\sin\left(\omega t + \alpha - \frac{\pi}{N}\right) + K_2 \text{ - - - - - - - (15)}$$

Hence, since i_1 is continuous at $\omega t = \frac{2\pi}{N}$ it follows that

$$K_1 - K_2 = \frac{2\hat{e}}{\omega L}\sin\frac{2\pi}{N}\sin\left(\alpha + \frac{2\pi}{N}\right)$$

As the phase groups are loaded symmetrically, the mean value of i_1 between the limits $\omega t = 0$ and $\omega t = \frac{4\pi}{N}$ is $\frac{1}{2}I_d$

$$\text{hence } \frac{1}{2}I_d = \frac{N}{4\pi}\left[\int_0^{\frac{2\pi}{N}} -\frac{2\hat{e}}{\omega L}\sin\frac{\pi}{N}\sin\left(\omega t + \alpha + \frac{\pi}{N}\right) + K_1 + \int_{\frac{2\pi}{N}}^{\frac{4\pi}{N}} \frac{2\hat{e}}{\omega L}\sin\frac{\pi}{N}\sin\left(\omega t + \alpha - \frac{\pi}{N}\right) + K_2\right]$$

$$= \frac{1}{2}(K_1 + K_2)$$

So that
$$K_1 = \frac{1}{2}I_d + \frac{\hat{e}}{\omega L}\sin\frac{2\pi}{N}\sin\left(\alpha + \frac{2\pi}{N}\right)$$

and
$$K_2 = \frac{1}{2}I_d - \frac{\hat{e}}{\omega L}\sin\frac{2\pi}{N}\sin\left(\alpha + \frac{2\pi}{N}\right)$$

hence from equation 14 between $\omega t = 0$ and $\omega t = \frac{2\pi}{N}$

$$i_1 = \frac{1}{2}I_d + \frac{\hat{e}}{\omega L}\left\{\sin\frac{2\pi}{N}\sin\left(\alpha+\frac{2\pi}{N}\right) - 2\sin\frac{\pi}{N}\sin\left(\omega t+\alpha+\frac{\pi}{N}\right)\right\} \text{------} (16)$$

and similarly between $\omega t = \frac{2\pi}{N}$ and $\omega t = \frac{4\pi}{N}$

$$i_1 = \frac{1}{2}I_d - \frac{\hat{e}}{\omega L}\left\{\sin\frac{2\pi}{N}\sin\left(\alpha+\frac{2\pi}{N}\right) - 2\sin\frac{\pi}{N}\sin\left(\omega t+\alpha-\frac{\pi}{N}\right)\right\} \text{---} (17)$$

For the 6-phase rectifier, i.e., $N=6$ the voltage v and the current i_1 are drawn for various values of α in Figs. 49 and 48 For the same values of α oscillograms of these quantities were taken on a 6-kW grid-controlled rectifier. These oscillograms are reproduced in Fig. 4 and 5 and ~~the~~ a close agreement will be observed with the calculated curves in Figs. 49 and 48

As is well known, the critical load is the minimum value of I_d for which i_a and i_b are continuous. Reference to Figs. 4, 5, 49 and 48 will show that the critical load I_{crit} equals twice the amplitude of the alternating component of i_a or i_b. From equation 16 it will be seen that the alternating component of i_a is given by:-

$$\frac{\hat{e}}{\omega L}\left\{\sin\frac{2\pi}{N}\sin\left(\alpha+\frac{2\pi}{N}\right) - 2\sin\frac{\pi}{N}\sin\left(\omega t+\alpha+\frac{\pi}{N}\right)\right\} \text{------} (18)$$

Denoting twice the maximum value of this function between $\omega t = 0$ and $\omega t = \frac{2\pi}{N}$ by $\frac{k\hat{e}}{\omega L}$ we may write

$$I_{crit} = \frac{k\hat{e}}{\omega L} \text{------------------} (19)$$

where k is a function of N and α only. Curves of k to a base of α for $N=6$ and $N=12$ are calculated from equation 18 and are shown in Fig. 52 Other values of N rarely occur in practice. These curves are intended to be used as references in order to simplify the design work.

If Φ denotes the flux in the core of the interphase transformer corresponding to (AT) total ampere-turns on the winding, then

$$\Phi = \frac{4\pi}{10}\frac{(AT)}{d/A_i\mu} \quad \text{- - - - - - - - - - - - -} \quad (20)$$

and $$(AT) = \tfrac{1}{2}T(i_a - i_b) = T(i_a - \tfrac{1}{2}I_d) \quad \text{- - - - - - -} \quad (21)$$

From equations 20 and 21 the flux density in the core is given by

$$B = \frac{4\pi\mu}{10\,d}\cdot T\left(i_a - \tfrac{1}{2}I_d\right)$$

From this equation and from equation 16 it will be seen that the wave form of the flux density in the core is directly proportional to and in phase with the a.c. component of the current i_a at any instant. The maximum value of B will therefore be $\frac{4\pi}{10}\cdot\frac{\mu T}{d}$ times the maximum value of $i_a - \frac{1}{2}I_d$ which we have already shown to be $\frac{k\hat{e}}{2\omega L}$ ~~from equations~~ ~~and~~

Hence $$\hat{B} = \frac{4\pi}{10}\frac{\mu}{d}\cdot T\cdot\frac{k\hat{e}}{2\omega L}$$

Multiplying by $A_i T$ and putting $L = \frac{4\pi}{10}\frac{A_i T^2}{d}\mu\, 10^{-8}$ we have that

$$\hat{B} A_i T = \frac{1}{2}\frac{k\hat{e}}{\omega 10^8} \quad \text{- - - - - - - - - - - -} \quad (22)$$

Assuming a window factor of k_s, a window area of A_ω and a conductor area $a\ mm^2$

$$k_s = \frac{Ta}{100\,A_\omega} \qquad \text{by definition,}$$

and if δ is the current density in the winding expressed in amps. per mm^2 then $A_w = \frac{T I_d}{100\,\delta k_s}$

So that $$A_i A_\omega = \frac{k\hat{e} I_d 10^6}{2\omega B \delta k_s} \quad \text{- - - - - - - - - - -} \quad (23)$$

The right hand side of equation 23 involves only design constants or data obtainable from the rectifier circuit for which the transformer is being designed, hence the product $A_i A_\omega$ may be evaluated. The relative values of A_i and A_ω are dependent on material costs, labour costs, standardization, etc., and there is no need to split up the product here. For the usual 2-limb, core-type of construction A_i is about ¼ of A_w.

Calculation of the Losses.

The losses in interphase transformers comprise copper losses in the windings and iron losses in the cores and yokes. The former are simple to compute and need not be mentioned further at this point, but an accurate estimation of the hysterises and eddy-current losses in the core is difficult because the variation of the flux density with time is not sinusoidal.

A method which is simple to use and yet sufficiently accurate for practical purposes is to calculate the iron losses due to the fundamental of the flux wave only, and to add a suitable amount for the losses due to the higher harmonics.

The fundamental of the flux wave is deduced from the fundamental of the voltage wave applied to the interphase transformer under working conditions. This can be determined by resolving the voltage wave into a Fourier series. Adopting the usual notation

$$A_n = \frac{N}{\pi}\int_0^{\frac{2\pi}{N}} v \cos n\omega t . \, d\omega t, \quad \text{and} \quad B_n = \frac{N}{\pi}\int_0^{\frac{2\pi}{N}} v \sin n\omega t \, d\omega t$$

Substituting the value of v from equation 13 and carrying out the integrations, remembering that n is an odd multiple of $\frac{1}{2}N$ we find

$$A_n = \frac{-2N\hat{e}}{\pi(n-1)(n+1)} \sin\frac{2\pi}{N} \sin\left(\alpha + \frac{2\pi}{N}\right) \quad *$$

and $$B_n = \frac{-2Nn\hat{e}}{\pi(n-1)(n+1)} \sin\frac{2\pi}{N} \cos\left(\alpha + \frac{2\pi}{N}\right) \quad *$$

---

* See appendix, page 73

Design of Interphase Transformers.

The frequency of the fundamental of the voltage $\hat{v}$ is $\frac{1}{2}Nf$, so that the amplitude of the fundamental is $(A_n^2+B_n^2)^{1/2}$ when $n=\frac{1}{2}N$. If this amplitude is denoted by $\hat{\epsilon}$ curves showing $\hat{\epsilon}/\hat{e}$ may be drawn to a base of α for any values of N. Such curves for $N=6$ and $N=12$ are given in Fig. 52 From these curves the amplitude of the fundamental of the flux density may be estimated from

$$\hat{\beta} = \frac{\hat{\epsilon}}{\hat{e}}\,\frac{\hat{e}\,10^8}{\pi N f A_i T} \text{ - - - - - - - - - - - - } (24)$$

In Fig. 53 the total iron loss expressed in watts. per lb. for Stalloy laminations 0·014" thick is plotted to a base of flux density for frequencies of 150 and 300 cycles per second. These frequencies are the ones required when 6 and 12 phase rectifiers are supplied at 50 cycles.

A Correction Factor for Losses due to Higher Harmonics.

(1) Hysterises Loss:- The hysterises loss may be assumed to vary with the square of the maximum value of the flux density in the core and directly as the frequency of the fundamental.

Denote the true value of the hysterises loss in the core by P_H and the value due to the fundamental only by ϕ_H

Then $$\frac{P_H}{\phi_H} = \frac{\hat{B}^2}{\hat{\beta}^2} = \left[\frac{\frac{1}{2}k\hat{e}\,10^8}{\omega A_i T}\Big/\frac{\hat{\epsilon}\,10^8}{\omega n T A_i}\right]^2 = \left[\frac{k n \hat{e}}{2\hat{\epsilon}}\right]^2$$

Fig. 54 shows graphs of P_H/ϕ_H for $N=6$ and $N=12$. It will be observed that in each case very little correction is required for the uncontrolled rectifier.

(2) Eddy-current Loss:- The eddy-current loss in the core of any transformer varies with the square of the applied voltage and is independent of the voltage wave-form.

Denote the true value of the eddy-current loss in the core by P_E and the eddy-current loss due to the fundamental of the voltage only by ϕ_E

Then $$\frac{P_E}{\phi_E} = \left[\frac{\text{r.m.s. value of the voltage wave}}{\text{r.m.s. value of fundamental}}\right]^2 \quad \text{- - - -} \quad (25)$$

The r.m.s. value of the voltage wave must now be calculated.

Denoting it by E we have that

$$E^2 = \frac{N}{2\pi}\int_0^{\frac{2\pi}{N}} v^2\, d\omega t$$

Substituting for v from equation 13 and integrating

$$E = 2\hat{e}\sin\frac{\pi}{N}\left[\frac{N}{4\pi}\cos\left(\frac{4\pi}{N}+2\alpha\right)\sin\frac{2\pi}{N}+\frac{\alpha}{2}\right]^{1/2}$$

Fig. 55 shows E drawn on a base of α for $N=6$ and $N=12$. From equation 25 graphs of P_E/ϕ_E for $N=6$ and $N=12$ are drawn in Fig. 54. These show the increase of the actual eddy-current losses compared with those estimated using the fundamental only.

Since the eddy-current and hysterises losses are roughly equal in iron from which the core is made and since they increase in approximately the same manner with increase of α, a suitable allowance for the increase in the total iron loss can be made by averaging the two losses. Curves of total iron loss due to the fundamental only are drawn in Fig. 54 for $N=6$ and $N=12$

The Critical Load:- From the definition of inductance

$$L = \frac{\phi T}{I}10^{-8} = \frac{\hat{B} A_i T\, 10^{8}}{(AT_{\hat{B}})}$$

where $(AT_{\hat{B}})$ denotes the resultant ampere-turns on the interphase transformer required to produce a flux density of $\hat{B}$ in the core. Making the area of the yokes and cores equal and denoting the length of the mean path of the flux by d then

$$L = \frac{B A_i T^2 10^{-8}}{(at_B)\, d} \quad \text{- - - - - - - - - - -} \quad (26)$$

where $(at_{\hat{B}})$ is the ampere turns per cm. required to produce a flux density of $\hat{B}$. Finally, substituting in equation 19 gives

$$I_{crit} = \frac{k \hat{e} (at_B) d.}{\omega \hat{B} A_i T^2 10^{-8}} \quad \text{- - - - - - - - - - -} \quad (27)$$

The Design of an Interphase Transformer for a 125-kW 50-Cycle Invertor.

Relevant Data:- Connection diagram, Fig. 50 Full-load direct current 260 A; Ignition angle, 180°; Secondary phase voltage, 450.

From Fig. 52 the value of k corresponding to an ignition angle of 180° is 0·5. Assuming a current density of 2·2 A/mm^2. and a window factor of 0·28, and limiting the flux density in the core to 8,000 lines per cm^2, the value of the product, $A_i A_\omega$ is found to be 27350 from equation 23

Choosing a 2-limb core-type of construction with one-half of the total turns wound on each limb, A_ω may be taken as approximately $4 A_i$

Hence $A_i = \frac{1}{2}\sqrt{27350} = 82{\cdot}5$ cm.

From equation 22 the number of turns, T is found to be 78, say 80, which gives 40 per limb.

The cross-sectional area of the conductor is $I_d/2\delta$ which evaluate to 59 mm^2. A 12 x 5 mm. strip insulated to 12·55 x 5·55 is therefore a suitable size.

Arranging the 40 turns on each limb in 5 layers of 8 turns each the height of the windows becomes 20 cm. allowing for shoulders and slack.

The nett-core section has already been fixed at 82·5 cm^2. Assuming a space factor of 0·9 and making the core square, the side is $\sqrt{(82{\cdot}5/0{\cdot}9)} = 9{\cdot}6$ cm.

Winding the coils on a former of external diameter 14 cm., the distance between the core centres becomes 22 cm., which allows a 1 cm. clearance between the two coils.

Iron Losses:- Making the core and yoke cross-sections equal, the weight of iron in the magnetic circuit is approximately 148 lb.

From. Fig. 52 the amplitude of the fundamental of the voltage across the interphase transformer is $0{\cdot}73\hat{e}$ for $\alpha = 180^\circ$. Hence from equation 24 the fundamental of the flux density is 7470 lines per cm^2.

Fig. 53 gives the specific iron loss for a sinusoidally varying flux density of this amplitude as 1.55W. per lb., and Fig. 54 shows that for $\alpha = 180^\circ$ this value should be multiplied by 1·1 to allow for the higher harmonics.

Hence the total core loss equals 1·1 x 1·55 x 148 = 259 W.

Copper Loss:- The resistance of the winding is 0·0147 ohm and the copper loss is therefore $\left(\frac{1}{2}I_d\right)^2 R$ = 249 W.

Critical Load:- From the dimensions of the cores and yokes already found, the length of the mean path of the flux is about 106 cm.

Fig. 56 gives $(at) = 1{\cdot}24$ for $B = 8000$ and hence from equation 26

$$L = 0{\cdot}321\ H$$

and

$$I_{crit.} = \frac{k\hat{e}}{\omega L} = 3{\cdot}22\ A$$

Application of Method to 12-phase Rectifiers.

The connections shown in Fig. 57 are used to some extent in practice and the design of the three interphase transformers call for special comment.

Transformers A and B are similar to the example worked through previously. It should be observed, however, that only one-half the full-load direct-current of the rectifier is used in equation 23

Transformer C is best dealt with by considering the equivalent circuit shown in Fig. 58 If the e.m.f. of each secondary phase in the latter figure is assumed to be $\frac{1}{2}\sqrt{3}$ times the actual value of the secondary phase e.m.f., then, so far as transformer C is concerned, Fig. 57 is equivalent to Fig. 58

From the ordinary theory of grid-controlled rectifiers α for transformer C is $\frac{\pi}{6}$ greater than the value taken for transformers A and B for any given output voltage. This fact must be appreciated when reading the values of k from the graphs in Fig. 52 In all other points the design is similar to the preceding example if the curves for $N=12$ are used in place of $N=6$.

APPENDIX

SECTION I

Elementary Voltage and Current Relation in Mercury-Arc Convertors.

Three simple relations of a fundamental nature will be derived here. The first is an expression for the overlap between anodes.

(1) Overlap angle, u .

During the normal operation of a convertor the arc is maintained between the cathode and each anode in turn. When the commutation from one anode to the next takes place the current falls to zero in one transformer secondary phase and rises to its full value (equal to the direct current) in the succeeding one. This change occupies a finite time, owing to the leakage reactance of the transformer windings. The interval during which two anodes are thus operating in parallel or "overlapping" is denoted by u radians. In the present treatment the effect of the resistance of the transformer windings on the time of commutation is neglected. A rigid proof showing that the effect of resistance is relatively unimportant is given ~~later~~ in (Paper III, ~~page~~).

Fig. 37 shows the simplest method of connecting an N-anode rectifier. Considering the instant shown when anode 1 and anode N are overlapping, it will be seen that Kirchhoff's Law may be applied to the closed circuit comprising anode 1, the arcs and anode N ; whence:

$$-l\frac{di_N}{dt}+e_N-\lambda+\lambda+l\frac{di_1}{dt}=0 \text{ - - - - - - - } (28)$$

where l is the leakage inductance of each secondary phase, e_1 and e_N the induced e.m.f.s. and i_1 and i_N the currents in anodes 1 and N respectively. λ, the arc drop is assumed to be independent of the current. Since two anodes are burning at the instant under consideration the direct current, I_d is equal to $i_N + i_1$ hence differentiating

$$\frac{di_1}{dt} + \frac{di_N}{dt} = \frac{dI_d}{dt}$$

Assuming that the inductance in the d.c. circuit is sufficiently large to maintain the direct current sensibly constant dI_d/dt will be zero and therefore

$$\frac{di_1}{dt} = -\frac{di_N}{dt} \quad \text{- - - - - - - - - - -} \quad (29)$$

Substituting in equation 28 and rearranging the terms

$$\frac{di_1}{dt} = \frac{1}{2l}(e_N - e_1)$$

Assuming that the applied voltage is sinusoidal, e_1, can be represented by $\hat{e}\sin(\omega t+\alpha)$ and e_N by $\hat{e}\sin(\omega t+\alpha+\frac{2\pi}{N})$ where α is the ignition angle and is measured in the manner shown in Fig. 33

Therefore $\frac{di_1}{dt} = \frac{\hat{e}}{l}\cos(\omega t+\alpha+\frac{\pi}{N})\sin\frac{\pi}{N}$

from which $i_1 = \frac{\hat{e}}{l}\sin\frac{\pi}{N}\int\cos(\omega t+\alpha+\frac{\pi}{N})\,dt + k'$

$$= \frac{\hat{e}}{\omega l}\sin\frac{\pi}{N}\sin(\omega t+\alpha+\frac{\pi}{N}) + k'$$

where k' is a constant of the integration. Assuming $\omega t = 0$ at the instant when current commences to flow in phase 1, i.e., when $i_1 = 0$ then

$$k' = \frac{\hat{e}}{\omega l}\sin\frac{\pi}{N}\sin(\alpha+\frac{\pi}{N})$$

Also when $\omega t = u$ commutation is complete and $i_1 = I_d$ therefore

$$I_d = \frac{\hat{e}}{\omega l}\sin\frac{\pi}{N}\left\{\sin(\alpha+\frac{\pi}{N}) - \sin(u+\alpha+\frac{\pi}{N})\right\}$$

$$\text{or} \quad \sin(u+\alpha+\frac{\pi}{N}) = \sin(\alpha+\frac{\pi}{N}) - \frac{\omega l I_d}{\hat{e}\sin\pi/N} \quad \text{- - - -} \quad (30)$$

From this expression u can be found for any values of $N, \alpha, \hat{e}, \omega l$ and I_d. A graph of u to a base of ignition angle for a constant value of direct current is given in Fig. 38 and graphs of u to a base of direct current for constant ignition angles are given in Figs. 39 and 40

Values ~~for~~ of $N=6$, $\omega l = 0{\cdot}462$ ohm and $\hat{e} = 371$ volts were chosen. These figures were taken from the 6-kW convertor used in the experimental work so that a comparison could be made with test results which were given elsewhere.

(2) Direct Voltage, V_d.

If the instantaneous value of the direct voltage is denoted by v_d then neglecting the arc drop and the resistance of the d.c. circuit

$$v_d = e_1 - l\frac{di_1}{dt}$$

and $v_d = e_n - l\frac{di_N}{dt}$ between $\omega t = 0$ and $\omega t = u$

Adding
$$v_d = \frac{e_1+e_N}{2} - \frac{l}{2}\left(\frac{di_1}{dt} + \frac{di_N}{dt}\right)$$
$$= \frac{e_1+e_N}{2} \quad \text{since} \quad \frac{di_1}{dt} + \frac{di_N}{dt} = 0$$

from equation 29

When commutation is complete and the entire load is carried by anode 1

$$v_d = e_1$$

This relation holds between $\omega t = u$ and $\omega t = \frac{2\pi}{N}$

Fig. 59 shows v_d in heavy outline. The mean value of the direct voltage can be found by integrating v_d between $\omega t = 0$ and $\omega t = \frac{2\pi}{N}$ thus

$$V_d = \frac{N}{2\pi}\int_0^u \frac{e_1+e_N}{2}\, d(\omega t) + \frac{N}{2\pi}\int_u^{\frac{2\pi}{N}} e_1\, d(\omega t)$$

$$= \frac{N\hat{e}}{2\pi}\left[\int_0^u \cos\frac{\pi}{N}\sin(\omega t+\alpha+\frac{\pi}{N})\, d(\omega t) + \int_u^{\frac{2\pi}{N}} \sin(\omega t+\alpha)\, d(\omega t)\right]$$

$$= \frac{N\hat{e}}{2\pi}\sin\frac{\pi}{N}\left[\sin(\frac{\pi}{N}+\alpha) + \sin(u+\alpha+\frac{\pi}{N})\right]$$

Substituting for $\sin(u+\alpha+\frac{\pi}{N})$ from equation 30

$$V_d = \hat{e}\frac{N}{\pi}\sin\frac{\pi}{N}\sin(\frac{\pi}{N}+\alpha) - \frac{N}{2\pi}\omega l I_d$$

If λ denotes the arc drop and R the resistance of the d.c. circuit then the voltage at the d.c. terminals will be

$$V_d = \hat{e}\frac{N}{\pi}\sin\frac{\pi}{N}\sin(\frac{\pi}{N}+\alpha) - (\frac{N}{2\pi}\omega l + R)I_d - \lambda \text{ - - - } (31)$$

This equation is true both for rectification and inversion. In the latter case, the value of α is such that the algebraic sign of V_d is negative.

Some oscillograms of the direct voltage between the cathode and the star-point of the secondary winding are given in Fig. 7 A, B and C

(3) Alternating Line Current.

The wave-form and r.m.s. value of the primary line current depends on the anode or secondary phase current and on the type of transformer connection used. All practical arrangements of connections have been investigated by Marte and Winograd, and later by Rissik.

The case of a 6-phase secondary and a 3-phase, 4-wire star-connected primary is investigated below. It serves as an illustration of the method of attacking such problems, but it is primarly included because the results obtained will be required later in the investigation.

Fig. 60 shows the current distribution in the windings of the transformer. Since the change of magnetic potential along the top or the bottom yoke is negligible, it follows that the sum of the ampere-turns on the three limbs must be equal at every instant. Denoting the resultant m.m.f. per limb by m we may write

$$m = T_1 i_R + T_2(a_1 - a_4) = T_1 i_Y + T_2(a_3 - a_6) = T_1 i_B + T_2(a_5 - a_2)$$

where T_1 and T_2 are the turns on the primary and on the secondary phases respectively; i_R , i_Y , and i_B the three primary phase currents; and $a_1, a_2, a_3 \dots$ the secondary phase currents. Since the primary phase currents may flow to the neutral independently of one another, the resultant ampere-turns m will always be zero, hence

$$i_R = \frac{T_2}{T_1}(a_1 - a_4) \quad - - - - - - - - \quad (32)$$

$$i_Y = \frac{T_2}{T_1}(a_3 - a_5) \quad - - - - - - - - \quad (33)$$

$$i_B = \frac{T_2}{T_1}(a_5 - a_2) \quad - - - - - - - - \quad (34)$$

$$i_n = i_R + i_Y + i_B$$
$$= \frac{T_2}{T_1}\left(a_1 + a_3 + a_5 - a_2 - a_4 - a_6\right) \quad \text{- - - -} (35)$$

In the case under consideration the wave-form of the anode current approximates to a rectangle whose height and base are I_d and $\frac{2\pi}{6}$ respectively. The line and neutral currents can be built up from equations 32, 33, 34 and 35 in the manner shown in Fig. 61. Oscillograms are shown in Fig. 6 B and C

SECTION II

Details of the grid-controlled Mercury-Arc Convertor referred to in the preceding papers.

The equipment was built by Messrs Hewittic Electric Co. Ltd., Surrey, and comprises the following:-

- Main transformer.
- Glass bulb.
- Ignition and excitation gear.
- Grid control gear.
- Interphase transformer.
- Smoothing reactor.

These will be dealt with under separate headings.

Main Transformer. The transformer is a 3-limbed, natural-air-cooled, core-type, transformer, designed to operate on a 50-cycle supply. The primary is wound for three phases, all the ends of which are brought to a terminal board. This permits either star or mesh connection to be used. The normal primary phase voltage is 254 and tappings for ±5% and ±10% are provided. The full-load current on the primary side is 12 amps per phase.

The secondary comprises 6 phases which are wound in two star-connected groups of three phases each. The three ends and the neutrals of each three-phase group are brought out to terminals. No tappings are provided on the secondary windings. The normal voltage and the full-load current per secondary phase are 252 volts and 8 amps respectively.

One auxiliary, mesh-connected, 3-phase winding supplies the grid-control apparatus at 110 volts. A second auxiliary winding provides a single-phase, 120-volt, centre-tapped supply for the ignition and excitation circuits.

Glass Bulb. A standard 6-arm glass bulb with a rated d.c. output of 50 amps at 500 volts was employed. At this rating the bulb would normally be fan-cooled, but in our case the output did not exceed 25 amps at 350 volts hence a fan was unnecessary. In addition to the usual graphite anodes and mercury cathode a control grid is situated in each limb just below the anode. This will be seen in the photographs ~~on Page~~ in Fig. 1. The grids are thin metal tubes the outside diameters of which are slightly less than the inside diameters of the glass limbs. From the inside of these tubes metal fins project radially into the arc path. Three small subsidiary limbs are fused on to the bulb near the mercury pool. Two of these are for the pilot or excitation anodes and the third contains the ignition electrode. The latter is a thin strip of spring steel sealed into the top end of the limb and projecting out into the bulb. A piece of graphite is fixed to the outer end and a soft-iron armature is attached midway between the seal and the graphite tip. The assembly is adjusted so that the graphite clears the mercury pool by about inch.

Ignition and Excitation. Fig. 62 shows the circuit diagram. E_1 and E_3 are connected across the outers and E_2 to the mid-point of the single-phase winding on the main transformer. When the supply is switched on the voltage between E_1 and E_2 is about 60 and since a and b are normally closed contactors a current flows in the solenoid S which is clamped to the ignition limb of the bulb below the soft iron armature. The armature is attracted to the solenoid and the ignition electrode pulled down into the mercury pool thereby short-circuiting the solenoid which consequently loses its magnetism and allows the ignition anode to spring out of the pool. This breaks the circuit in the bulb and the resulting spark ionises the mercury vapour. The presence of a small quantity of ionised mercury vapour is sufficient to allow the excitation anodes and the cathode to begin operating as a full-wave rectifier. The direct-current output from this rectifier flows in the cathode lead and excites the relay r which then opens contactors a and ~~b~~ b thereby isolating the ignition system. In order to limit the current in the excitation circuit, a choke is included in each anode lead. The two coils are mounted on one magnetic circuit, the top yoke of which can be adjusted to vary the airgap. This permits the exciting current to be adjusted to an optimum value. Oscillograms pertaining to the excitation circuit are shown in Fig. 7 G and H

Grid Excitation Apparatus. The system known as "peaky-wave control" is employed. The circuit is shown in Fig. 63 and will be dealt with under the following sub-headings:-

Phase-shifting transformer.
Peaking transformers.
D.C. Bias supply.

Phase-shifting transformer. A standard 2-pole, Neco, ¼ h.p., 110-V, 3-phase, 50-cycle, wound-rotor induction motor is used. The phase-turn ratio between stator and rotor is unity and all the leads of both stator and rotor are brought out to terminals mounted on the carcase. A graduated scale divided into 360 degrees is mounted on the shaft and enables the phase displacement between the stator and rotor voltages to be read directly. From the connection diagram in Fig. 63 it will be seen that the stator is fed directly from the 3-phase auxiliary winding on the main transformer.

Peaking transformers. These transformers are designed to give a secondary voltage with a maximum value of 450 V and a duration of less than $\frac{1}{5}$th of a cycle when a sinusoidal voltage of 65 is applied to the primary. Three transformers are employed. The primaries are star-connected and are fed from the rotor of the phase shifting transformer. The mid-points of the secondaries are connected together to give a 6-phase output with a maximum value between line and neutral of 225 volts.

80-V, D.C. grid-bias supply. This is obtained from a full-wave Westinghouse copper-oxide rectifier which is supplied at 110 V from one phase of the 3-phase auxiliary winding on the main transformer. Relevant oscillograms are shown in Fig. 7 D, E and F

Interphase Transformer. A 2-limb interphase transformer with a nett core area of 14·4 cm^2 and 84 turns per limb form~~ed~~ing part of the equipment supplied by the makers was found to be unsuitable, and it was replaced by one designed and built by the writer using the method described in Paper IV. Relevant data are core area, 18 cm^2 and turns per limb, 100.

Smoothing Equipment. Unless stated otherwise, an iron-cored series reactor of which details are given below, was connected in the cathode lead.

Type:	2-limb, core-type, natural-air-cooled.
Nett core area:	26 cm per limb.
Total turns:	180, 90 per limb.
Air-gap:	Adjustable, normally $\frac{1}{8}$ inch.
Mean length of flux path:	Approximately 60 cm.
Inductance:	10 mH at 20 A increasing to 30 mH at 5 A.

In the tests described on page 20 an air-cored reactor was used in order to avoid variation of inductance with load current. Details are given below.

Number of Turns:	120.
Mean diameter:	55 cm.
Length:	16 cm.
Inductance:	11·2 mH.
Resistance:	0·3 ohms.

A photograph of the convertor is shown in Fig. 1

SECTION III

Details of the cathode-ray oscillograph used in the investigation.

Introduction: Early in the investigation it was realised that a good oscillograph was necessary if full advantage was to be taken of the laboratory work. Some time was spent experimenting with various standard oscillograph models of both moving-strip and cathode-ray types in an endeavour to find a satisfactory instrument for this purpose. These preliminary tests showed that no standard equipment available at that time was entirely suitable, so the writer developed and built the equipment described below, in which special attention has been devoted to simplicity of operation; absence of distortion; suitability for recording satisfactorily voltages between 5 and 500, and currents between 10 mH and 30 A; and finally a simple and accurate method of photographing the trace.

General Arrangement: A cathode-ray tube is supplied with the necessary auxiliary voltages to give a sharply defined spot on the screen. The "test" voltage is applied across one pair of deflector plates and appears as a horizontal line on the screen. If it is necessary for the operator to see the wave-form, a mirror is rotated at a constant speed in front of the screen. If, however, a permanent record of the wave-form is required the image of the trace is focussed on to a photographic plate arranged to move in front of the screen with a suitable velocity.

Cathode-Ray Tube: A Cossor 3271/J tube of the high vacuum type (described in Cossor leaflet 1934, L 146) was used. A high vacuum type was used in preference to one of the gas-filled variety to avoid origin distortion. A direct voltage of about 3000 is necessary between the third anode and the shield. The voltages for the intermediate electrodes - cathode, first and second anodes - are obtained from variable potential dividers connected across the 3000-V terminals. The tube and the potential dividers are assembled as a unit and the 3000-V leads, the cathode heater leads, and the four deflector plates are brought out to terminals mounted in an accessible position. Since the heater voltage is less than two volts a fixed resistor was wired in the heater circuit to permit a 2-volt cell to be connected directly to the heater terminals of the unit. Focussing is carried out by adjusting the three variable potentiometers mounted on the tube unit. The circuit diagram and other data necessary for assembling the unit are given in Fig. 64 ~~page~~ . Fig. 3A ~~page~~ shows a photograph of the complete unit.

High-Voltage Supply: The high voltage is obtained from a half-wave rectifier comprising a 1-phase, 50-cycle, 250/3000-V transformer and a Cossor S.U. 2130 half-wave rectifying valve. The filament of the rectifying valve is supplied at 2 V from an auxiliary winding on the main transformer. A smoothing circuit comprising condensers and series resistors is connected to the output. The rectifier is mounted in a wooden box provided with output and input terminals. The circuit diagram and the values of the components are given in Fig. 65

Rotating mirror system for visual examination of the wave-form: Four similar rectangular mirrors are mounted in the manner shown in Fig. 3B The mirror system is driven through a 10:1 reduction gear from a $\frac{1}{40}$-h.p., 250-V, 50-cycle, 1500-r.p.m., 1-phase, synchronous motor fed from a supply having the same frequency as the wave being examined. By this means "locking" of the image is achieved. The idea was obtained from the Duddell mechanical oscillograph and modified for use with cathode-ray tubes.

Photographic Equipment: A light-tight wooden slide about 6 feet long and designed to allow a 4¼" x 3¼" photographic plate to slip through it with a minimum clearance was borrowed from a mechanical oscillograph of which it formed part. About 4 feet from the top end there was a narrow horizontal aperture through which the trace on the oscillograph screen could be focussed on a plate travelling past the aperture. The slide was clamped on to the edge of the bench in a vertical position such that the aperture was level with the centre of the oscillograph screen. The image was focussed on to the plate by interposing a pan-tacher, f 1·8 lens between the tube and the slide, the distances being adjusted until a clearly defined image of suitable size was obtained on a dummy plate lowered down the slide until it was opposite the aperture. Tube and lens were then clamped in this position. The sensitive plates were introduced into the top of the slide, and removed from the bottom after exposure in special light-tight cloth bags. Near the top of the slide a small spring catch held the plate until any required instant when it could be released by pulling a light cord. Since the plate is falling past the aperture undergravity the velocity is not quite uniform but the error is less than would be imagined as the cushioning effect of the air column inside the slide and also the friction of the plate in the guides tends to limit the velocity. Measurement shows that the error is sufficiently small to be neglected. The prints reproduced here are reduced from the original negatives. Ilford Iso-Zenith plates

(H and D 7000) were found to be most suitable.

Current Deflection: The current was passed through deflecting coils arranged symmetrically over the cathode-ray tube in the normal manner. Different coils were used for each range in preference to using shunts, as the latter would have had to be designed with the same time constant as the coil they were shunting.

Conclusion: The instrument has worked exceedingly well in practice, and it has enabled the investigation to be carried out without difficulty.

SECTION IV

A. On the determination of the fundamental of the anode current.

Pertaining to page 12 :

$$A_1 = \frac{1}{\pi}\int_{\alpha+u}^{\alpha+\frac{2\pi}{N}+u} i_1 \cos\omega t \; d\omega t$$

Substituting for i_1 from equations 3 and 4

~~page~~ $$A_1 = \frac{1}{\pi}\Big[\int_{\alpha}^{\alpha+u}\frac{\hat{e}}{\omega l}\sin\frac{\pi}{N}\Big\{\sin(\alpha+\frac{\pi}{N}) - \sin(\omega t+\frac{\pi}{N})\Big\}\cos\omega t \; d\omega t$$

$$+\int_{\alpha+u}^{\alpha+\frac{2\pi}{N}} I_d \cos\omega t \; d\omega t$$

$$+\int_{\alpha+\frac{2\pi}{N}}^{\alpha+\frac{2\pi}{N}+u} I_d\cos\omega t - \frac{\hat{e}}{\omega l}\sin\frac{\pi}{N}\Big\{\sin(\alpha+\frac{\pi}{N}) - \sin(\omega t-\frac{\pi}{N})\Big\}\cos\omega t\Big]$$

$$= \frac{1}{\pi}\Big[\frac{\hat{e}}{\omega l}\sin\frac{\pi}{N}\Big\{\sin(\alpha+\frac{\pi}{N})\sin\omega t + \frac{1}{4}\cos(2\omega t+\frac{\pi}{N}) - \frac{1}{2}\sin\frac{\pi}{N}\cdot\omega t\Big\}_{\alpha}^{\alpha+u}$$

$$+ I_d \sin\omega t\Big|_{\alpha+u}^{\alpha+2\pi/N}$$

$$+ I_d\sin\omega t\Big|_{\alpha+\frac{2\pi}{N}}^{\alpha+\frac{2\pi}{N}+u} - \frac{\hat{e}}{\omega l}\sin\frac{\pi}{N}\Big\{\sin(\alpha+\frac{\pi}{N})\sin\omega t + \frac{1}{4}\cos(2\omega t-\frac{\pi}{N}) + \frac{1}{2}\sin\frac{\pi}{N}\cdot\omega t\Big\}_{\alpha+\frac{2\pi}{N}}^{\alpha+\frac{2\pi}{N}+u}\Big]$$

$$= \frac{1}{\pi}\Big[\frac{\hat{e}}{\omega l}\sin\frac{\pi}{N}\Big\{2\sin(\alpha+\frac{\pi}{N})\sin\frac{u}{2}\cos(\alpha+\frac{u}{2}) - 2\sin(\alpha+\frac{\pi}{N})\sin\frac{u}{2}\cos(\alpha+\frac{u}{2}+\frac{2\pi}{N})$$

$$+\frac{1}{2}\sin u\,\sin(2\alpha+u+\frac{3\pi}{N}) - \frac{1}{2}\sin u\,\sin(2\alpha+u+\frac{\pi}{N}) - \sin\frac{\pi}{N}\cdot u$$

$$+ 2I_d\sin\frac{u}{2}\cos(\alpha+\frac{u}{2}+\frac{2\pi}{N}) + 2I_d\cos(\alpha+\frac{u}{2}+\frac{\pi}{N})\sin(\frac{\pi}{N}-\frac{u}{2})\Big]$$

Now from equation 30 ~~page~~ we may write

$$\frac{\hat{e}}{\omega l}\sin\frac{\pi}{N} = \frac{I_d}{\sin(\alpha+\frac{\pi}{N}) - \sin(\alpha+\frac{\pi}{N}+u)}$$

Substituting in the previous expression

$$A_1 = \frac{2I_d}{\pi}\left[\frac{2\sin(\alpha+\frac{\pi}{N})\sin\frac{u}{2}\sin(\alpha+\frac{u}{2}+\frac{\pi}{N})\sin\frac{\pi}{N}+\frac{1}{2}\sin u\cos(2\alpha+u+\frac{2\pi}{N})\sin\frac{\pi}{N}-\frac{1}{2}\sin\frac{\pi}{N}\cdot u}{\sin(\alpha+\frac{\pi}{N})-\sin(\alpha+\frac{\pi}{N}+u)}\right.$$

$$\left. + \cos(\alpha+\frac{u}{2}+\frac{2\pi}{N})\sin\frac{u}{2} + \cos(\alpha+\frac{u}{2}+\frac{\pi}{N})\sin(\frac{\pi}{N}-\frac{u}{2})\right]$$

which can be simplified to

$$\frac{2I_d}{\pi}\sin\frac{\pi}{N}\left[\frac{\sin u\cos(2\alpha+u+\frac{2\pi}{N})+u}{4\cos(\alpha+\frac{\pi}{N}+\frac{u}{2})\sin u/2}\right]$$

Similarly $$B_1 = \frac{1}{\pi}\int_{\alpha}^{\alpha+\frac{2\pi}{N}+u} i_1 \sin\omega t \, d\omega t$$

$$= \frac{1}{\pi}\left[\int_{\alpha}^{\alpha+u}\frac{\hat{e}}{\omega \ell}\sin\frac{\pi}{N}\left\{\sin(\alpha+\frac{\pi}{N})\sin\omega t - \sin(\omega t+\frac{\pi}{N})\sin\omega t\right\}d\omega t\right.$$

$$+ \int_{\alpha+u}^{\alpha+2\pi/N} I_d\sin\omega t \, d\omega t$$

$$\left. + \int_{\alpha+\frac{2\pi}{N}}^{\alpha+\frac{2\pi}{N}+u} I_d\sin\omega t - \frac{\hat{e}}{\omega \ell}\sin\frac{\pi}{N}\left\{\sin(\alpha+\frac{\pi}{N})\sin\omega t - \sin(\omega t-\frac{\pi}{N})\sin\omega t\right\}d\omega t\right]$$

$$= \frac{1}{\pi}\left[\frac{\hat{e}}{\omega \ell}\sin\frac{\pi}{N}\left\{-\sin(\alpha+\frac{\pi}{N})\cos\omega t+\frac{1}{4}\sin(2\omega t+\frac{\pi}{N})-\frac{1}{2}\cos\frac{\pi}{N}.\omega t\right\}_{\alpha}^{\alpha+u}\right.$$

$$- I_d\cos\omega t \Big|_{\alpha+u}^{\alpha+\frac{2\pi}{N}} - I_d\cos\omega t\Big|_{\alpha+\frac{2\pi}{N}}^{\alpha+\frac{2\pi}{N}+u}$$

$$\left. - \frac{\hat{e}}{\omega \ell}\sin\frac{\pi}{N}\left\{-\sin(\alpha+\frac{\pi}{N})\cos\omega t+\frac{1}{4}\sin(2\omega t-\frac{\pi}{N})-\frac{1}{2}\cos\frac{\pi}{N}.\omega t\right\}_{\alpha+\frac{2\pi}{N}}^{\alpha+\frac{2\pi}{N}+u}\right]$$

$$= \frac{1}{\pi}\left[\frac{\hat{e}}{\omega \ell}\sin\frac{\pi}{N}\left\{-2\sin(\alpha+\frac{\pi}{N})\sin\frac{u}{2}\sin(\alpha+\frac{u}{2}) - 2\sin(\alpha+\frac{\pi}{N})\sin\frac{u}{2}\sin(\alpha+\frac{u}{2}+\frac{2\pi}{N})\right.\right.$$

$$\left. + \frac{1}{2}\sin u\cos(2\alpha+u+\frac{\pi}{N}) - \frac{1}{2}\sin u.\cos(2\alpha+u+\frac{3\pi}{N})\right\}$$

$$\left. + 2I_d\sin\frac{u}{2}\sin(\alpha+\frac{u}{2}+\frac{2\pi}{N}) + 2I_d\sin(\alpha+\frac{\pi}{N}+\frac{u}{2})\sin(\frac{\pi}{N}-\frac{u}{2})\right]$$

$$= \frac{2I_d}{\pi}\left[\frac{-2\sin(\alpha+\frac{\pi}{N})\sin\frac{u}{2}\cos(\alpha+\frac{u}{2}+\frac{\pi}{N})\sin\frac{\pi}{N}+\frac{1}{2}\sin u\sin(2\alpha+u+\frac{2\pi}{N})\sin\frac{\pi}{N}}{\sin(\alpha+\frac{\pi}{N})-\sin(\alpha+\frac{\pi}{N}+u)}\right.$$

$$\left. + \sin(\alpha+\frac{u}{2}+\frac{2\pi}{N})\sin\frac{u}{2} + \sin(\alpha+\frac{\pi}{N}+\frac{u}{2})\sin(\frac{\pi}{N}-\frac{u}{2})\right]$$

which can be simplified to

$$\frac{2I_d}{\pi}\sin\frac{\pi}{N}\sin(\alpha+\frac{\pi}{N}+\frac{u}{2})\cos\frac{u}{2}$$

B. On the r.m.s. value of the anode current.

Pertaining to page 13

$$I_a = \left[\frac{1}{2\pi}\int_{\alpha}^{\alpha+\frac{2\pi}{N}+u} i_1^2 \, d\omega t\right]^{\frac{1}{2}}$$

Substituting for i_1 from equations 3 and 4 ~~page~~

we find that

$$I_a = \frac{1}{\sqrt{2\pi}}\Bigg[\int_{\alpha}^{\alpha+u}\left(\frac{\hat{e}}{\omega L}\sin\frac{\pi}{N}\right)^2\left\{\sin\left(\alpha+\frac{\pi}{N}\right)-\sin\left(\omega t+\frac{\pi}{N}\right)\right\}^2 d\omega t$$

$$+\int_{\alpha+u}^{\alpha+\frac{2\pi}{N}} I_d^2 \, d\omega t$$

$$+\int_{\alpha+\frac{2\pi}{N}}^{\alpha+2\pi/N+u}\left\{I_d^2-\frac{\hat{e}}{\omega L}\sin\frac{\pi}{N}\sin\left(\alpha+\frac{\pi}{N}\right)+\frac{\hat{e}}{\omega L}\sin\frac{\pi}{N}\sin\left(\omega t-\frac{\pi}{N}\right)\right\}^2 d\omega t\Bigg]^{\frac{1}{2}}$$

$$= \frac{1}{\sqrt{2\pi}}\Bigg[\left(\frac{\hat{e}}{\omega L}\sin\frac{\pi}{N}\right)^2\left\{\sin^2\left(\alpha+\frac{\pi}{N}\right)\omega t+2\sin\left(\alpha+\frac{\pi}{N}\right)\cos\left(\omega t+\frac{\pi}{N}\right)+\frac{1}{2}-\frac{1}{4}\sin\left(2\omega t+\frac{2\pi}{N}\right)\right\}_{0}^{\alpha+u}$$

$$+ I_d^2\,\omega t\Big|_{\alpha+u}^{\alpha+\frac{2\pi}{N}} + I_d^2\,\omega t\Big|_{\alpha+\frac{2\pi}{N}}^{\alpha+\frac{2\pi}{N}+u} + \left(\frac{\hat{e}}{\omega L}\sin\frac{\pi}{N}\right)^2\Big\{\sin^2\left(\alpha+\frac{\pi}{N}\right).\,\omega t \cdots\cdots$$

$$\cdots\cdots 2\sin\left(\alpha+\frac{\pi}{N}\right)\cos\left(\omega t-\frac{\pi}{N}\right)+\frac{1}{2}\omega t-\frac{1}{4}\sin\left(2\omega t-\frac{2\pi}{N}\right)\Big\}_{\alpha+\frac{2\pi}{N}}^{\alpha+\frac{2\pi}{N}+u}$$

$$-2I_d\frac{\hat{e}}{\omega L}\sin\frac{\pi}{N}\left\{\sin\left(\alpha+\frac{\pi}{N}\right)\omega t+\cos\left(\omega t-\frac{\pi}{N}\right)\right\}_{\alpha+\frac{2\pi}{N}}^{\alpha+\frac{2\pi}{N}+u}\Bigg]^{\frac{1}{2}}$$

$$= \frac{1}{\sqrt{2\pi}}\Bigg[\left(\frac{\hat{e}}{\omega L}\sin\frac{\pi}{N}\right)^2\Big\{\sin^2\left(\alpha+\frac{\pi}{N}\right)u+\frac{u}{2}-4\sin\left(\alpha+\frac{\pi}{N}\right)\sin\left(\alpha+\frac{u}{2}+\frac{\pi}{N}\right)\sin\frac{u}{2}-\cdots$$

$$\cdots\frac{1}{2}\cos\left(2\alpha+u+\frac{2\pi}{N}\right)\sin u\Big\}$$

$$+I_d^2\left(\frac{2\pi}{N}-u\right)+I_d^2 u+\left(\frac{\hat{e}}{\omega L}\sin\frac{\pi}{N}\right)^2\Big\{\sin^2\left(\alpha+\frac{\pi}{N}\right)u+\frac{u}{2}\cdots\cdots$$

$$\cdots\cdots-4\sin\left(\alpha+\frac{\pi}{N}\right)\sin\left(\alpha+\frac{\pi}{N}+\frac{u}{2}\right)\sin\frac{u}{2}-\frac{1}{2}\cos\left(2\alpha+\frac{2\pi}{N}+u\right)\sin u\Big\}$$

$$-2I_d\frac{\hat{e}}{\omega L}\sin\frac{\pi}{N}\left\{\sin\left(\alpha+\frac{\pi}{N}\right)u-2\sin\left(\alpha+\frac{\pi}{N}+\frac{u}{2}\right)\sin\frac{u}{2}\right\}\Bigg]^{\frac{1}{2}}$$

Substituting for $\frac{\hat{e}}{\omega l}\sin\frac{\pi}{N}$ from equation 30 ~~page~~ and rearranging the terms the above expression becomes equal to

$$\frac{I_d}{\sqrt{N}}\left[1-\frac{N}{\pi}\left\{\frac{-\sin(\alpha+\frac{\pi}{N})u-2\sin(\alpha+\frac{\pi}{N}+\frac{u}{2})\sin\frac{u}{2}}{\sin(u+\alpha+\frac{\pi}{N})-\sin(\alpha+\frac{\pi}{N})}-\frac{\sin^2(\alpha+\frac{\pi}{N})u+\frac{u}{2}-4\sin(\alpha+\frac{\pi}{N})\sin(\alpha+\frac{\pi}{N}+\frac{u}{2})-\frac{1}{2}\cos(2\alpha+\frac{2\pi}{N}+u)\sin u}{\left|\sin(u+\alpha+\frac{\pi}{N})-\sin(\alpha+\frac{\pi}{N})\right|^2}\right\}\right]^{\frac{1}{2}}$$

C. On the Fourier analysis of the interphase transformer voltage.

Pertaining to page 48

$$A_n = \frac{N}{\pi}\int_0^{\frac{2\pi}{N}} v \cos n\omega t \;\; d\omega t$$

Between $\omega t = 0$ and $\omega t = \frac{2\pi}{N}$

$$\begin{aligned} v &= e_1 - e_N \\ &= 2\hat{e}\sin\frac{\pi}{N}\cos\left(\omega t + \alpha + \frac{\pi}{N}\right) \end{aligned}$$

hence

$$\begin{aligned} A_n &= -\frac{N}{\pi}\int_0^{\frac{2\pi}{N}} 2\hat{e}\sin\frac{\pi}{N}\cos\left(\omega t+\alpha+\frac{\pi}{N}\right)\cos n\omega t \;\; d\omega t \\ &= -\frac{N}{\pi}\hat{e}\sin\frac{\pi}{N}\int_0^{\frac{2\pi}{N}}\cos\left\{(n+1)\omega t+\alpha+\frac{\pi}{N}\right\}+\cos\left\{(n-1)\omega t-\alpha-\frac{\pi}{N}\right\} d\omega t \\ &= -\frac{2N}{\pi}\hat{e}\sin\frac{\pi}{N}\left[\frac{1}{n+1}\cos\left\{(n+1)\frac{\pi}{N}+\alpha+\frac{\pi}{N}\right\}\sin(n+1)\frac{\pi}{N}\right. \\ &\qquad\qquad \left. + \frac{1}{n-1}\sin(n-1)\frac{\pi}{N}\cos\left\{(n-1)\frac{\pi}{N}-\alpha-\frac{\pi}{N}\right\}\right] \end{aligned}$$

n is restricted to odd multiples of $\frac{1}{2}N$

hence

$$\begin{aligned} A_n &= -\frac{2N}{\pi}\hat{e}\sin\frac{\pi}{N}\cos\frac{\pi}{N}\sin\left(\alpha+\frac{2\pi}{N}\right)\left\{\frac{1}{n-1}-\frac{1}{n+1}\right\} \\ &= \frac{-2N\hat{e}}{\pi(n-1)(n+1)}\sin\frac{2\pi}{N}\sin\left(\alpha+\frac{2\pi}{N}\right) \end{aligned}$$

Similarly

$$\begin{aligned} B_n &= \frac{N}{\pi}\int_0^{\frac{2\pi}{N}} v \sin n\omega t \;\; d\omega t \\ &= -\frac{N}{\pi}\int_0^{\frac{2\pi}{N}} 2\hat{e}\sin\frac{\pi}{N}\cos\left(\omega t+\alpha+\frac{\pi}{N}\right)\sin n\omega t \;\; d\omega t \\ &= \frac{N}{\pi}\hat{e}\sin\frac{\pi}{N}\int_0^{\frac{2\pi}{N}}\sin\left\{(n+1)\omega t+\alpha+\frac{\pi}{N}\right\}+\sin\left\{(n-1)\omega t-\alpha-\frac{\pi}{N}\right\} d\omega t \\ &= \frac{2N}{\pi}\hat{e}\sin\frac{\pi}{N}\left[\frac{1}{n+1}\sin\left\{(n+1)\omega t+\alpha+\frac{\pi}{N}\right\}\sin(n+1)\frac{\pi}{N}\ldots\ldots\right. \\ &\qquad\qquad + \frac{1}{n-1}\sin\left\{(n-1)\frac{\pi}{N}-\alpha-\frac{\pi}{N}\right\}\sin(n-1)\frac{\pi}{N} \end{aligned}$$

as before n is restricted to odd multiples of $\frac{1}{2}N$

hence

$$B_n = -\frac{2N\hat{e}}{\pi}\sin\frac{\pi}{N}\cos\frac{\pi}{N}\cos\left(\alpha+\frac{2\pi}{N}\right)\left[\frac{1}{n+1}+\frac{1}{n-1}\right]$$

$$= \frac{2Nn\hat{e}}{\pi(n+1)(n-1)}\sin\frac{2\pi}{N}\cos\left(\alpha+\frac{2\pi}{N}\right).$$

BIBLIOGRAPHY

Convertor Technology.

(1) W. Dallenbach and E. Gerecke:
"The current and voltage relations of the mercury-arc rectifier"
Archiv fur Elektrotechnik, 1925, vol. 14, p 171.

(2) D.C. Prince and F.B. Vogdes:
"Principles of mercury-arc rectifiers and their circuits"
McGraw-Hill, 1927.

(3) K. Muller-Lubeck:
"Der quicksilberdamf gleichrichter"
Julius Springer, 1929.

(4) O.K. Marti and W. Winograd:
"Mercury-arc power rectifiers"
McGraw-Hill, 1930.

(5) H. Rissik:
"Mercury-arc current convertors"
Sir Isaac Pitman & Sons, 1935.

(6) A. Glaser - K. Muller-Lubeck:
"Theorie der stromrichter"
Julius Springer, 1935.

(7) W. Schilling:
"Die gleichrichterschaltungen"
R. Oldenbourg, 1938.

Pertaining to power factor.

(8) L.P. Krijger:
"The measurement of wattless power in the case of mercury-arc rectifiers"
Elektrotechnische Zeitschrift, 1925, vol. 46, p 48.

(9) M. Schenkel:
"The wattless power consumption of rectifier installations and its measurement"
Elektrotechnische Zeitschrift, 1925, vol. 46, p 1369 and 1399.

(10) H. Rissik:
"The influence of mercury-arc rectifiers upon the power factor of the supply system"
I.E.E. journal, 1933, vol. 72, p 435.

(11) A.E. Knowlton:
"Reactive power concepts in need of classification"
American I.E.E. journal, 1933, vol. 52, p 259.

(12) J.A. Johnson:
"Operating aspects of reactive power"
American I.E.E. journal, 1933, vol. 52, p 262.

(13) V.G. Smith:
"Reactive and fictitious power"
American I.E.E. journal, 1933, vol. 52, p 268.

(14) C. Dannat:
"The metering of mercury-arc rectifier supplies"
I.E.E. journal, 1937, vol. 81, p 256.

(15) R. Feinberg:
–

Elektrotechnik und Machinenbau, 1937, vol. 35,
p 137.

(16) E.V. Clark:
Discussion on "The metering of mercury-arc rectifier supplies"
I.E.E. journal, 1938, vol. 82, p 324.

Invertor Short-Circuit Conditions.

(17) H. Keller:
"The load diagram of the d.c. - a.c. mutator"
The Brown-Boveri Review, Dec. 1934, p 228.

Interphase Transformer Design.

(18) H. Jungmichl:
"The phase-equalizer in heavy duty rectifier installations"
Wissenschaftliche Veroffentlichungen aus dem Siemens-Konzern, 1928, vol. 6, p 34.

(19) –
"The interphase reactor in six-phase transformer rectifier circuits"
Johnson & Phillips transformer book, 1937.

OSCILLOGRAMS and PHOTOGRAPHS

Fig. 1. The grid-controlled mercury-arc convertor on which the experimental work was carried out.

A full description of the plant is given on page 60.

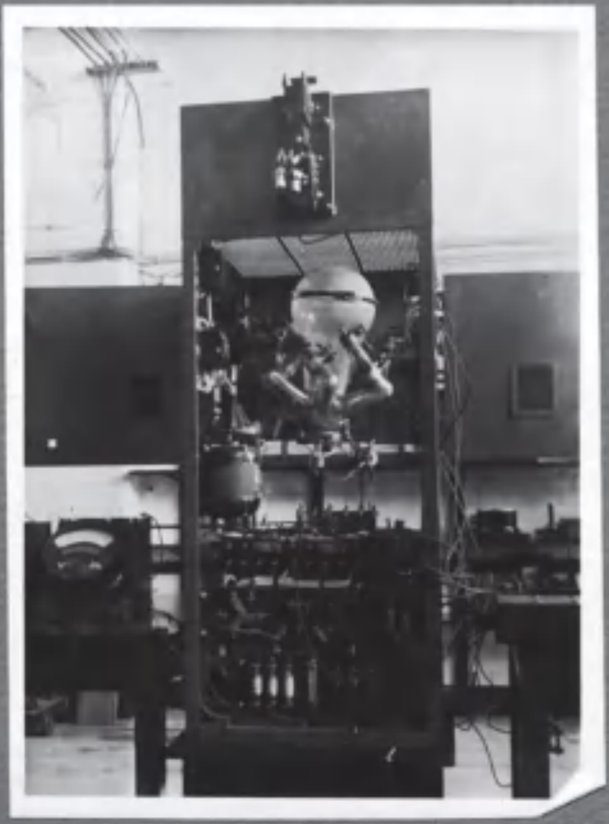

FIG. 1

A. The stroboscope used for measuring the overlap angle.

B. The Tinsley co-ordinate a.c. potentiometer.

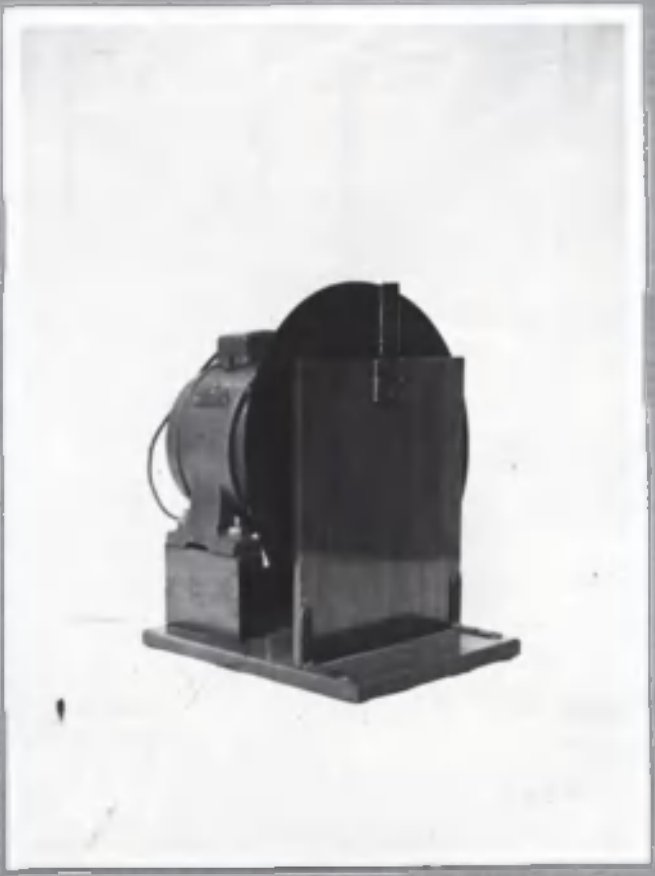

A

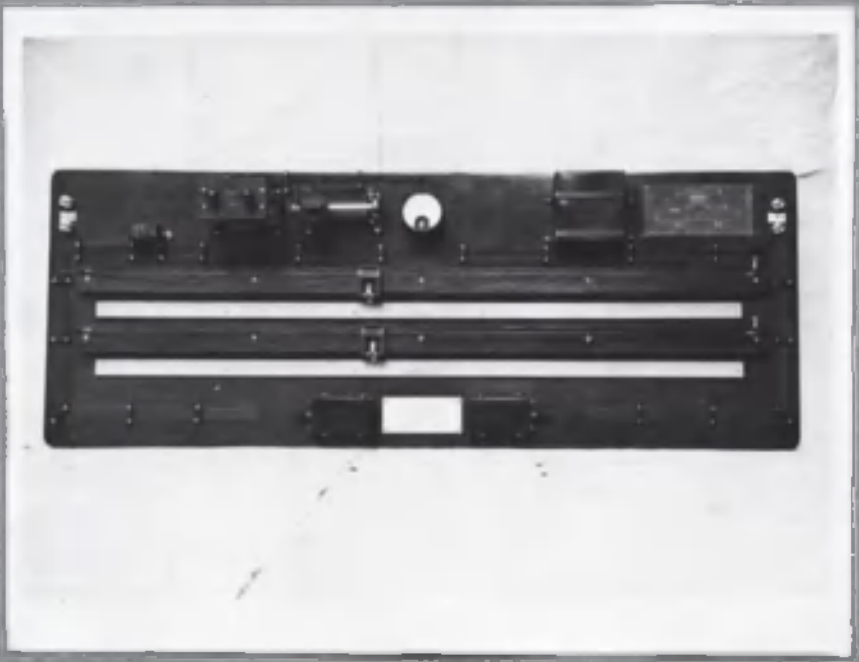

B

FIG. 2

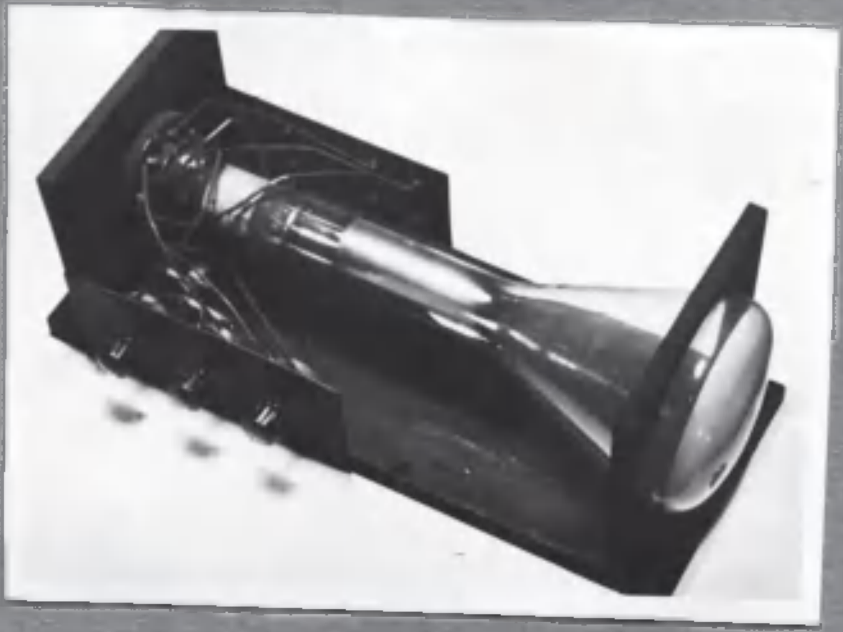

A

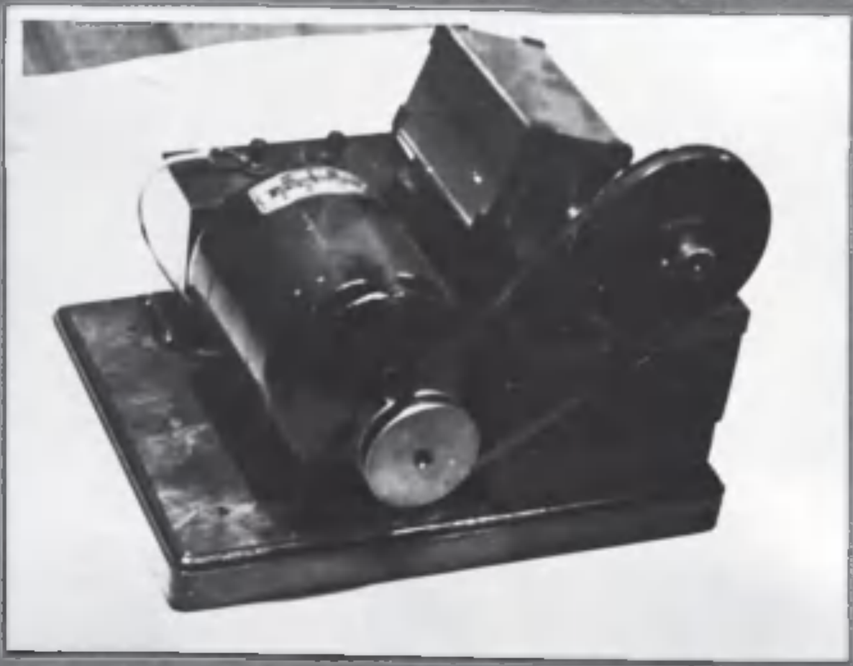

B

FIG. 3

A. The 3,000-V cathode-ray tube with focussing controls.

B. The synchronously rotating mirrors used as a time base.

Oscillogram of the voltage across the interphase transformer with the main transformer connected as in Fig. 50, $I_d = 5A$.

A. $\alpha = 30°$ B. $\alpha = 60°$

C. $\alpha = 90°$ D. $\alpha = 120°$

E. $\alpha = 150°$ F. $\alpha = 180°$

NOTE: Time is measured from left to right.

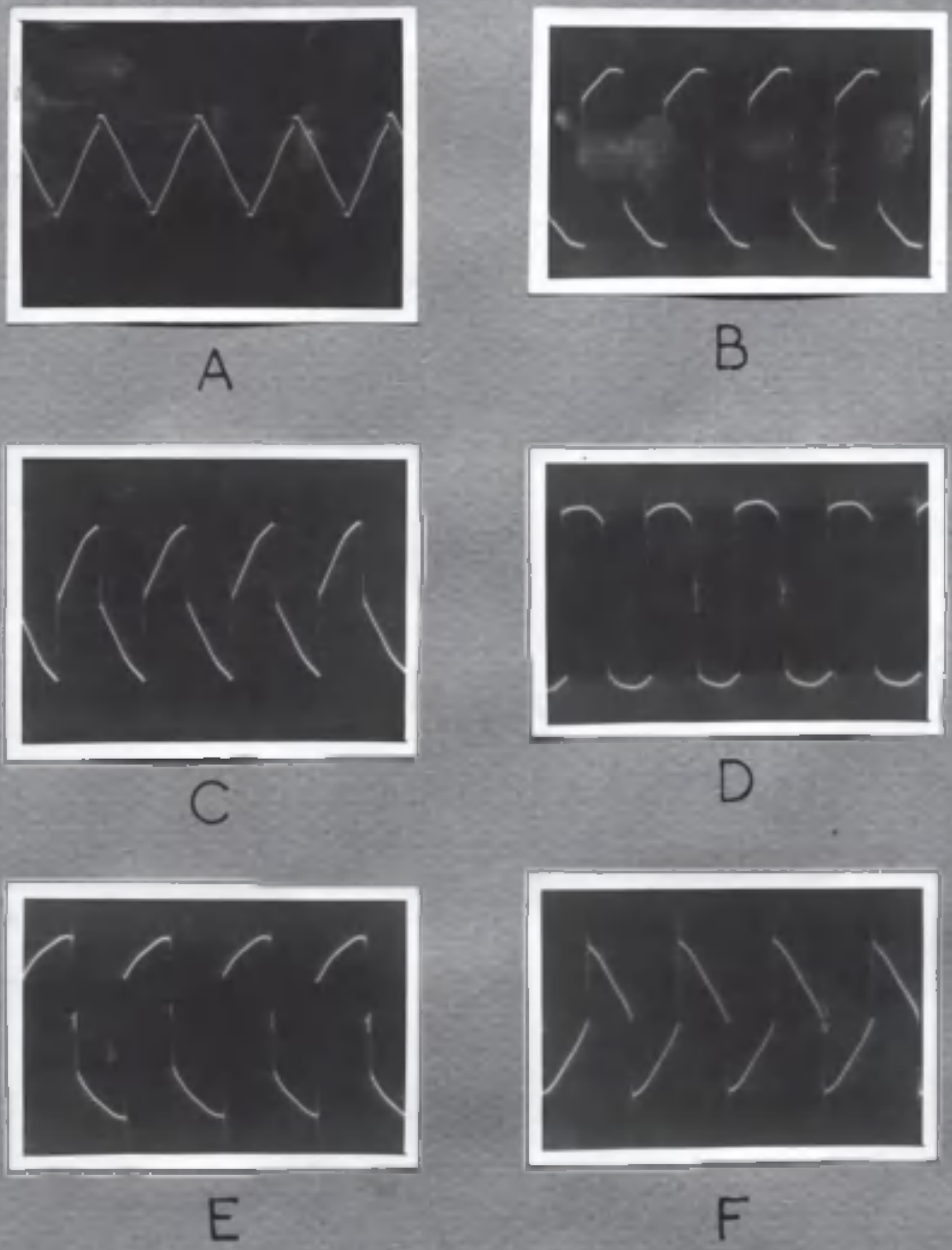

FIG. 4

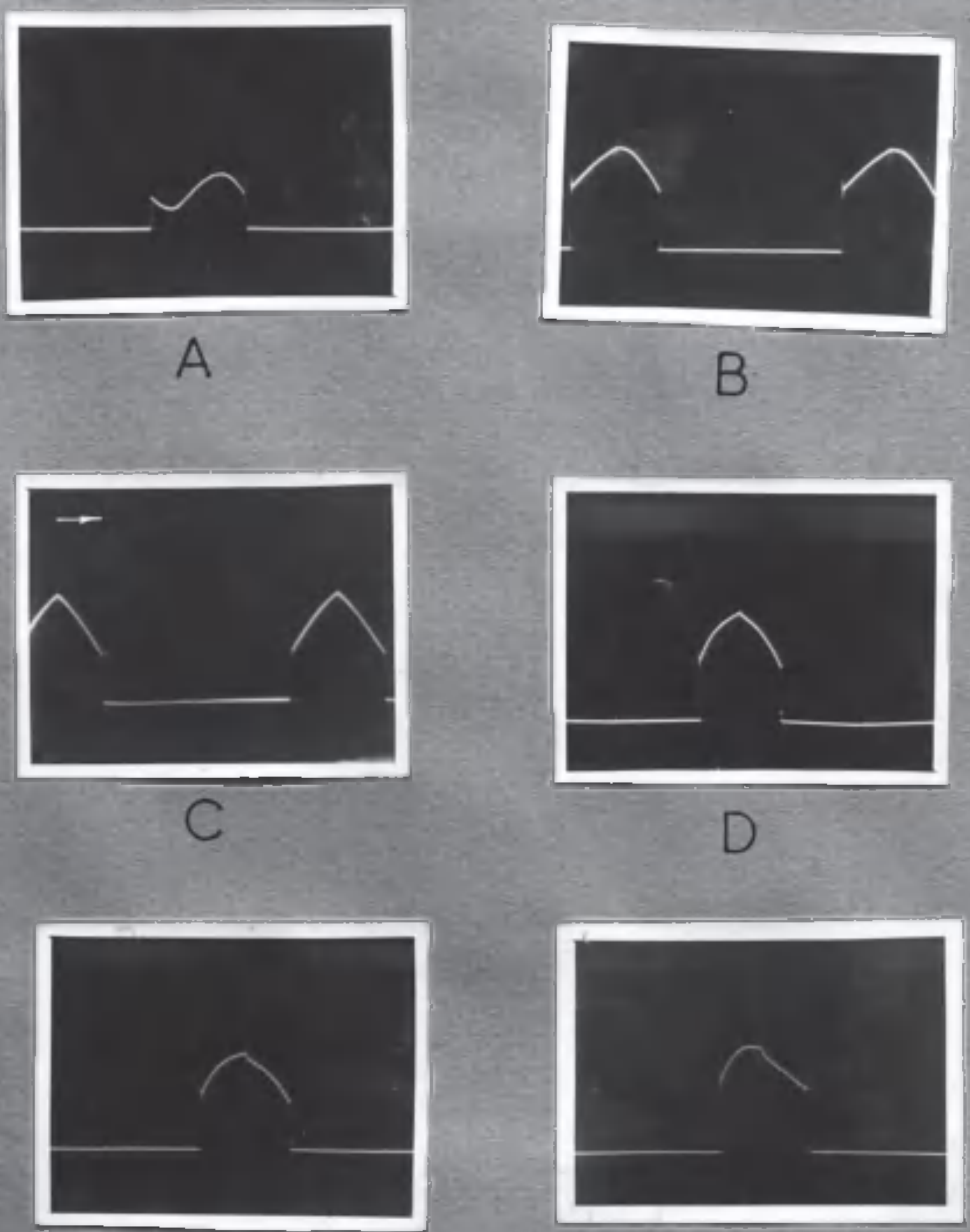

A B C D E F

FIG. 5

Oscillograms of the anode currents with the transformer connections as in Fig. 50, $I_d = 5A$

A. $\alpha = 30°$

B. $\alpha = 60°$

C. $\alpha = 90°$

D. $\alpha = 120°$

E. $\alpha = 150°$

F. $\alpha = 180°$

NOTE: Time is measured from left to right.

MISCELLANEOUS OSCILLOGRAMS

A. The voltage of the a.c. mains supplying the convertor.

B. The a.c. line current with transformer connected as in Fig. 10. $\alpha = 210^\circ$, $I_d = 15A$.

C. The neutral current under the same conditions as (B).

D. The a.c. line current with transformer connected 3-wire star/double star with interphase transformer $\alpha = 180$, $I_d = 5A$.

E. The a.c. line current with transformer connected 3-wire star/6-phase star $\alpha = 180^\circ$ and $I_d = 10A$

F. As in (E) with $\alpha = 30^\circ$

G. As in (E) with $\alpha = 180^\circ$ and $I_d = 20A$

H. The anode current with the transformer connected 3-wire star/6-phase star $\alpha = 180^\circ$, $I_d = 20A$

I. As in (H) with $I_d = 10A$

J. The anode current with the transformer connected as in Fig. 10 $\alpha = 210$ and $I_d = 15A$.

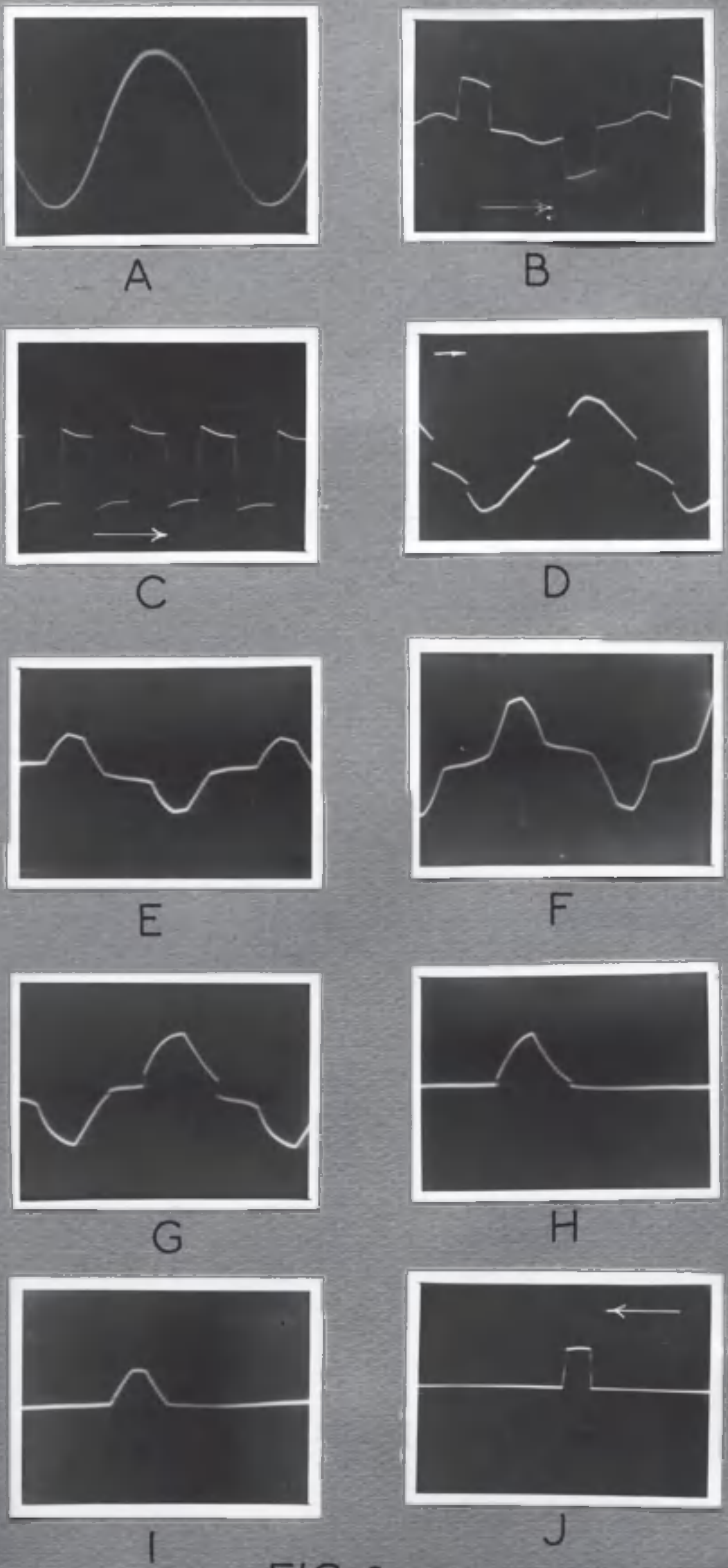

FIG. 6

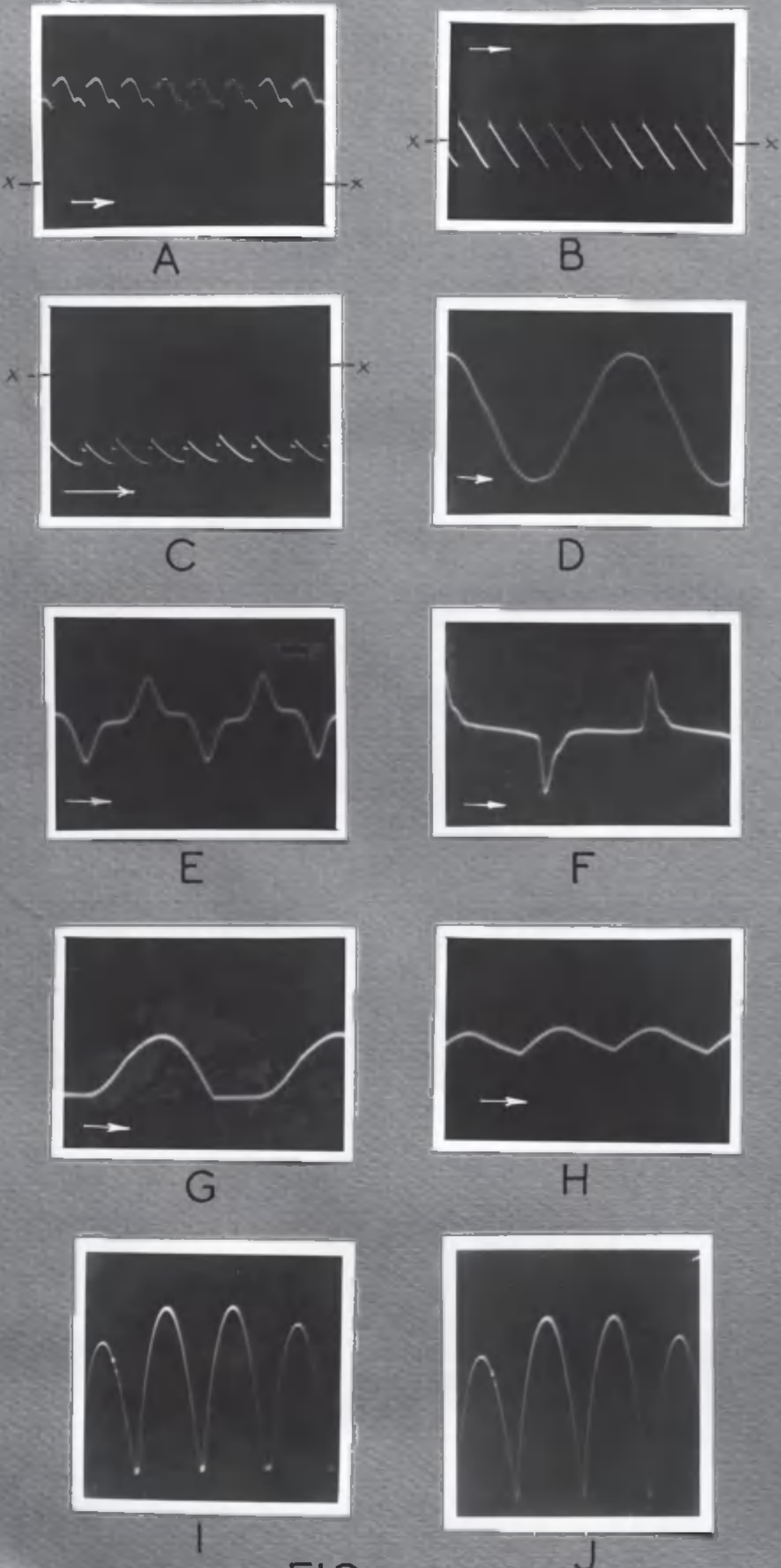

FIG. 7

MISCELLANEOUS OSCILLOGRAMS

A. The cathode-to-neutral voltages for $\alpha = 60^\circ$
xx indicates the zero line.

B. As (A) for $\alpha - 150^\circ$

C. As (A) for $\alpha = 210^\circ$

D. The current in the primary of the grid-control circuit "peaking" transformers.

E. The current in the primary of the Westinghouse metal rectifier transformer.

F. The voltage across the secondary of the "peaking" transformers.

G. The current in the excitation anode leads.

H. The current in the lead from the excitation circuit to the cathode.

I & J. Pertaining to the discussion on voltage regulation, page 19.

Photographs of the bulb on load taken through the stroboscope.

A. Commutation of the arc from the right-hand to the left-hand anode commences.

B. Commutation of the arc from the right-hand to the left-hand anode is nearly completed.

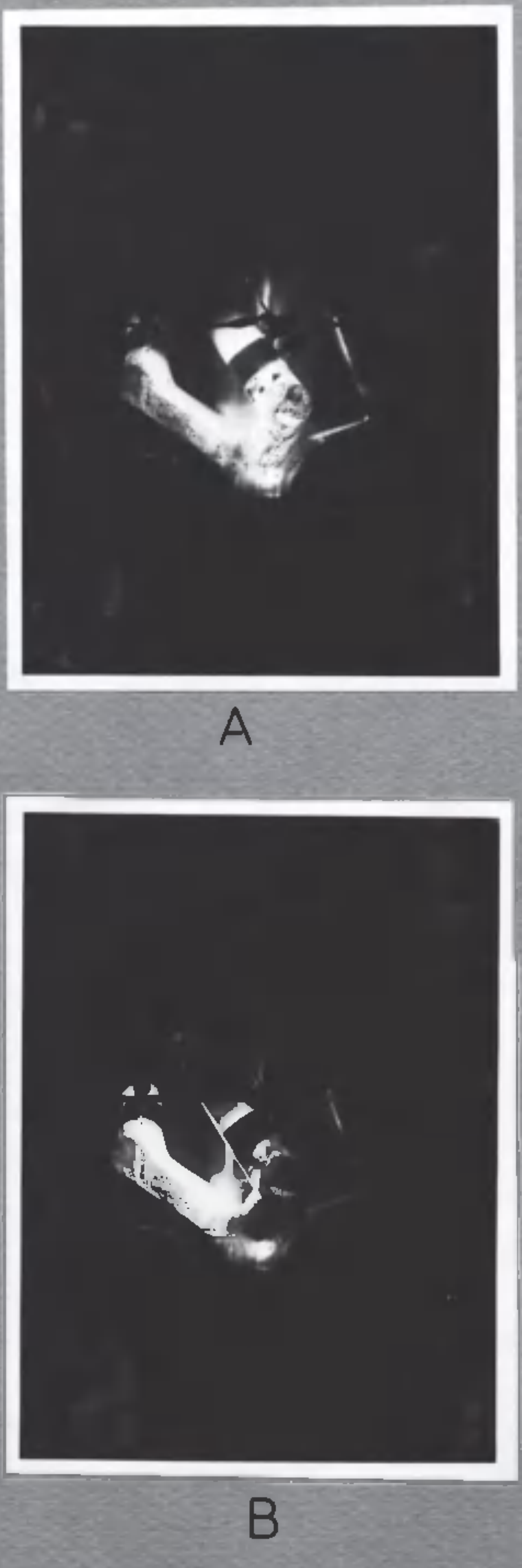

FIG. 8

CONNECTION DIAGRAMS AND GRAPHS.

Fig. 9. Motor-generator connections for loading convertor.

Fig. 10. Transformer connections.

Fig. 11. Wattmeter connections for measuring displacement factor.

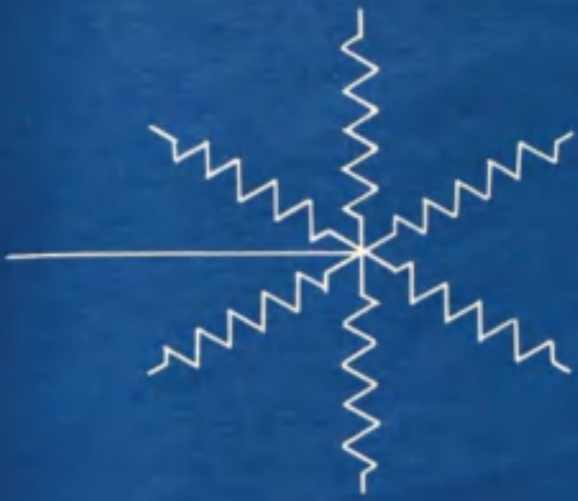

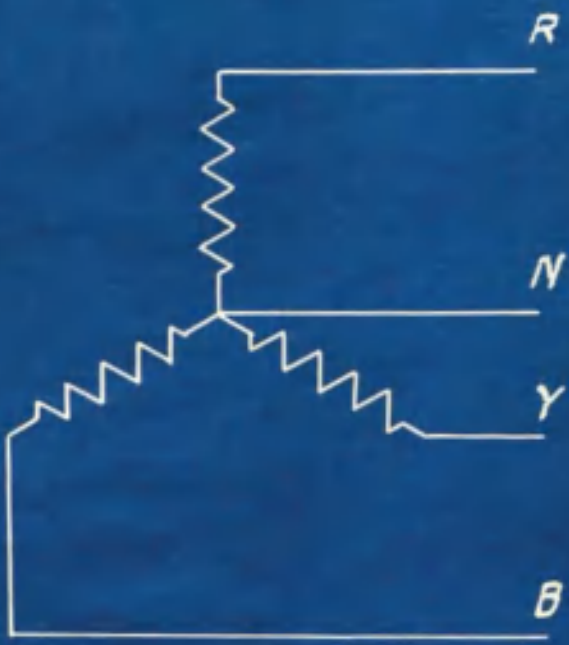
R
N
Y
B

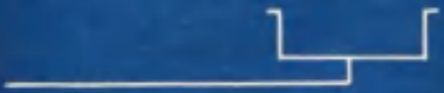

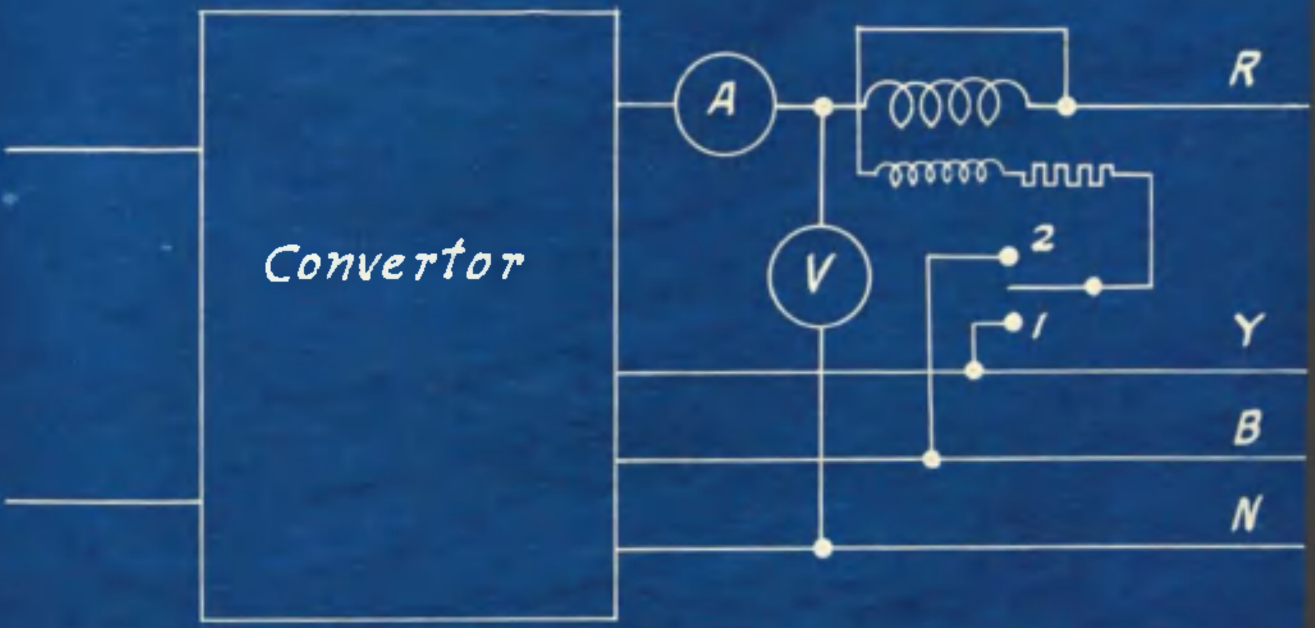
Convertor
A
V
2
1
R
Y
B
N

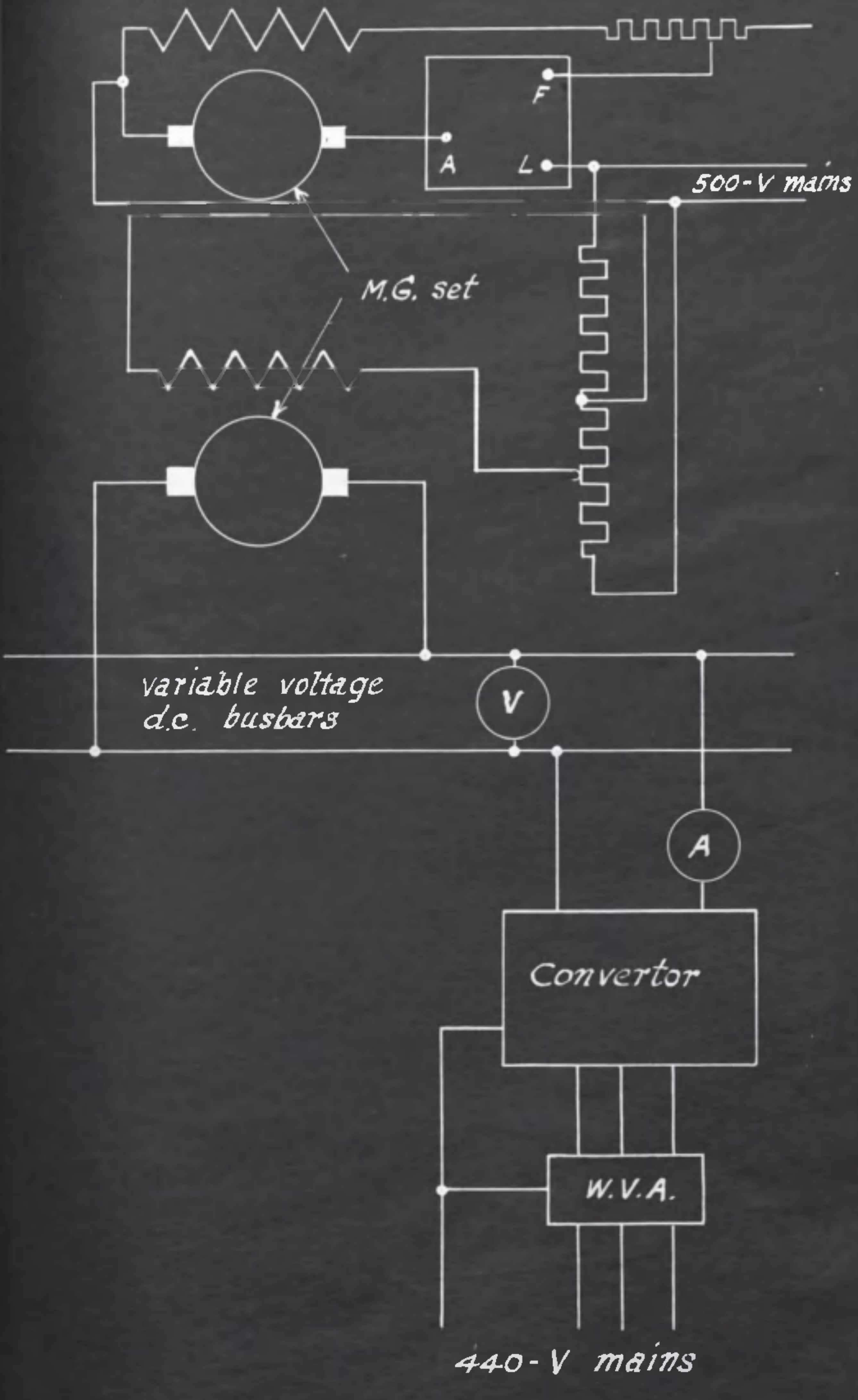
F
A
L
500-V mains
M.G. set
V
variable voltage
d.c. busbars
A
Convertor
W.V.A.
440-V mains

Fig. 12. Load test results: transformer connections as in Fig. 10: $\alpha = 60°$

The direct voltage curves obtained analytically and from the load test are coincident except at very small values of direct current.

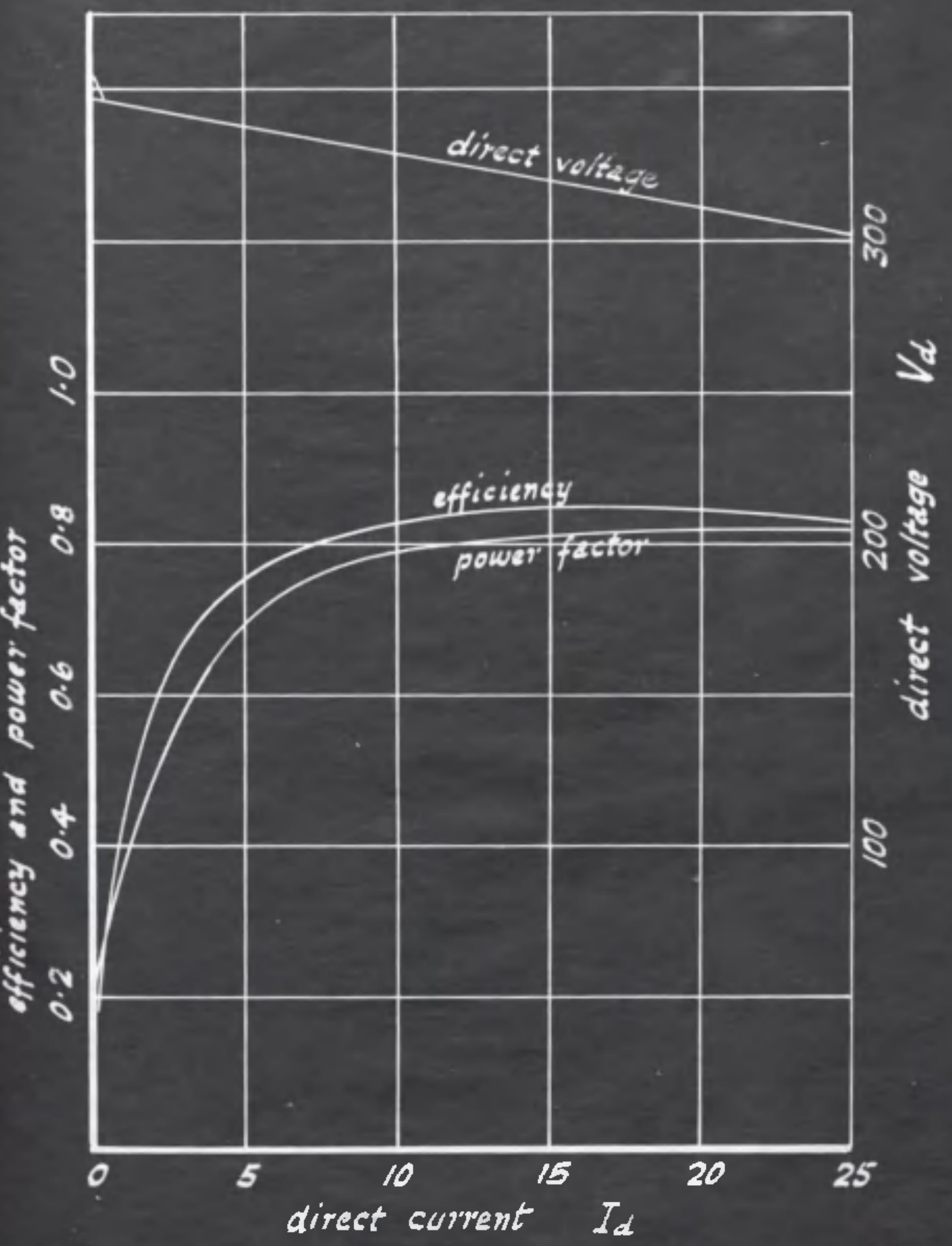
direct voltage
efficiency
power factor
efficiency and power factor
0·2
0·4
0·6
0·8
1·0
100
200
300
direct voltage Vd
0
5
10
15
20
25
direct current Id

Fig. 13. Load test results: transformer connections as in Fig. 10: $\alpha = 210^\circ$

The direct voltage curves obtained analytically and from the load test are coincident except at small values of direct current.

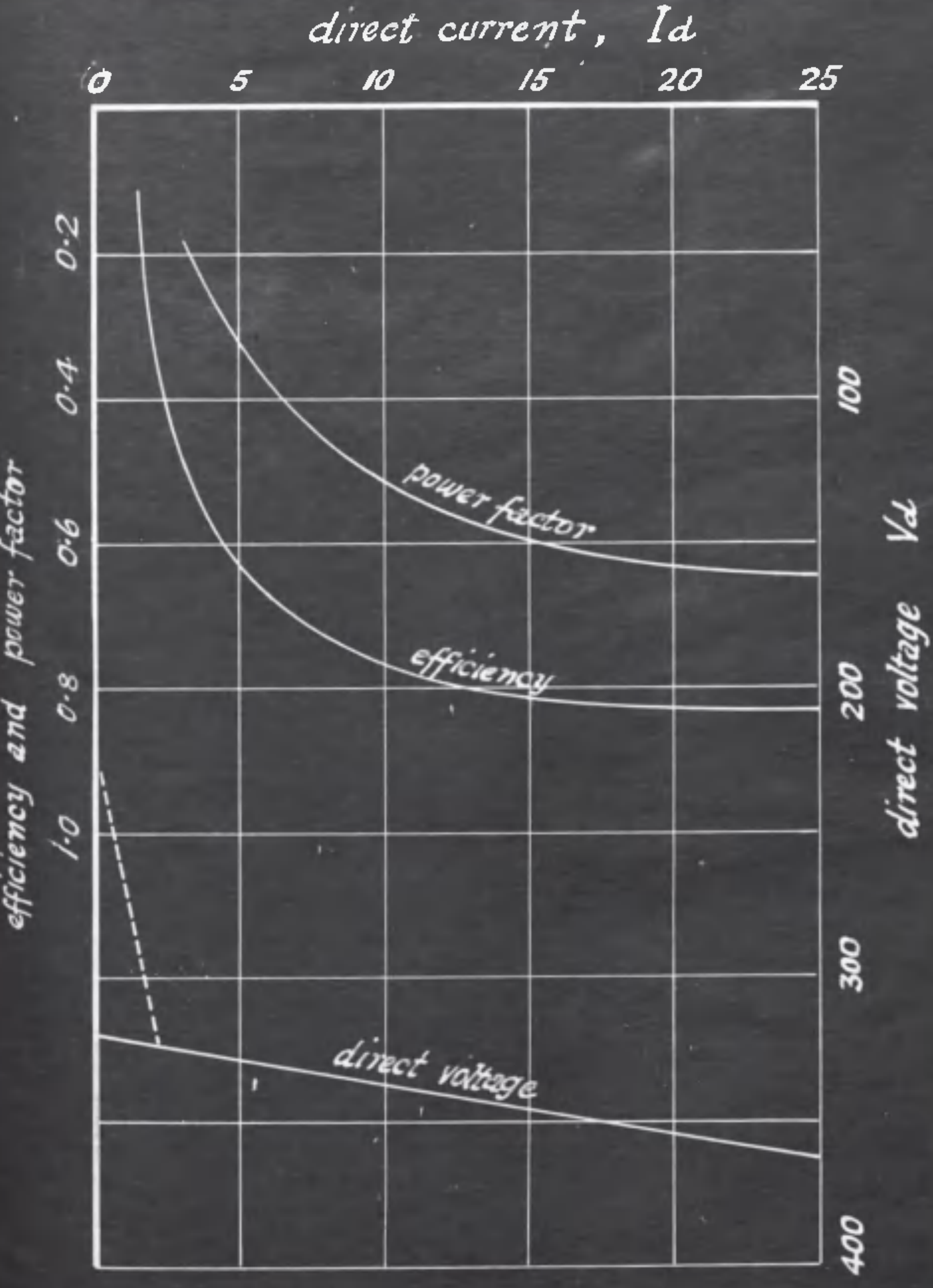
direct current, Id
0
5
10
15
20
25
efficiency and power factor
0·2
0·4
0·6
0·8
1·0
direct voltage Vd
100
200
300
400
power factor
efficiency
direct voltage

Fig. 14. Load test results: transformer connections as in Fig. 10: $I_d = 15A$

The direct voltage curves obtained analytically and from the load test are coincident.

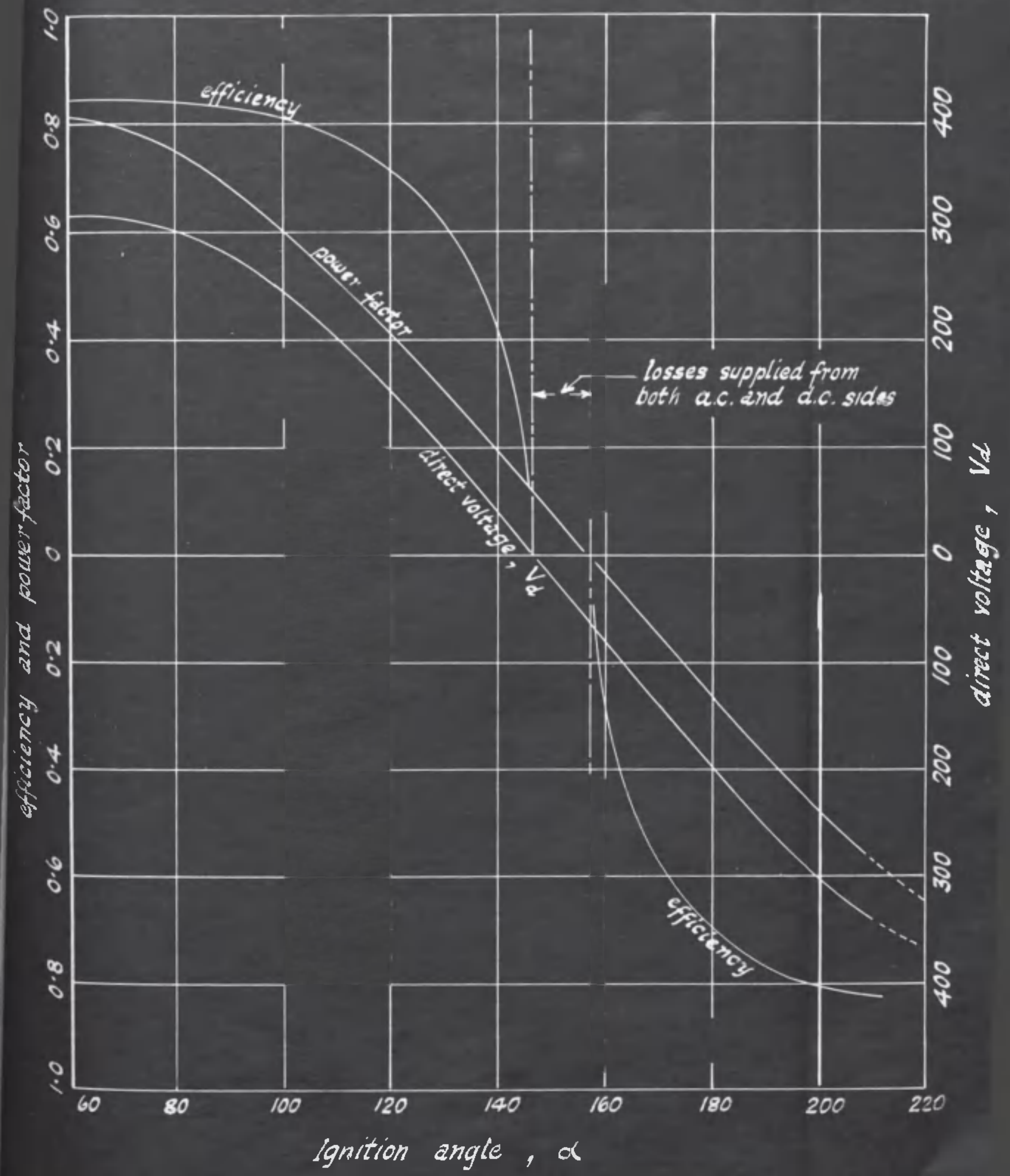
efficiency
power factor
direct voltage, Vd
losses supplied from both a.c. and d.c. sides
efficiency
efficiency and power factor
1.0
0.8
0.6
0.4
0.2
0
0.2
0.4
0.6
0.8
1.0
direct voltage, Vd
400
300
200
100
0
100
200
300
400
60
80
100
120
140
160
180
200
220
Ignition angle, α

Fig. 15. Separation of losses.

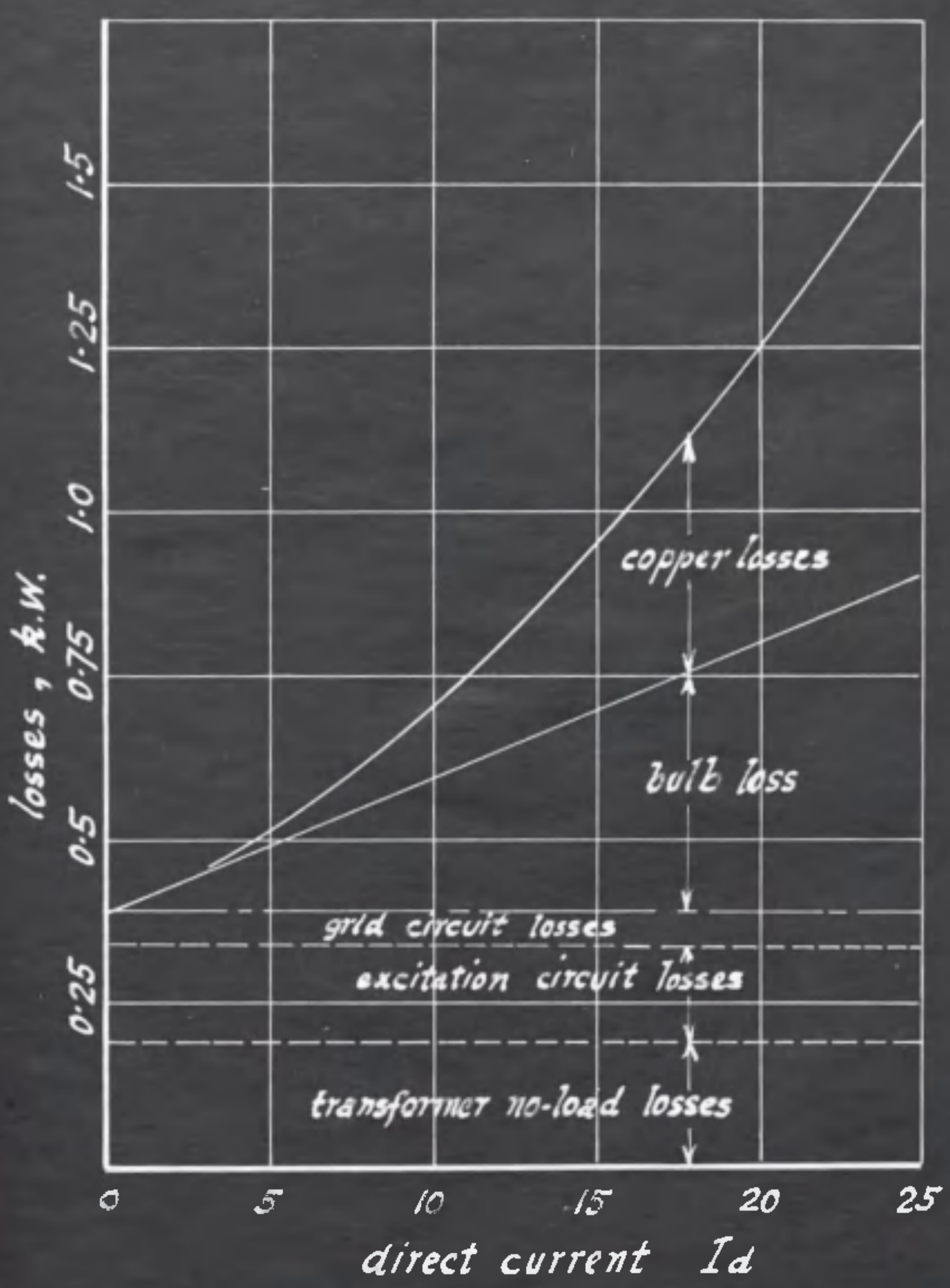
losses , k.W.
1·5
1·25
1·0
0·75
0·5
0·25
copper losses
bulb loss
grid circuit losses
excitation circuit losses
transformer no-load losses
0
5
10
15
20
25
direct current Id

Fig. 16. Efficiency curves. $I_\alpha = 15A$

By loss method ————

From load tests - - - - - -

$\alpha = 60$

$\alpha = 210°$

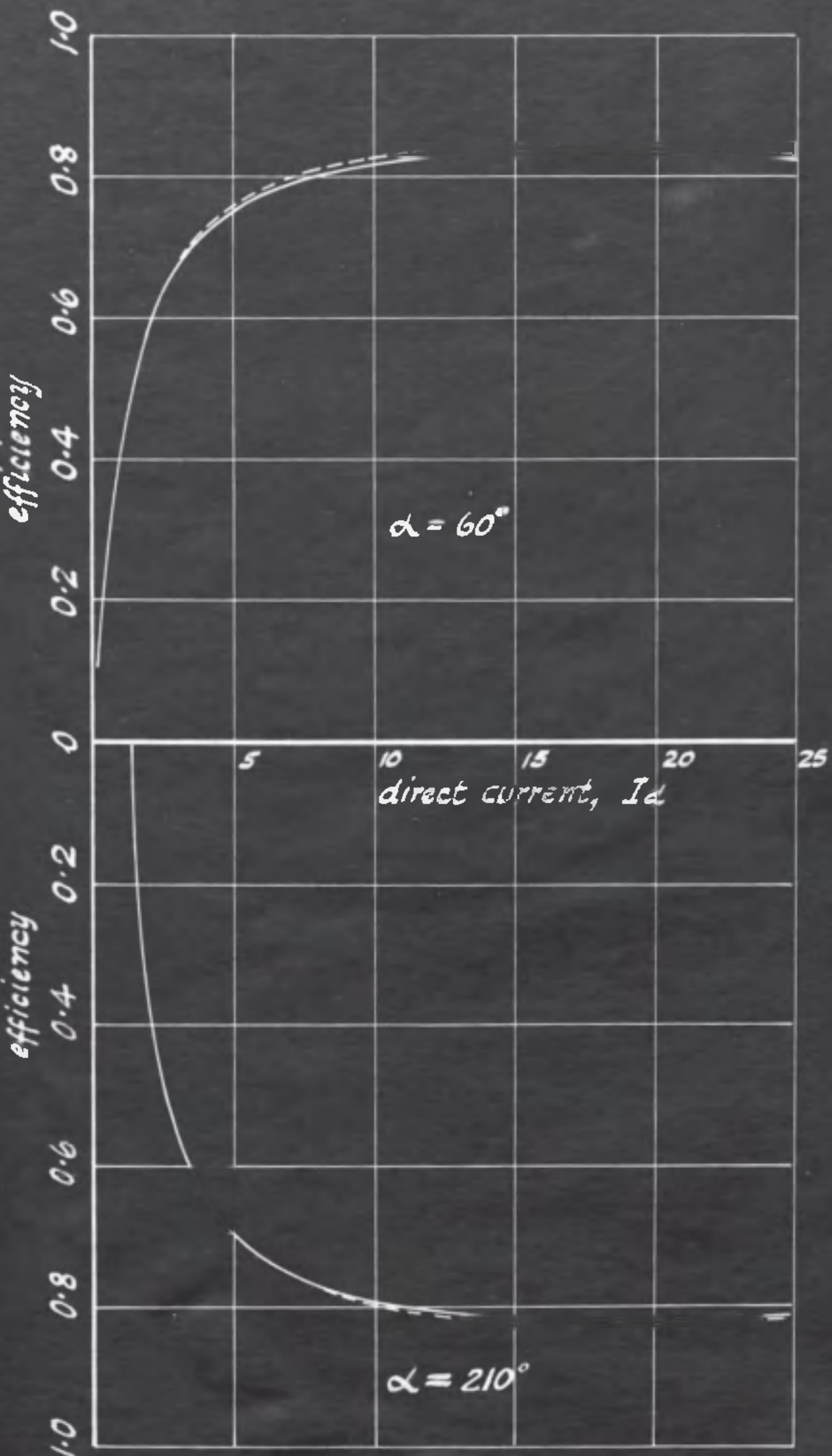
1·0
0·8
0·6
efficiency
0·4
0·2
0
α = 60°
5
10
15
20
25
direct current, Id
0·2
efficiency
0·4
0·6
0·8
α = 210°
1·0

Fig. 17. Pertaining to the calculation of displacement and distortion factors.

Fig. 18. Displacement, distortion and power factor curves drawn for $\alpha = 100^\circ$

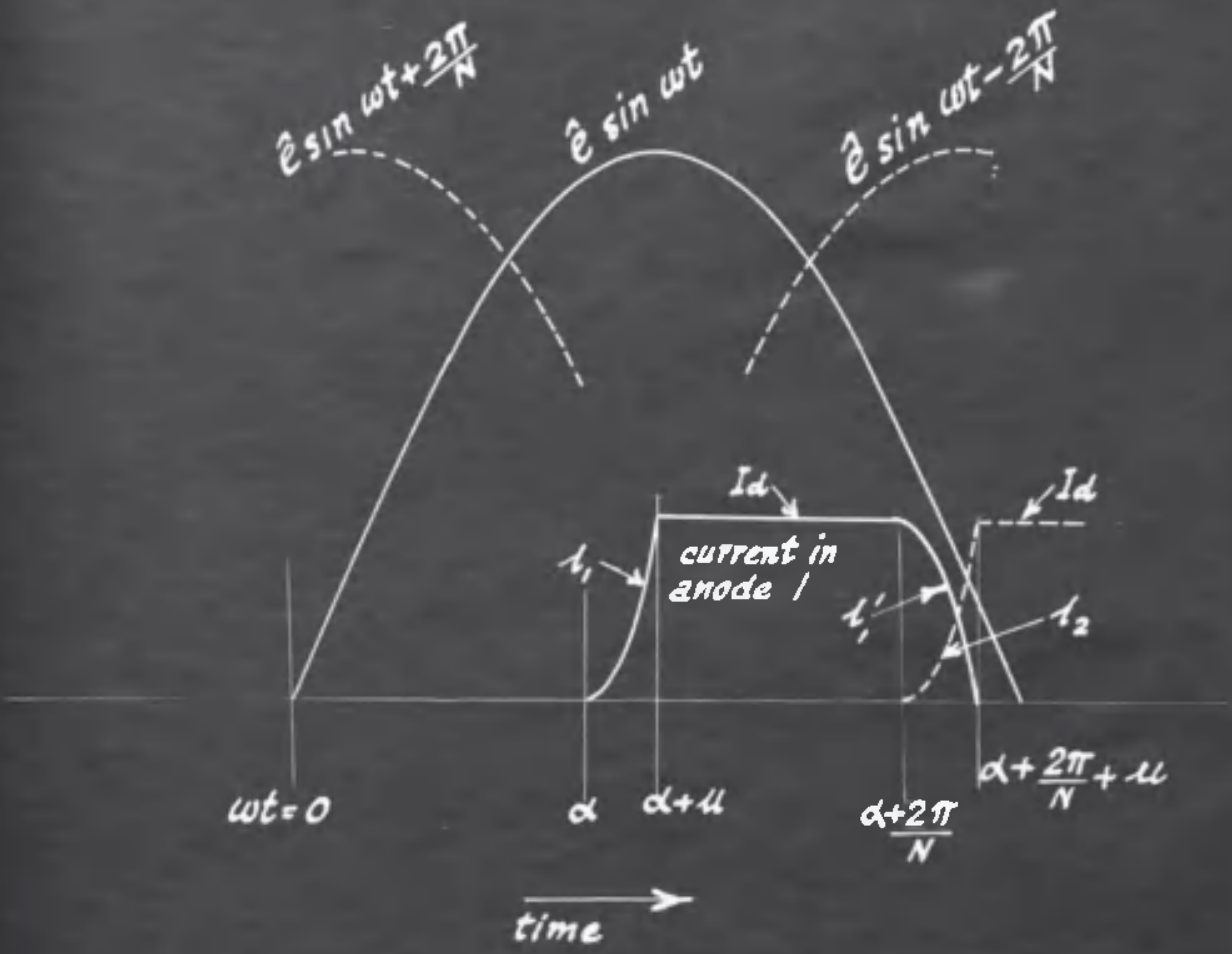
$\hat{e}\sin\left(\omega t+\frac{2\pi}{N}\right)$
$\hat{e}\sin\omega t$
$\hat{e}\sin\left(\omega t-\frac{2\pi}{N}\right)$
I_d
I_d
i_1
current in anode 1
i_1'
i_2
$\omega t=0$
α
$\alpha+u$
$\alpha+\frac{2\pi}{N}$
$\alpha+\frac{2\pi}{N}+u$
time

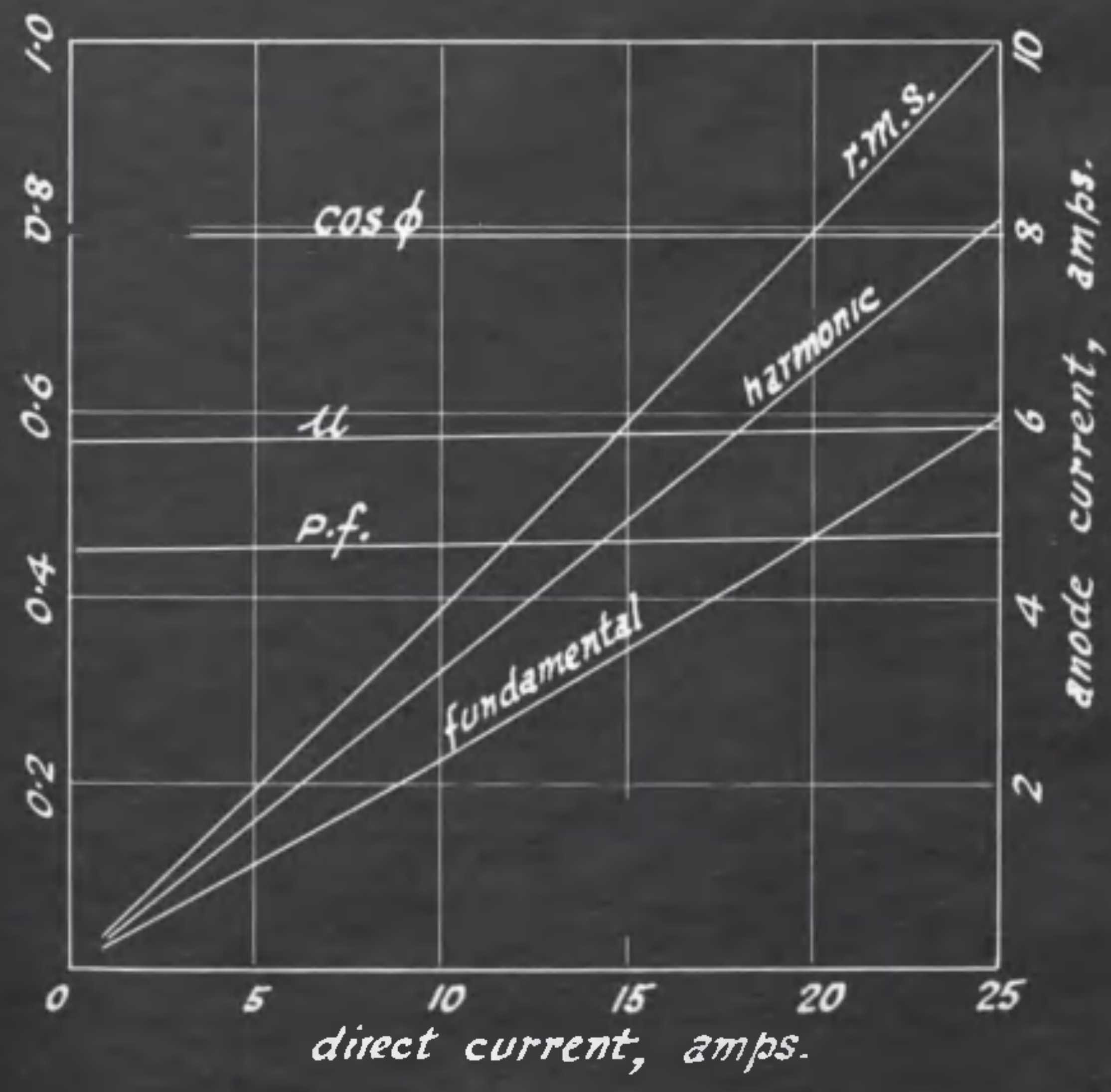
1·0
0·8
0·6
0·4
0·2
0
5
10
15
20
25
direct current, amps.
10
8
6
4
2
anode current, amps.
r.m.s.
harmonic
fundamental
cos φ
u
p.f.

Fig. 19. Pertaining to the calculation of displacement and distortion factors.

Fig. 20. Pertaining to the calculation of displacement and distortion factors.

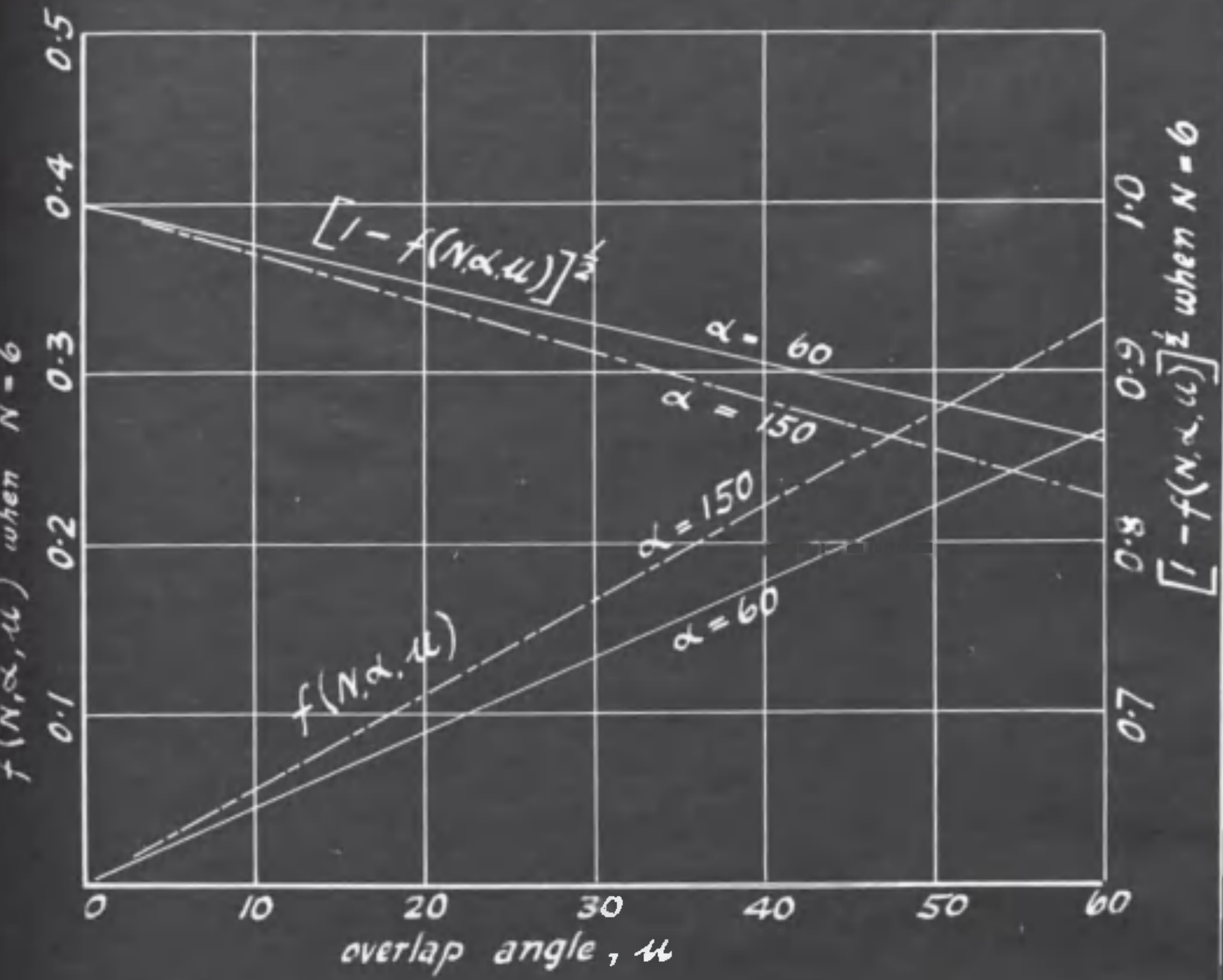

f(N, α, u) when N = 6
[1 − f(N, α, u)]^½ when N = 6
[1 − f(N, α, u)]^½
α = 60
α = 150
α = 150
α = 60
f(N, α, u)
0.1
0.2
0.3
0.4
0.5
0.7
0.8
0.9
1.0
0
10
20
30
40
50
60
overlap angle, u

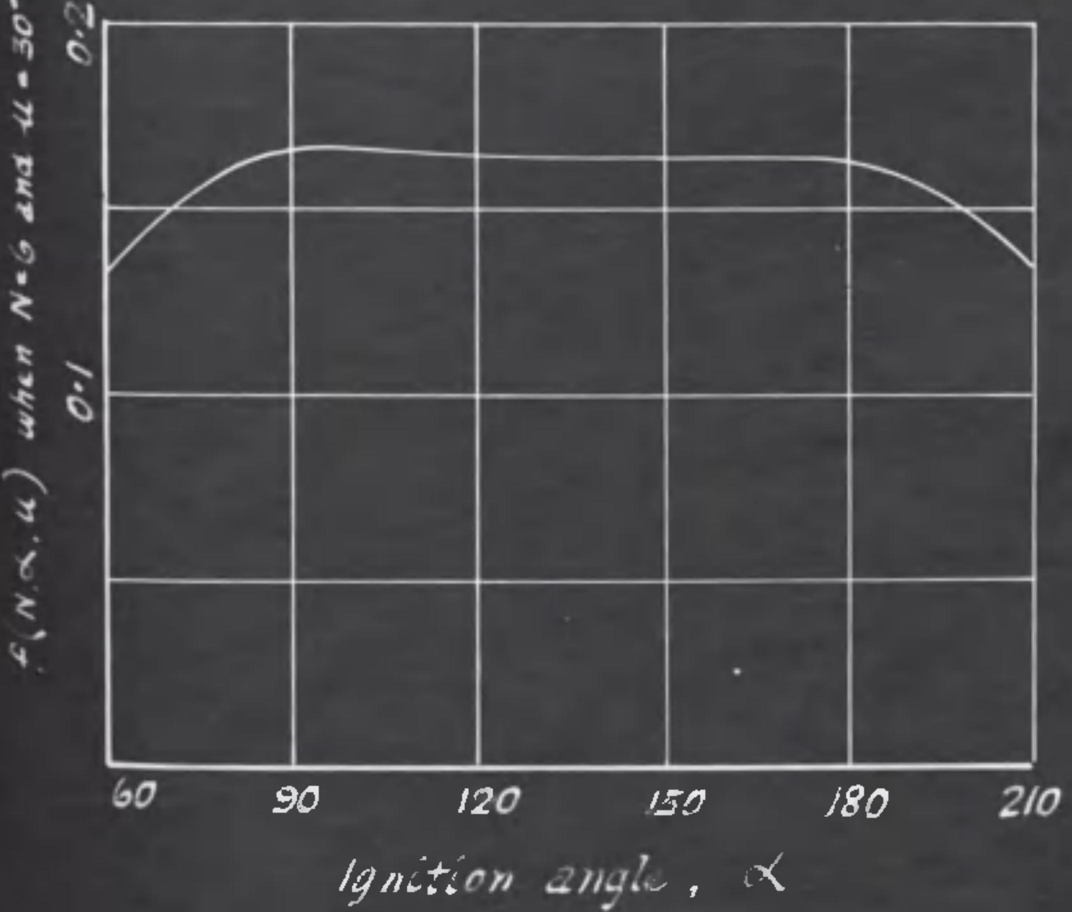

f(N, α, u) when N = 6 and u = 30°
0.1
0.2
60
90
120
150
180
210
Ignition angle, α

Fig. 21. Displacement, distortion and power factor curves drawn for $I_d = 15A$

— - — - — calculated.

———— experimental.

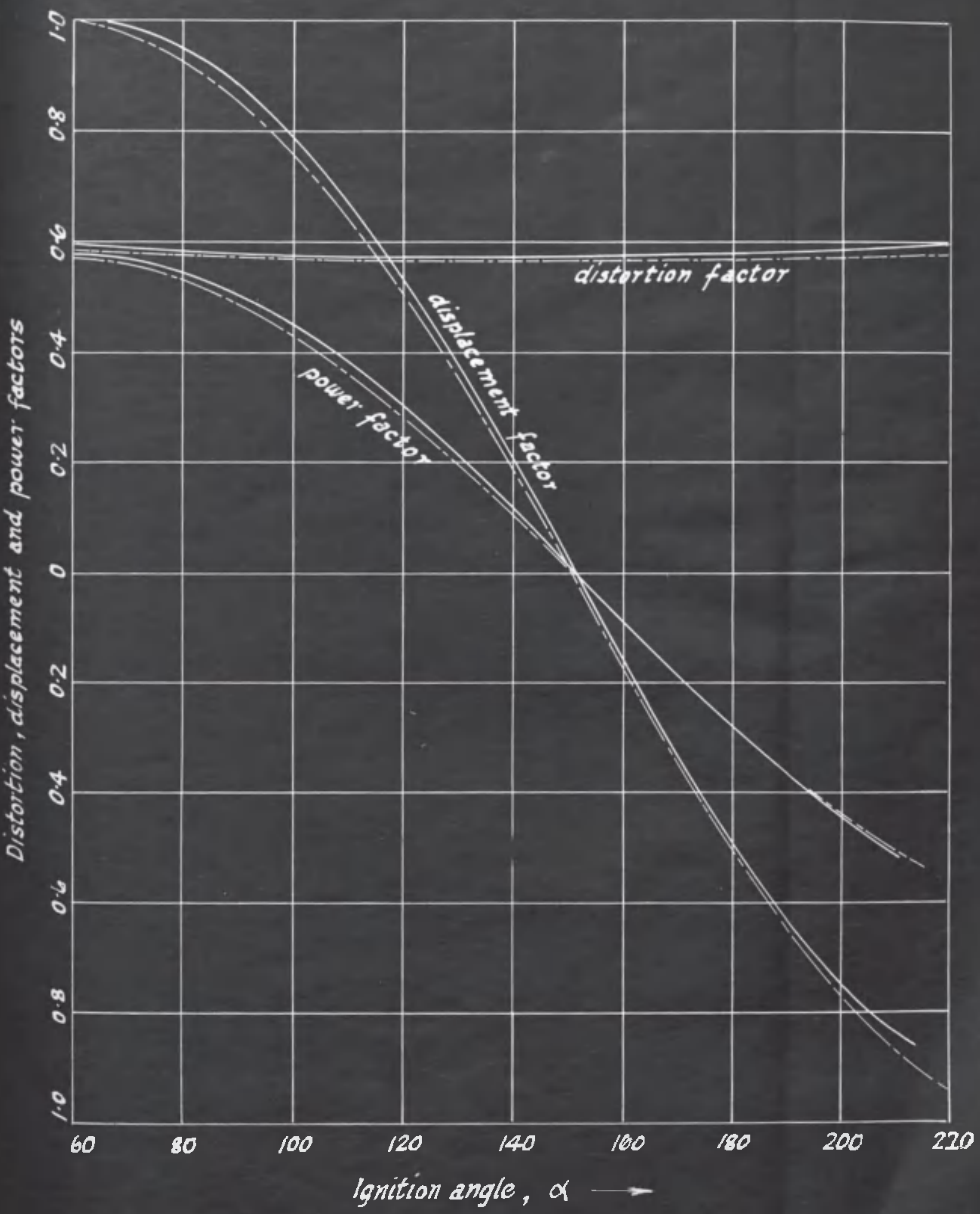
Distortion, displacement and power factors
1·0
0·8
0·6
0·4
0·2
0
0·2
0·4
0·6
0·8
1·0
distortion factor
displacement factor
power factor
60
80
100
120
140
160
180
200
220
Ignition angle, α →

Fig. 22. Pertaining to the measurement of the displacement factor of the anode current.

Fig. 23. Measurement of the arc drop with direct current.

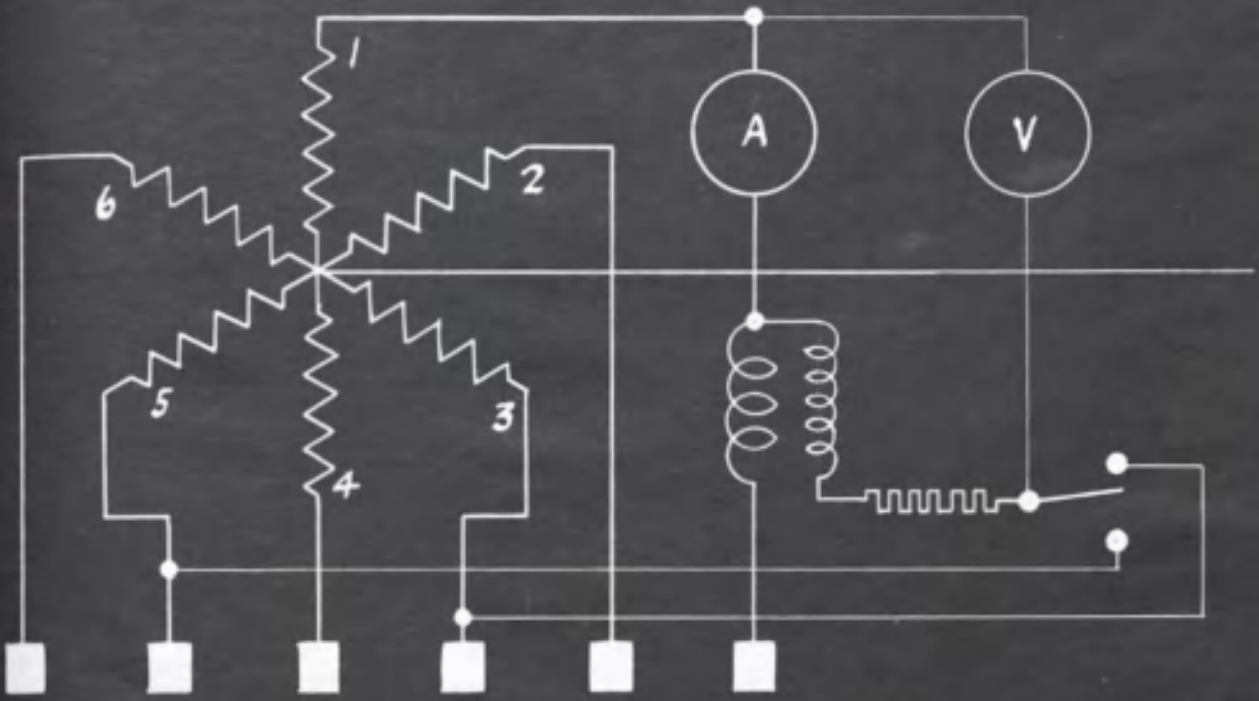
A
V

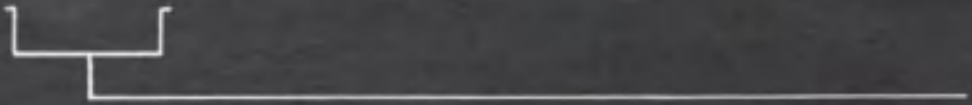

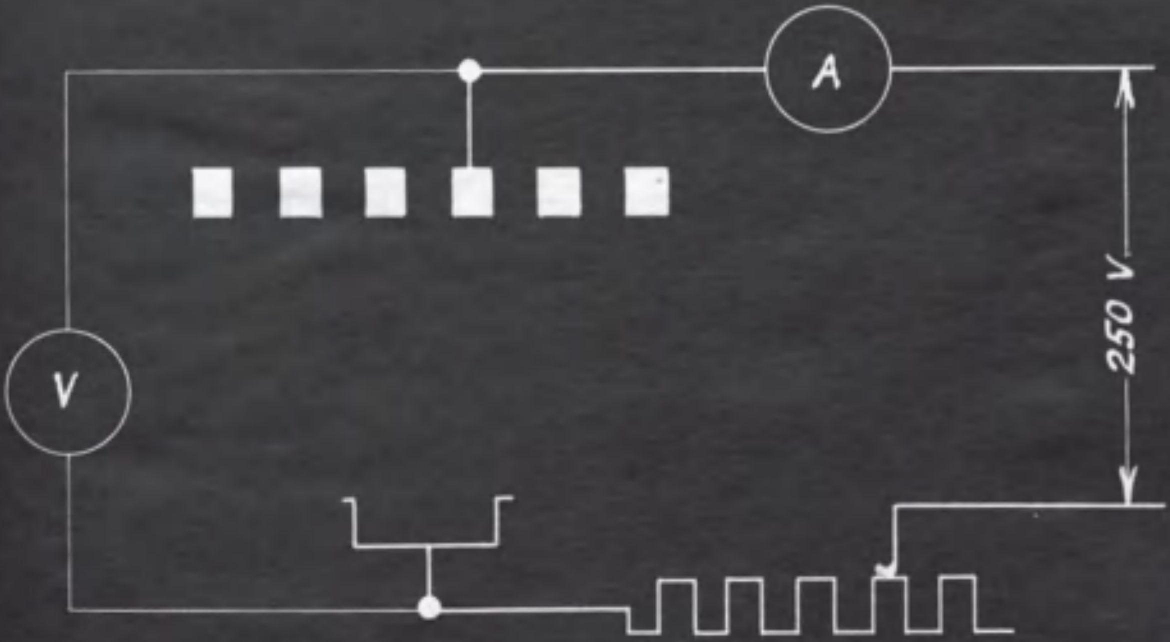
A
V
250 V

Fig. 24. Pertaining to the voltage regulation calculations.

Fig. 25. Pertaining to the calculation of the neutral current when the main transformer is connected 4-wire star/double star with interphase transformer.

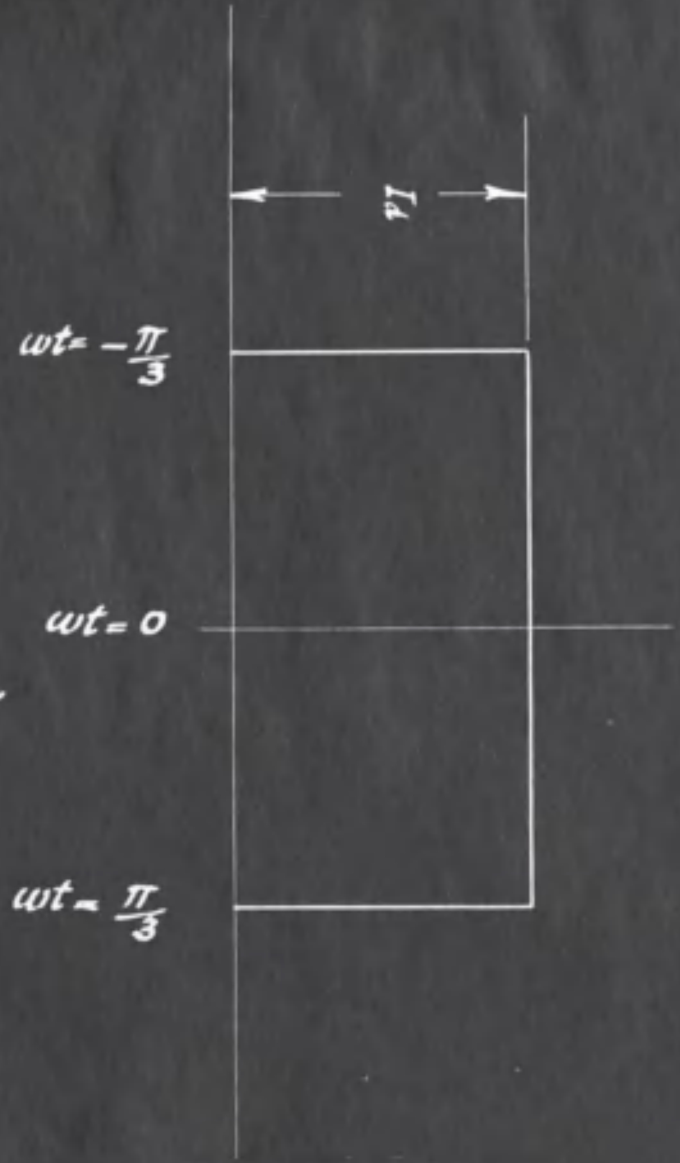
I_d
$\omega t = -\frac{\pi}{3}$
$\omega t = 0$
$\omega t = \frac{\pi}{3}$

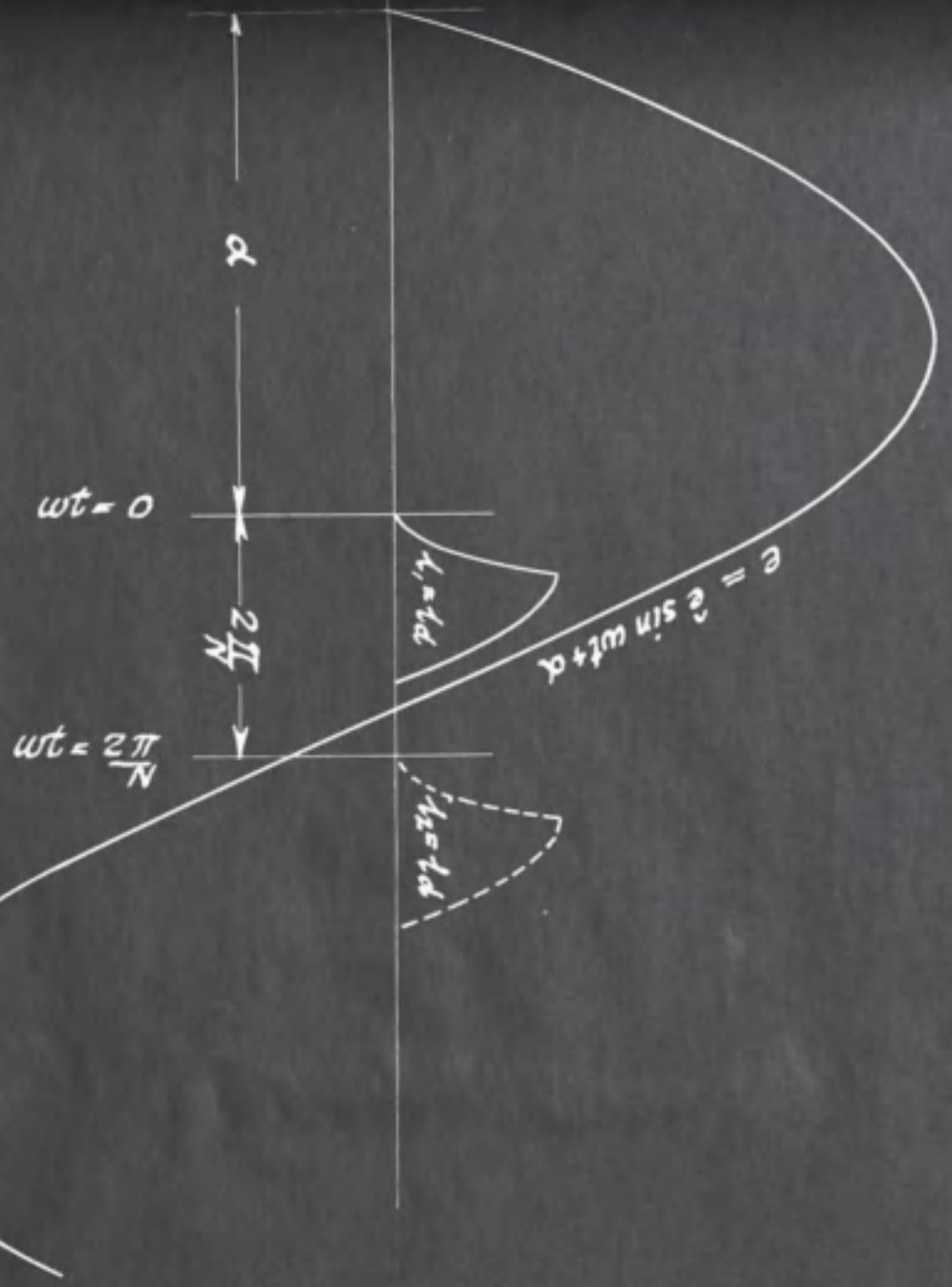
α
$\omega t = 0$
$\frac{2\pi}{N}$
$\omega t = \frac{2\pi}{N}$
$i_1 = i_d$
$i_2 = i_d$
$e = \hat{e} \sin \omega t + \alpha$

Fig. 26. Voltage regulation characteristic.

– – – – – calculated.

———— from load test.

$\alpha = 120°$; $L' = 11{\cdot}2\,mH$;

Fig. 27. Pertaining to the discussion on battery chargers.

Direct current/ignition angle characteristic.

$L' = 11{\cdot}2\,mH$; $V_d = 78V$

———— calculated.

– – – – from load test.

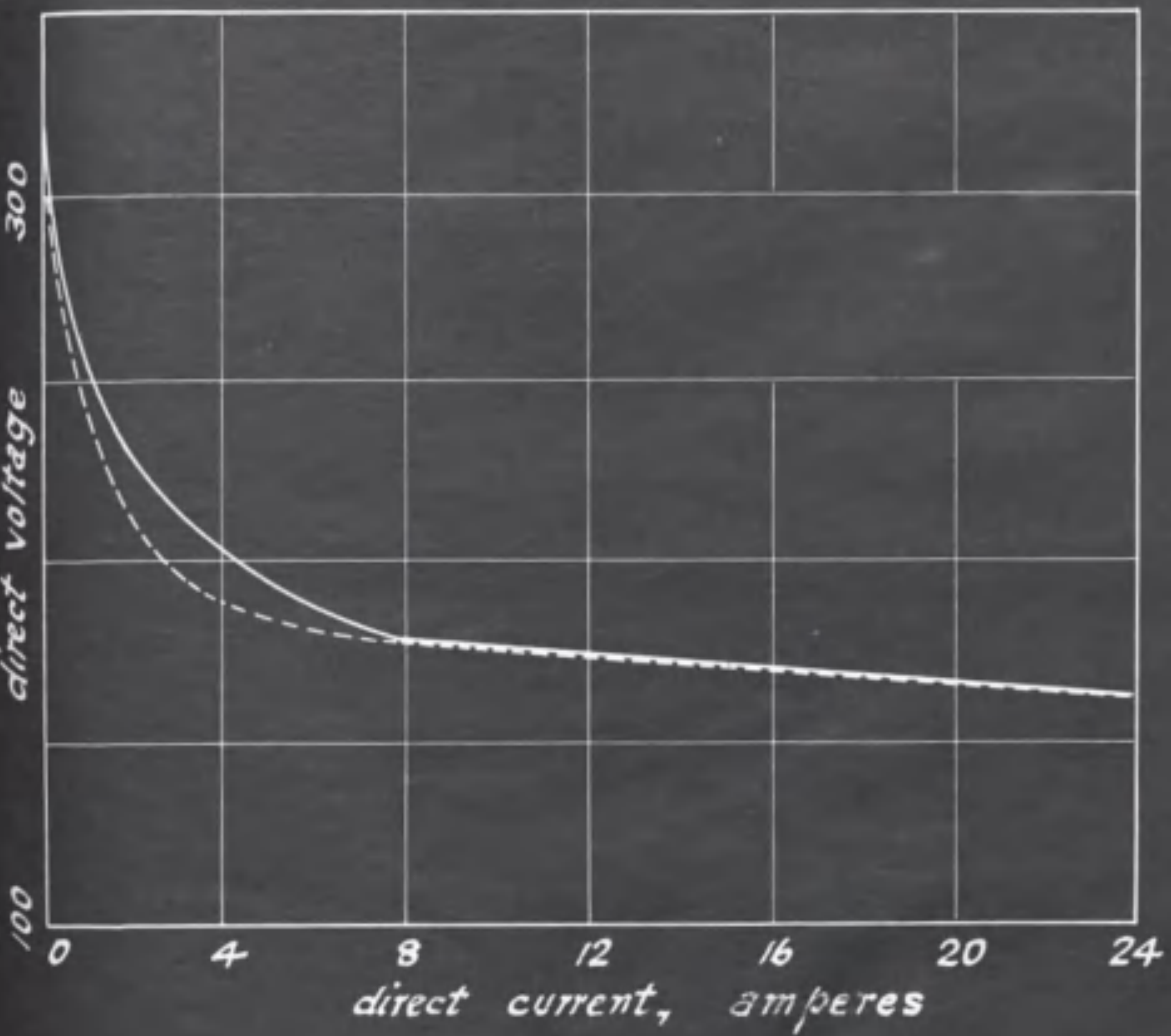
300
direct voltage
100
0
4
8
12
16
20
24
direct current, amperes

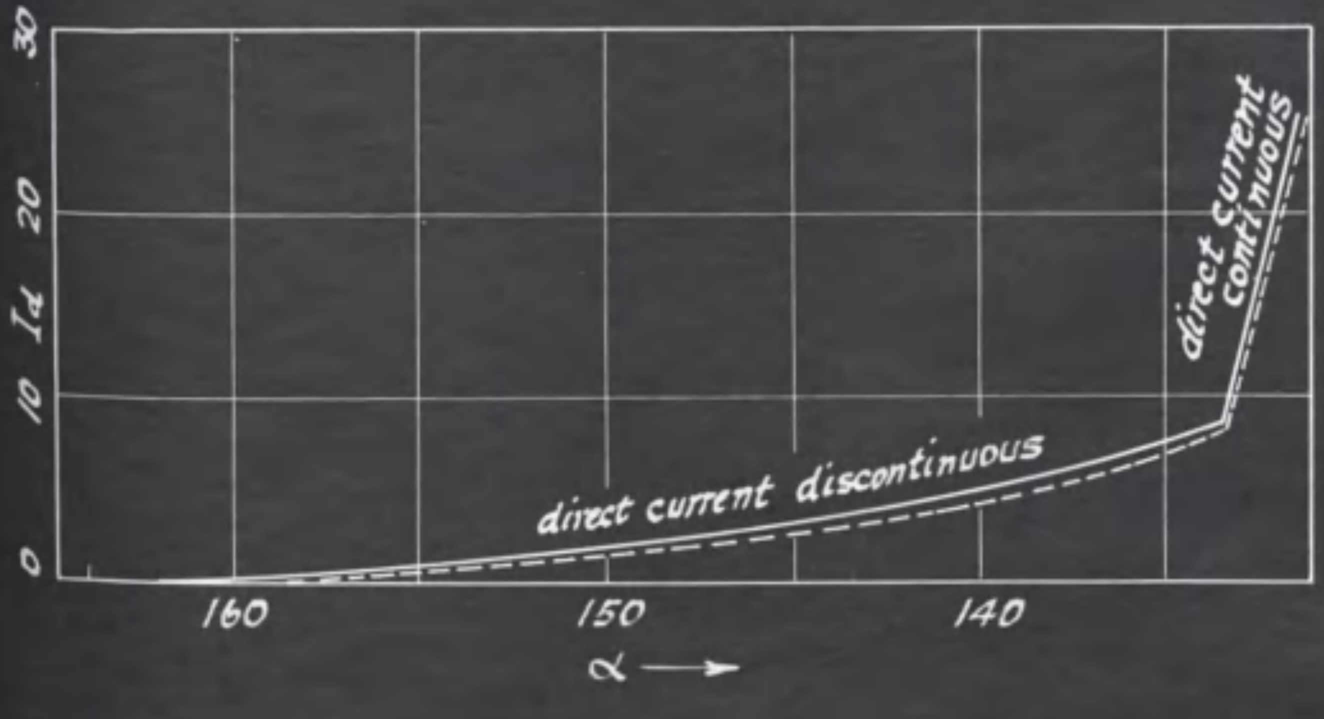
30
20
Id
10
0
direct current continuous
direct current discontinuous
160
150
140
α →

Fig. 28. Load test results with transformer connected star/double star with interphase transformer, $\alpha = 170^\circ$

Fig. 29. Load test results with transformer connected 3-wire star/6-phase star, $\alpha = 170^\circ$

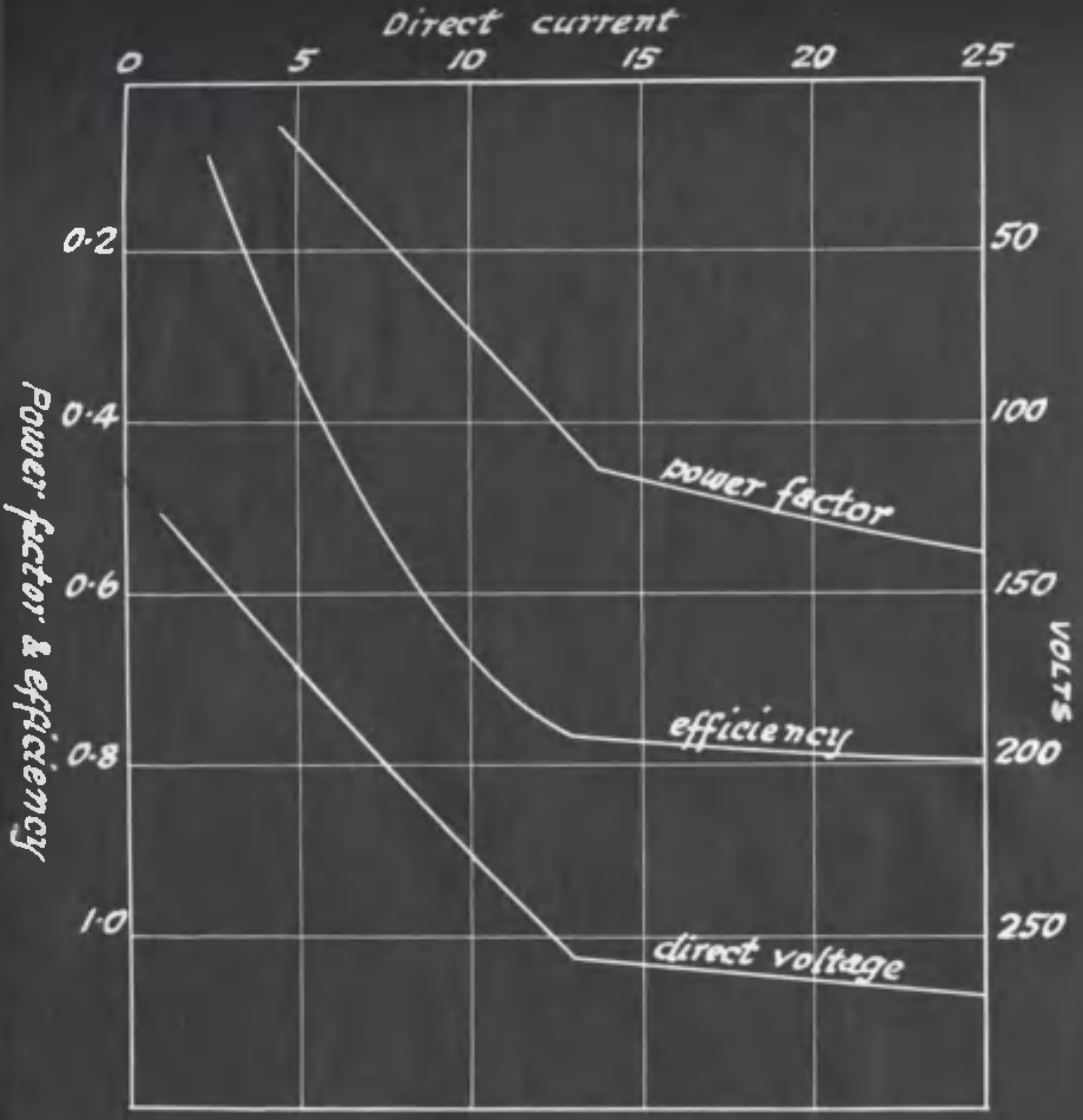
Direct current
0
5
10
15
20
25
0·2
0·4
0·6
0·8
1·0
Power factor & efficiency
50
100
150
200
250
VOLTS
power factor
efficiency
direct voltage

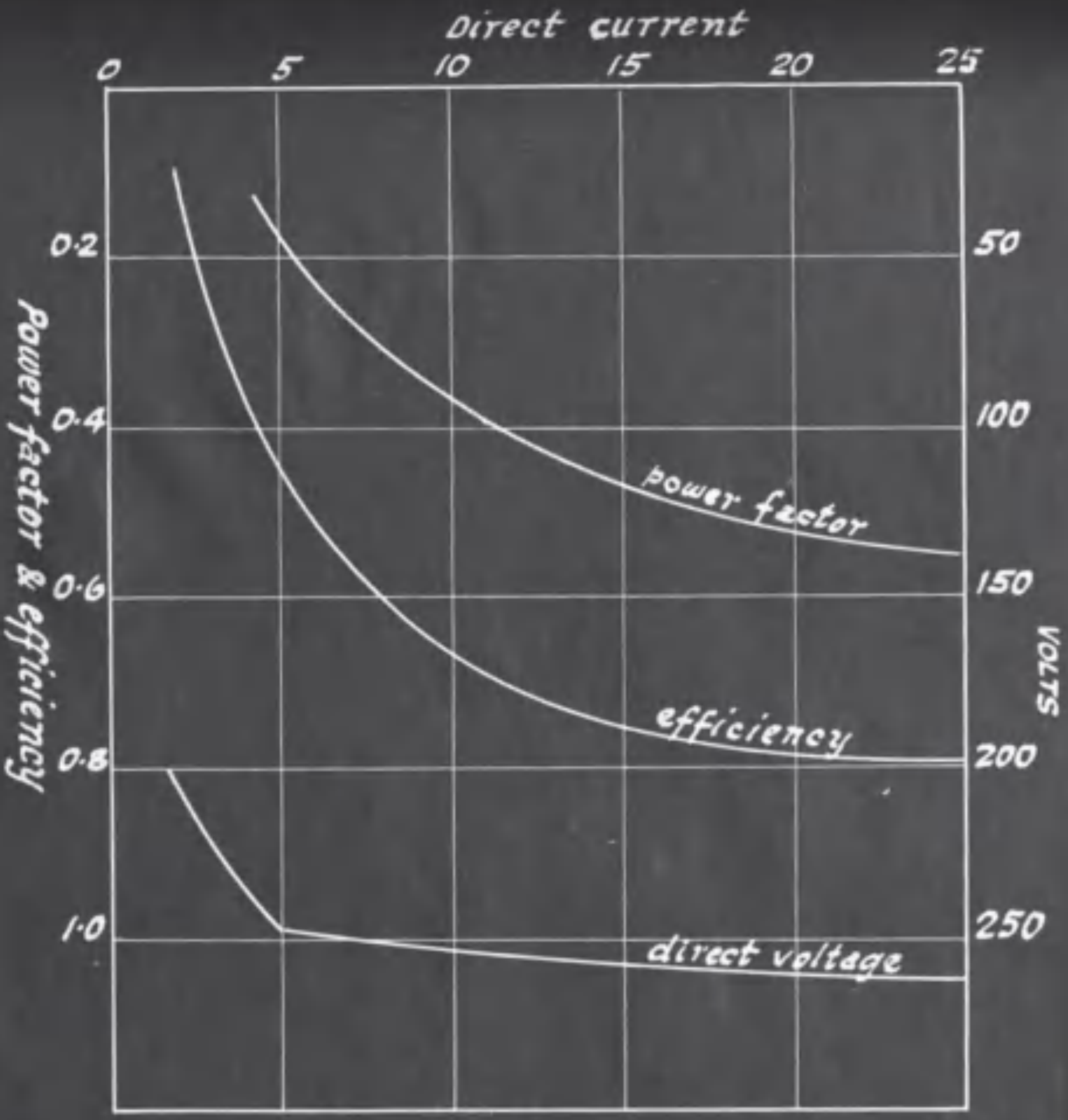
Direct current
0
5
10
15
20
25
0·2
0·4
0·6
0·8
1·0
Power factor & efficiency
50
100
150
200
250
VOLTS
power factor
efficiency
direct voltage

Fig. 30. Transformer windings showing leakage fluxes for different connections.

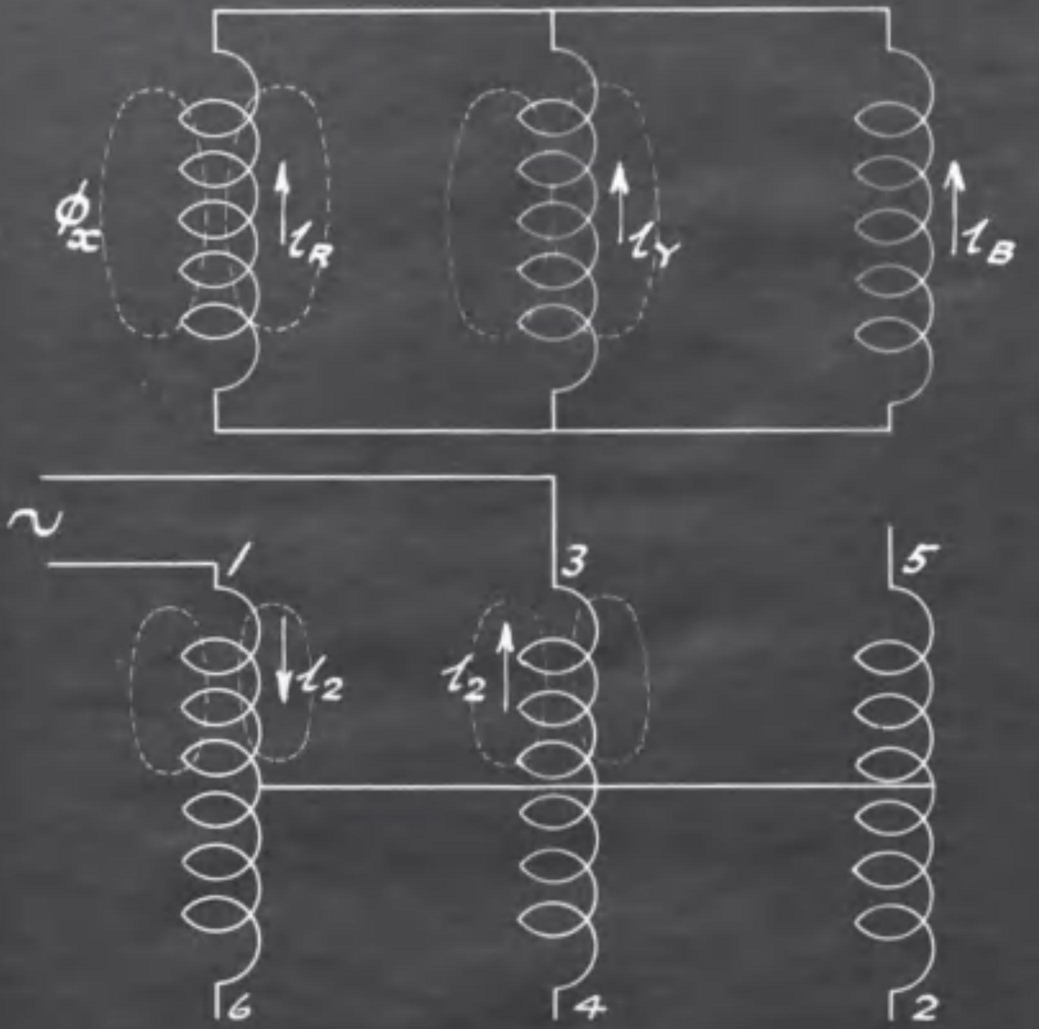

ϕ_x
i_R
i_Y
i_B
~
1
3
5
i_2
i_2
6
4
2

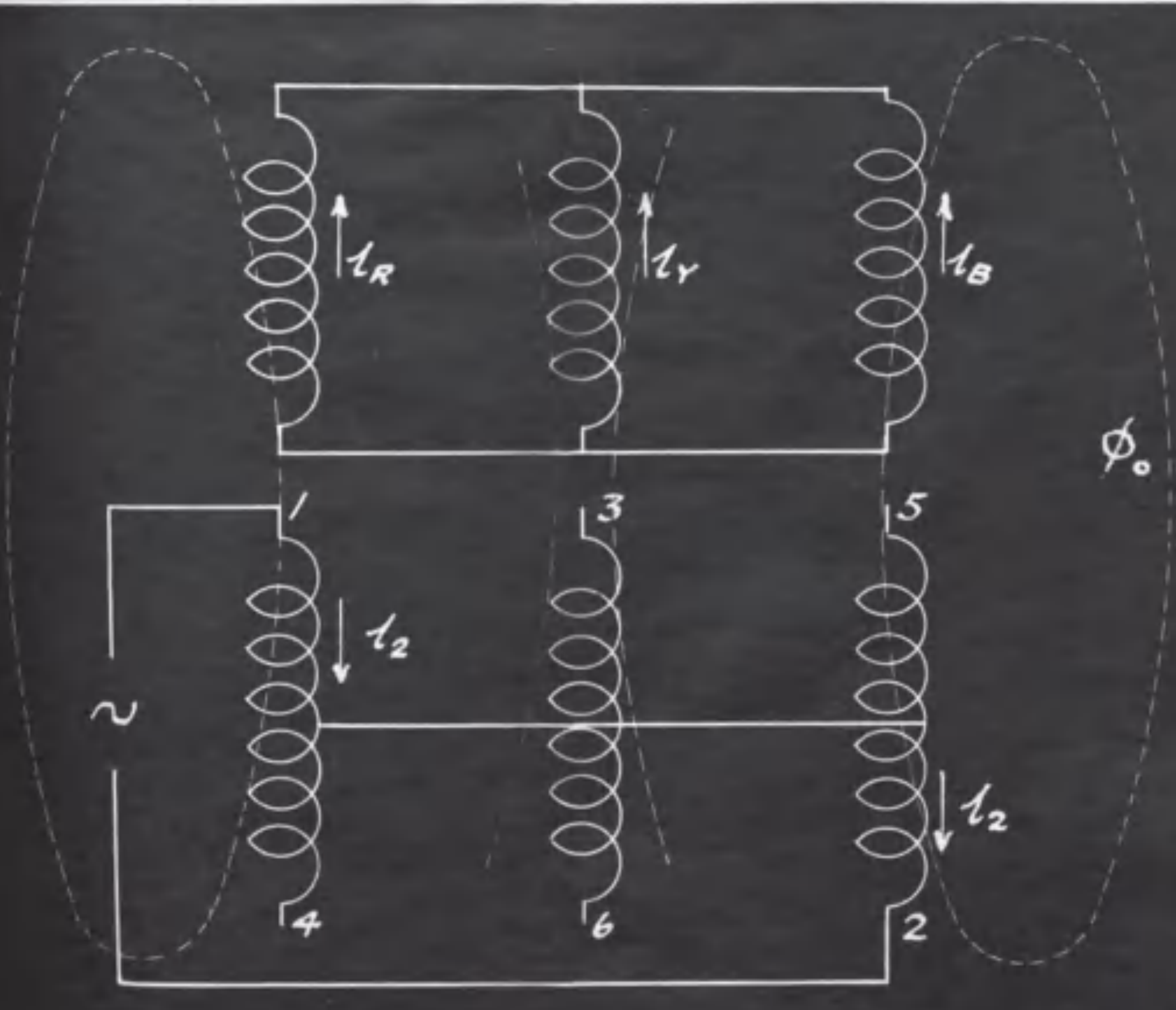

i_R
i_Y
i_B
ϕ_0
1
3
5
~
i_2
i_2
4
6
2

Fig. 31. Line current wave form deduced from anode current wave form.

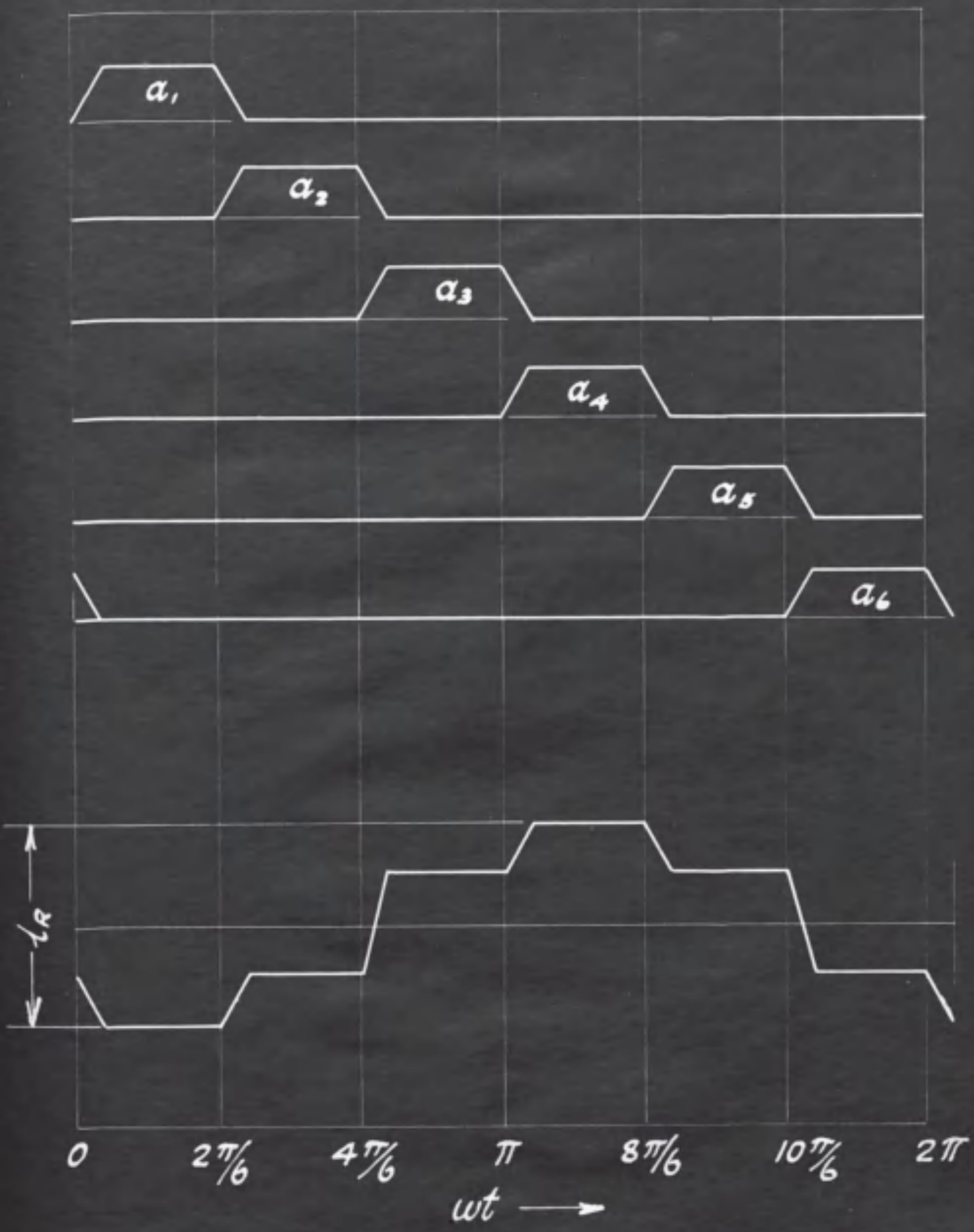

a_1
a_2
a_3
a_4
a_5
a_6
i_R
0
$2\pi/6$
$4\pi/6$
π
$8\pi/6$
$10\pi/6$
2π
$\omega t \longrightarrow$

Fig. 32. Line current wave form deduced from anode current wave forms.

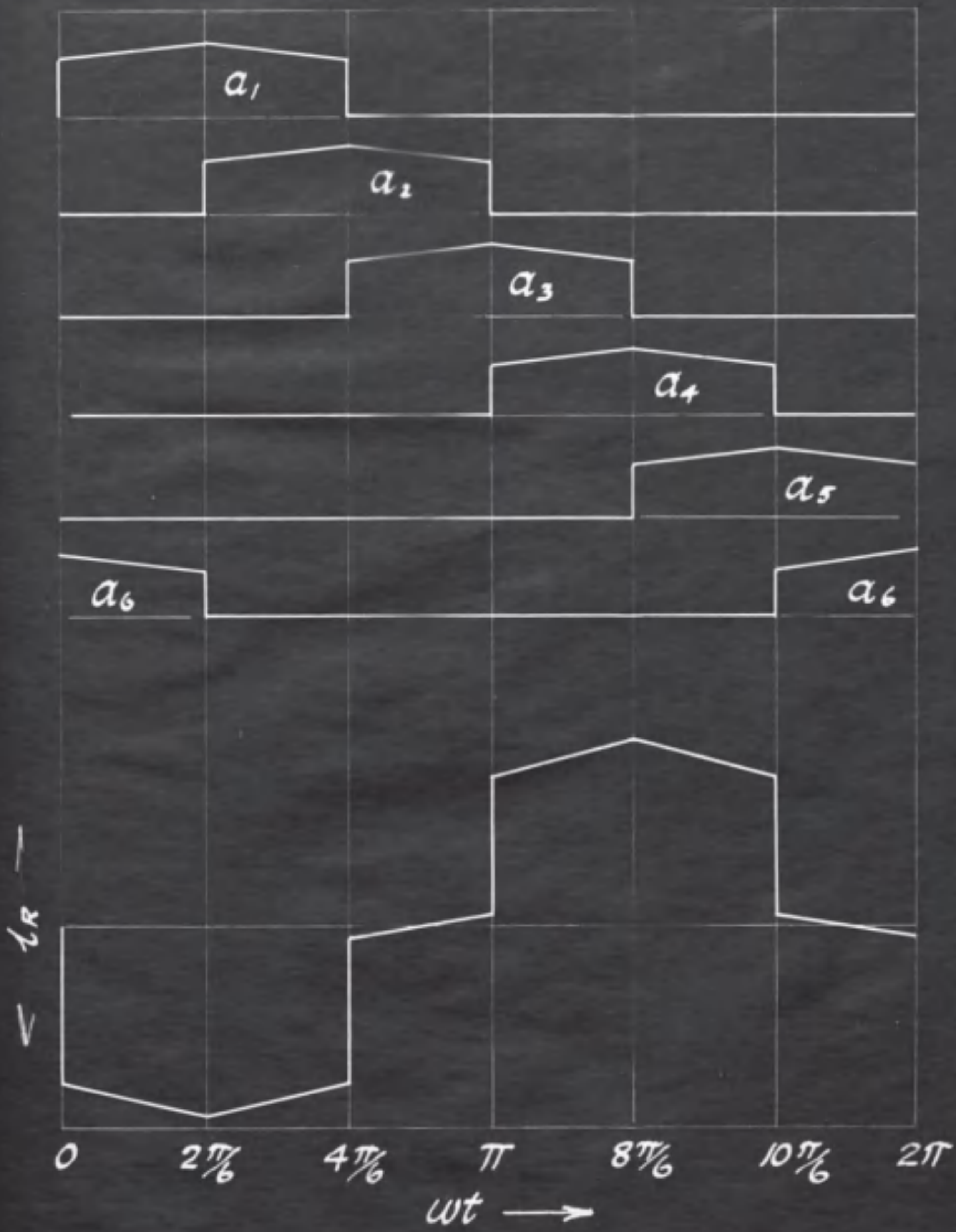
a1
a2
a3
a4
a5
a6
a6
i_R
0
2π/6
4π/6
π
8π/6
10π/6
2π
ωt →

Fig. 33. Pertaining to the short-circuit of invertors.

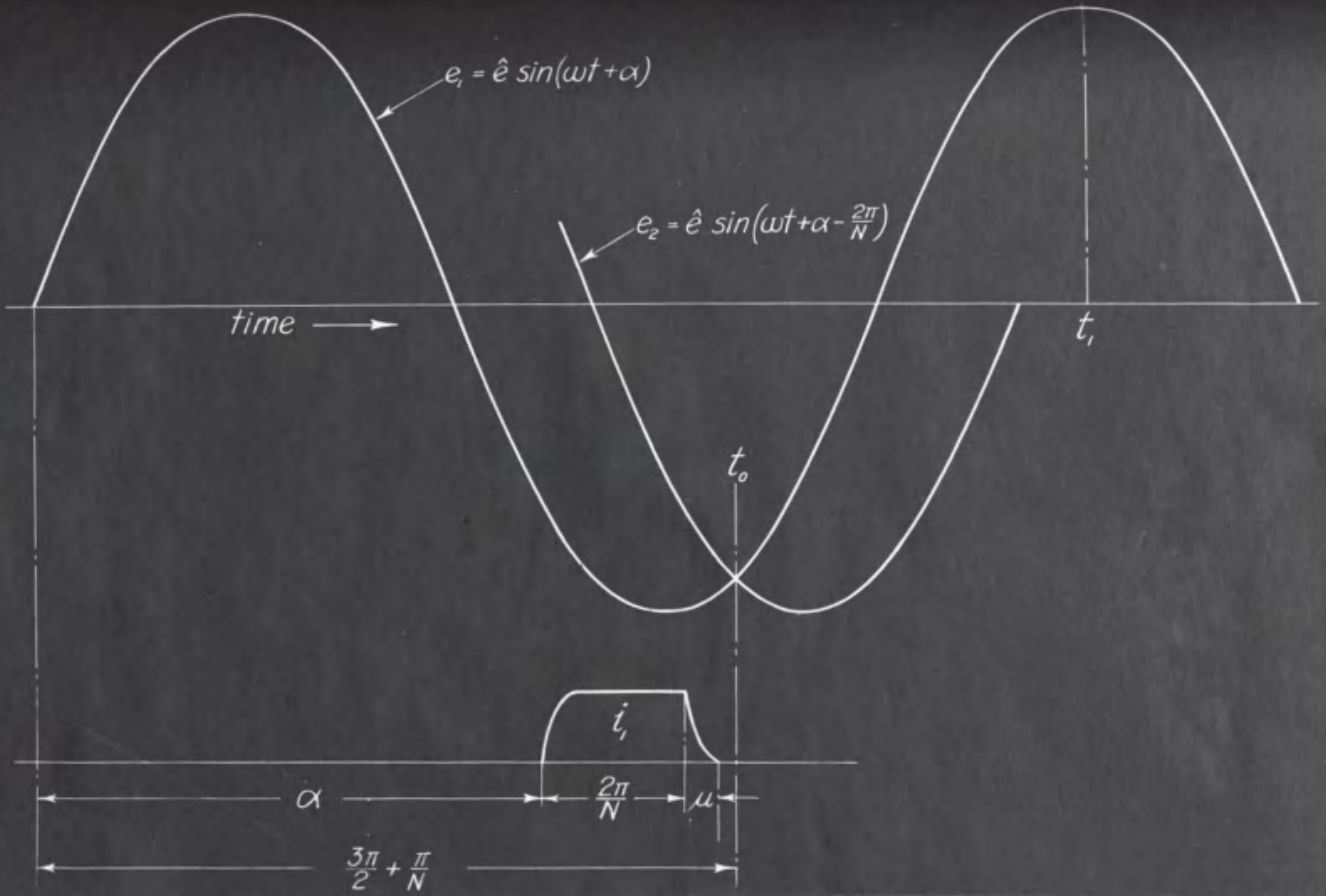
$e_1 = \hat{e} \sin(\omega t + \alpha)$
$e_2 = \hat{e} \sin(\omega t + \alpha - \frac{2\pi}{N})$
time →
t_1
t_0
i_1
α
$\frac{2\pi}{N}$
μ
$\frac{3\pi}{2} + \frac{\pi}{N}$

Fig. 34. Pertaining to the short-circuit of invertors.

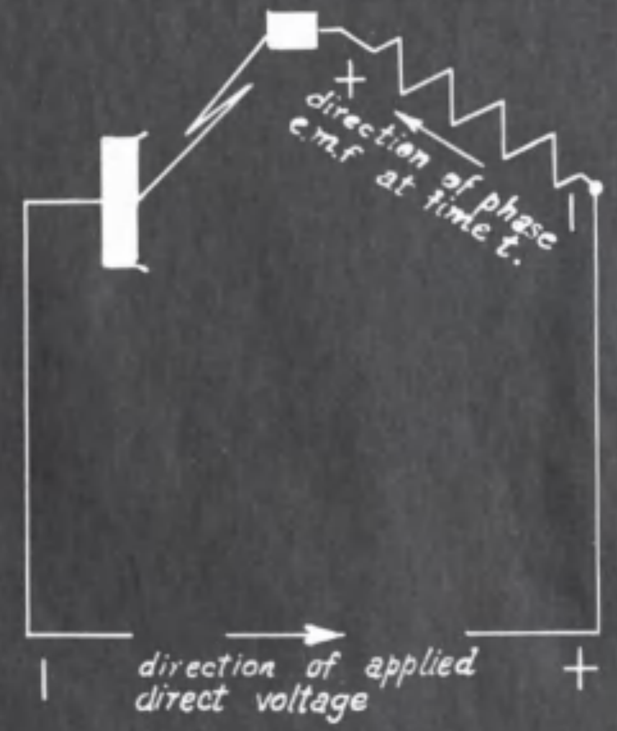
+
direction of phase
e.m.f at time t.
−
−
direction of applied
direct voltage
+

Fig. 35. Pertaining to the short-circuit of invertors.

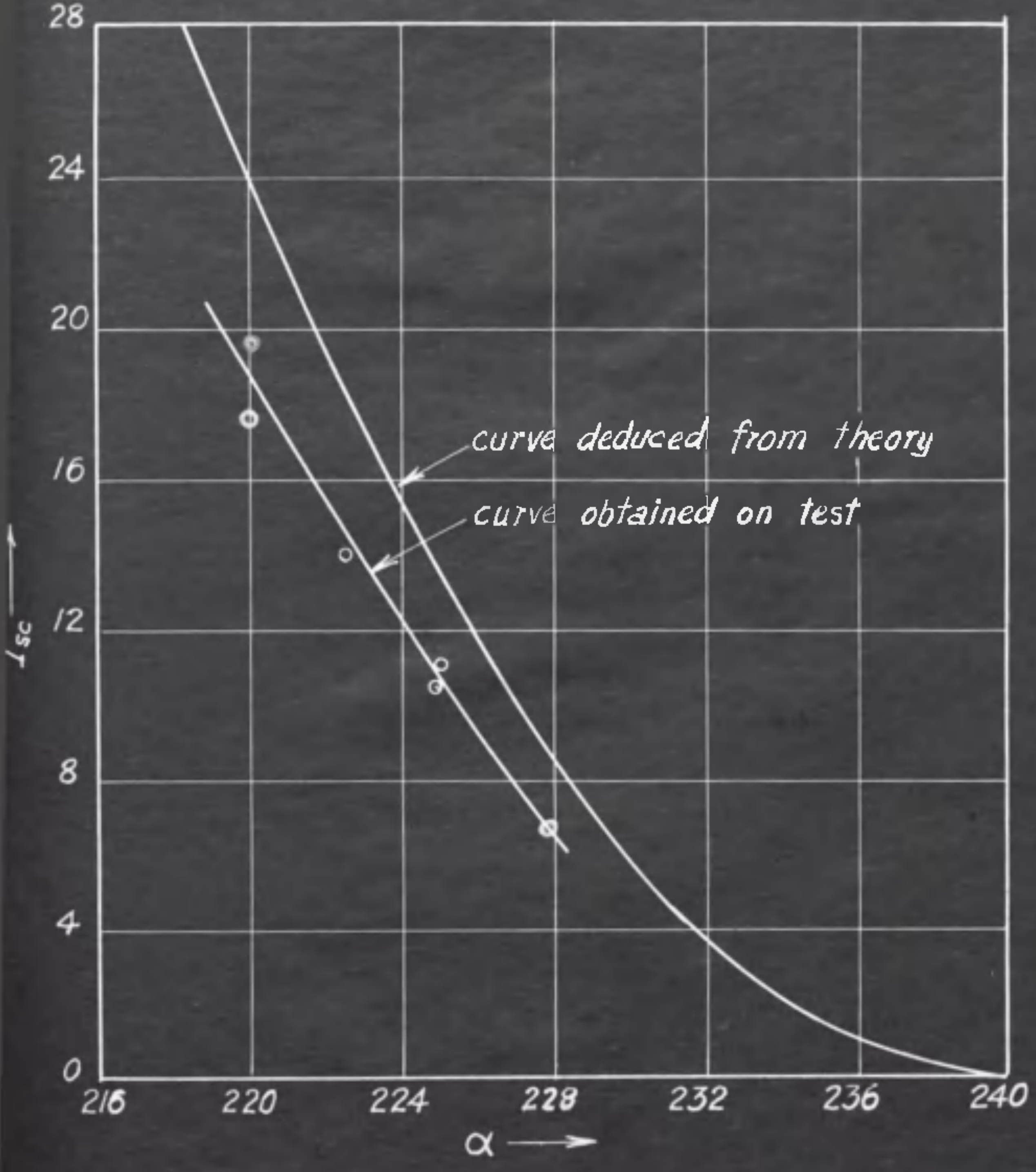
28
24
20
16
12
8
4
0
I_{sc}
216
220
224
228
232
236
240
α
curve deduced from theory
curve obtained on test

Fig. 36. A load diagram for 6-phase invertors.

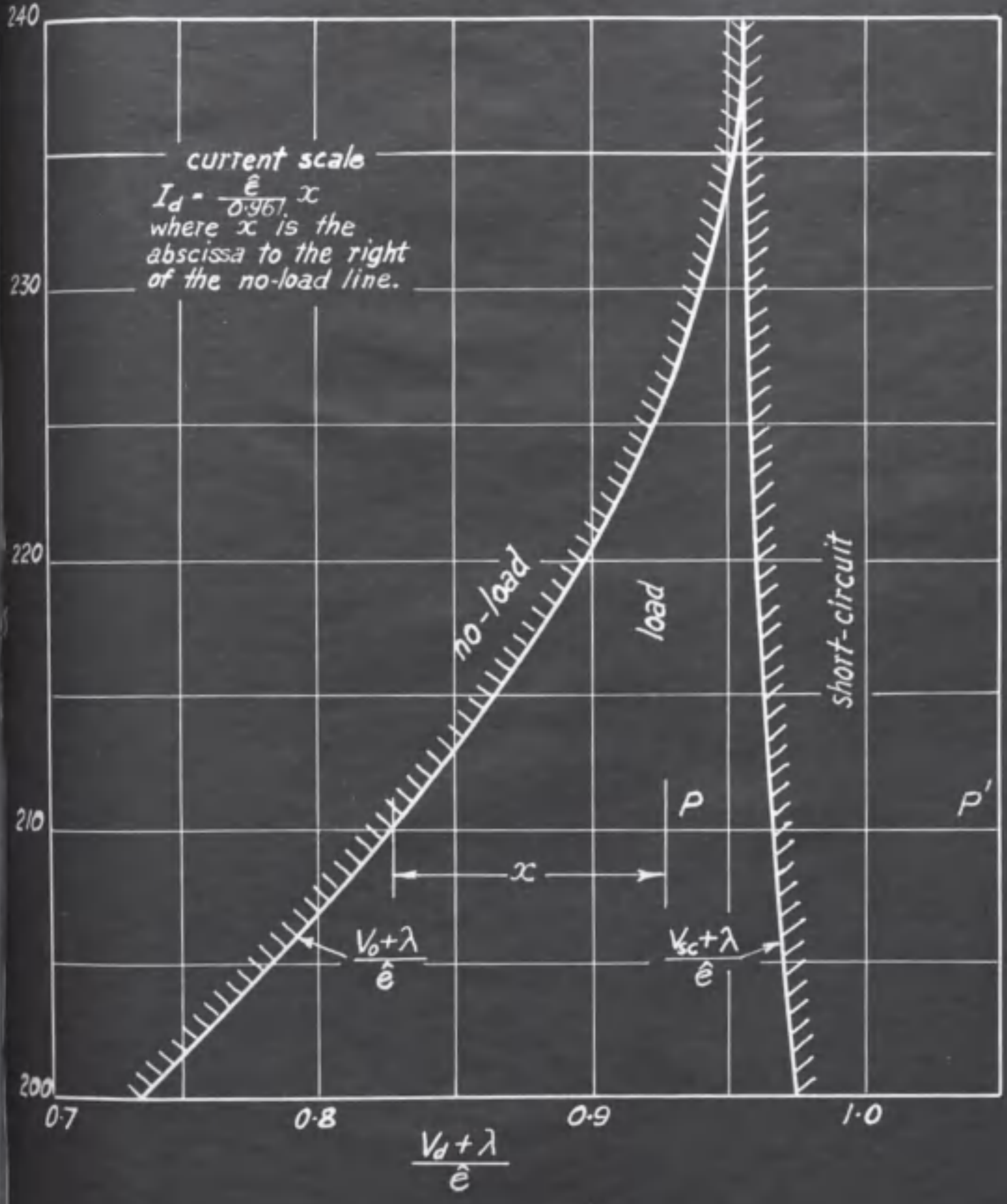
240
230
220
210
200
0·7
0·8
0·9
1·0
$\frac{V_d+\lambda}{\hat{e}}$
current scale
$I_d = \frac{\hat{e}}{0{\cdot}961}\,x$
where x is the
abscissa to the right
of the no-load line.
no-load
load
short-circuit
P
P′
x
$\frac{V_0+\lambda}{\hat{e}}$
$\frac{V_{sc}+\lambda}{\hat{e}}$

Fig. 37. Pertaining to commutation.

Fig. 38. Relation between u and α for $I_d = 15A$.

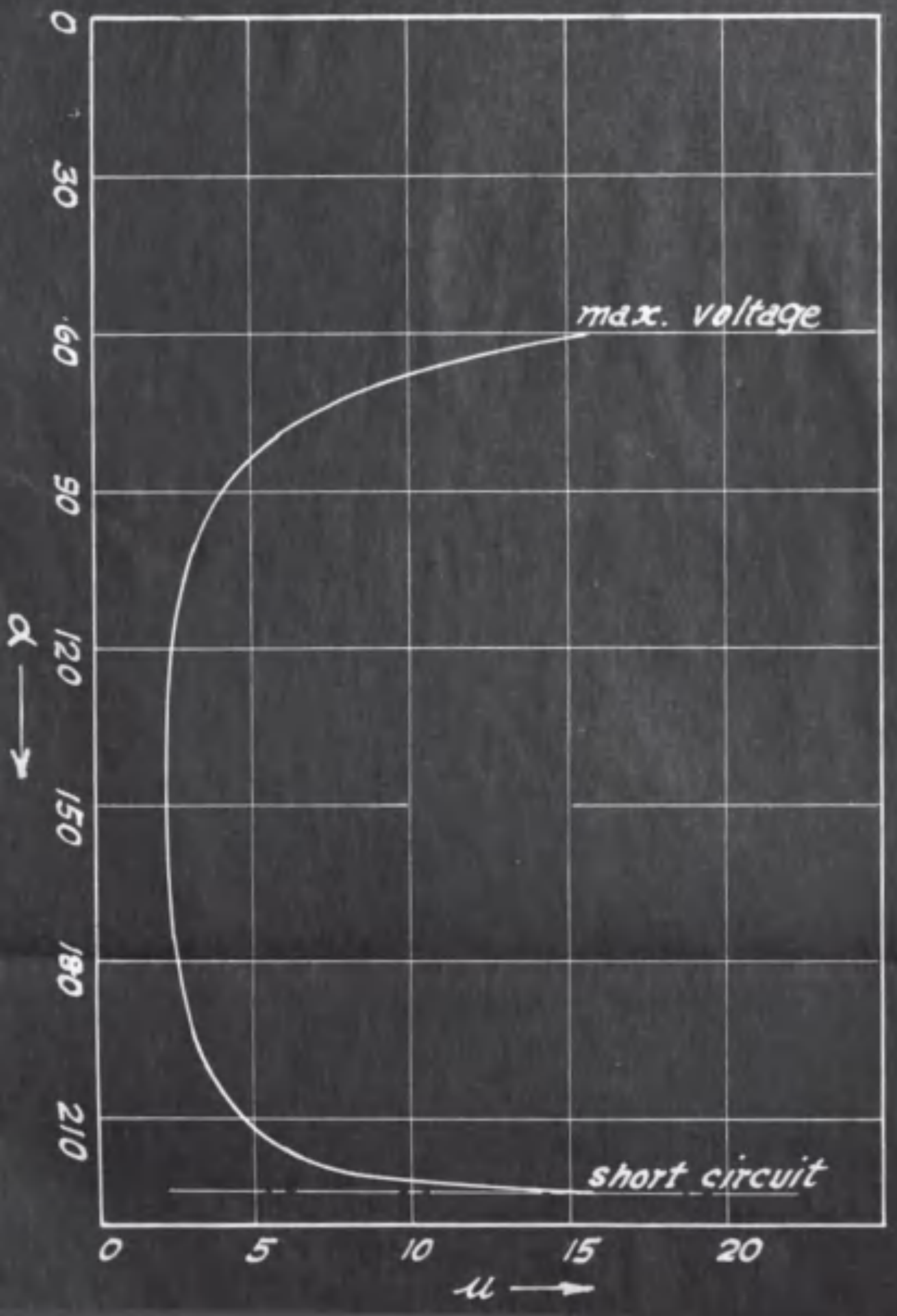
max. voltage
short circuit
0
30
60
90
120
150
180
210
α ⟶
0
5
10
15
20
u ⟶

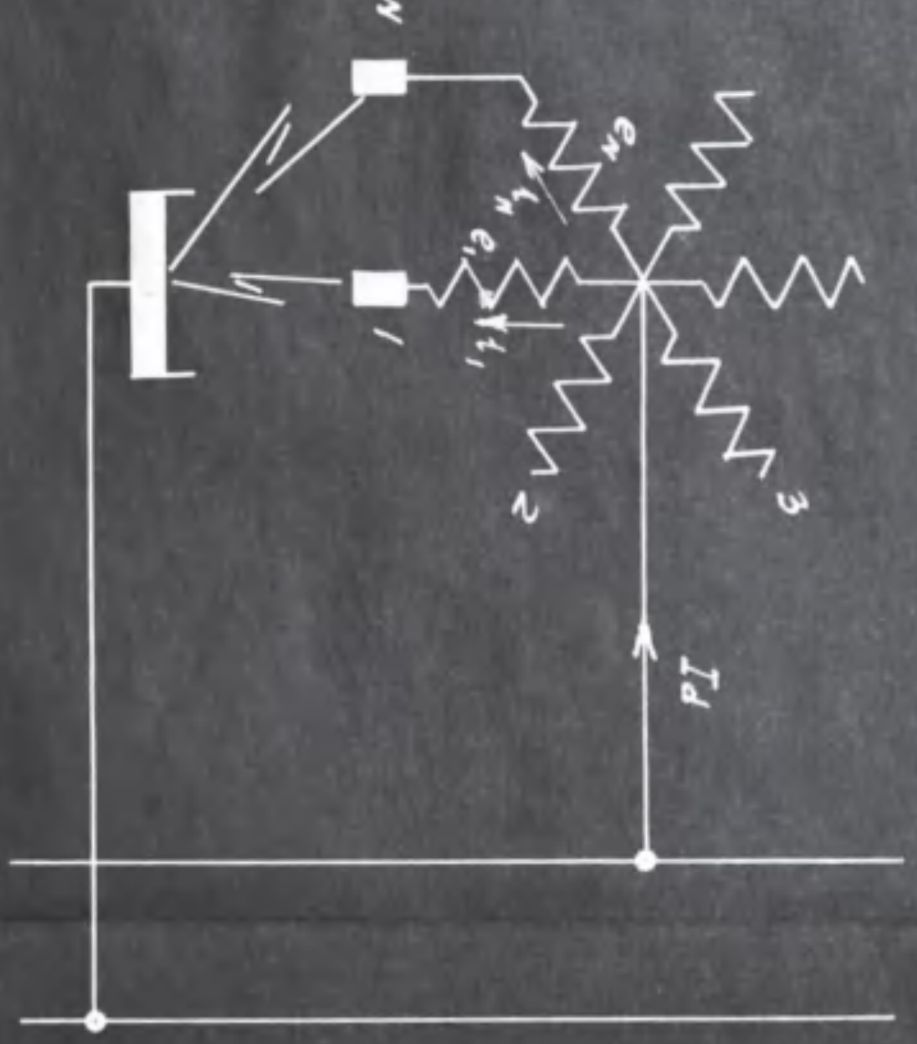
N
1
2
3
e_N
i_N
e_1
i_1
I_d

Fig. 39. Relation between u and I_d for various values of α

a .. calculated, neglecting τ
b .. calculated, including τ
c .. from stroboscope measurements.
Transformer connections as Fig. 10.

Fig. 40. a .. calculated, neglecting τ
b .. calculated, including τ
c .. from stroboscope measurements.
Transformer connections as Fig. 10.

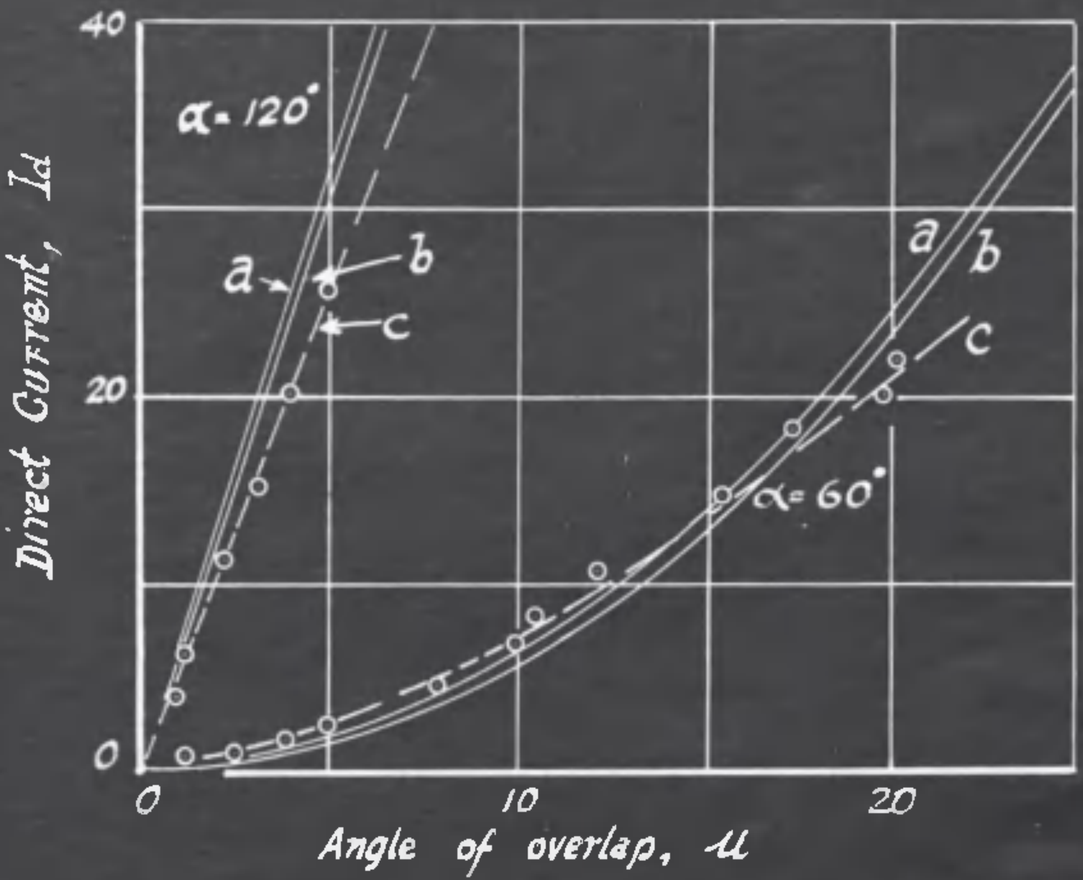
α = 120°
a
b
c
a
b
c
α = 60°
Direct Current, I_d
Angle of overlap, u
0
10
20
0
20
40

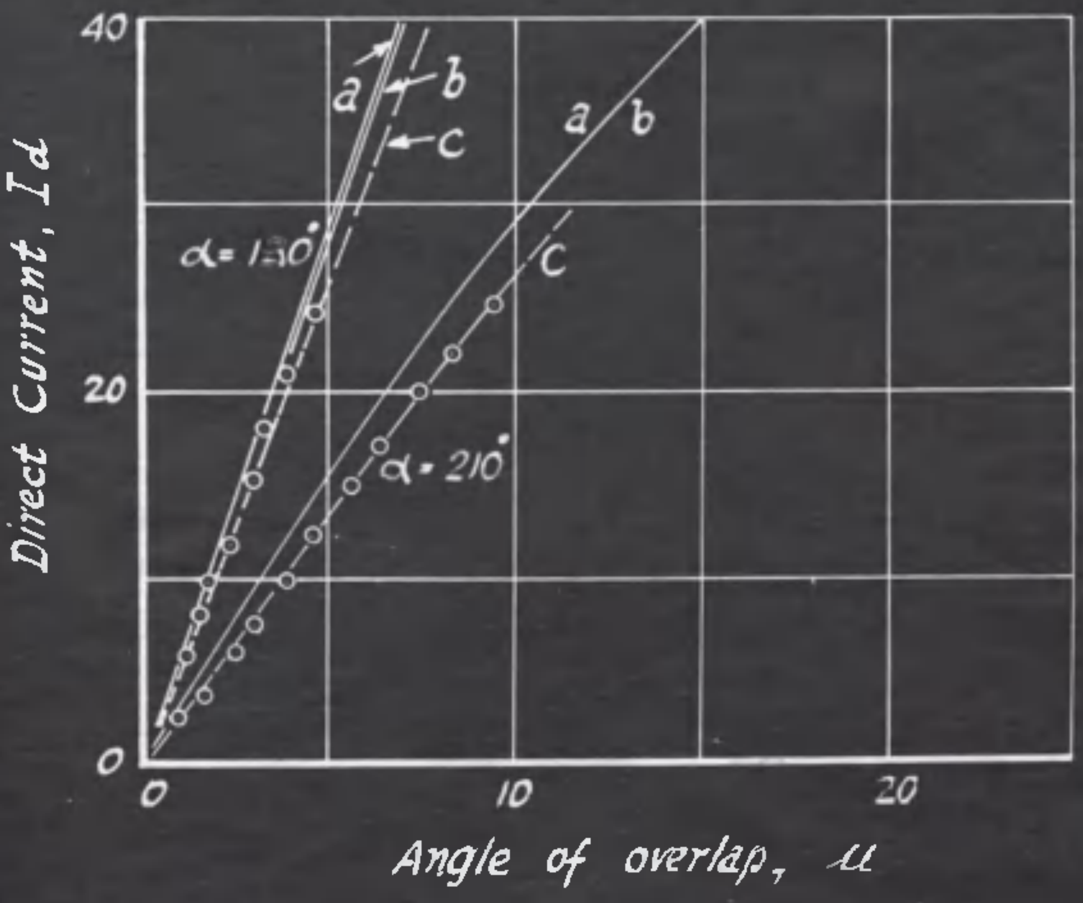
a
b
c
a
b
c
α = 150°
α = 210°
Direct Current, I_d
Angle of overlap, u
0
10
20
0
20
40

Fig. 41. Pertaining to commutation.

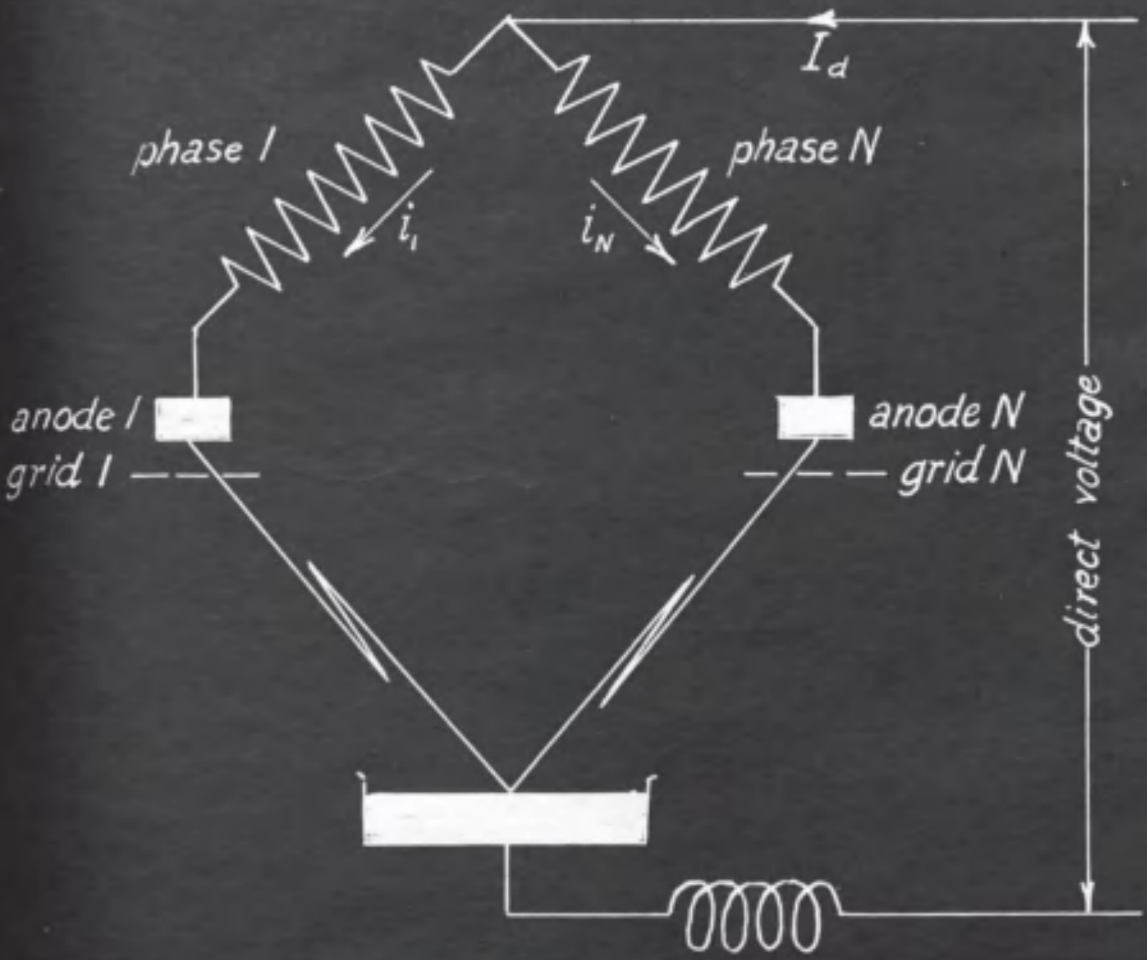
I_d
phase I
phase N
i_1
i_N
anode I
grid I
anode N
grid N
direct voltage

Fig. 42. Pertaining to commutation.

Fig. 43. Pertaining to commutation.
a.. calculated, neglecting r
b.. calculated, including r

Fig. 44. Pertaining to the construction of Fig. 43.

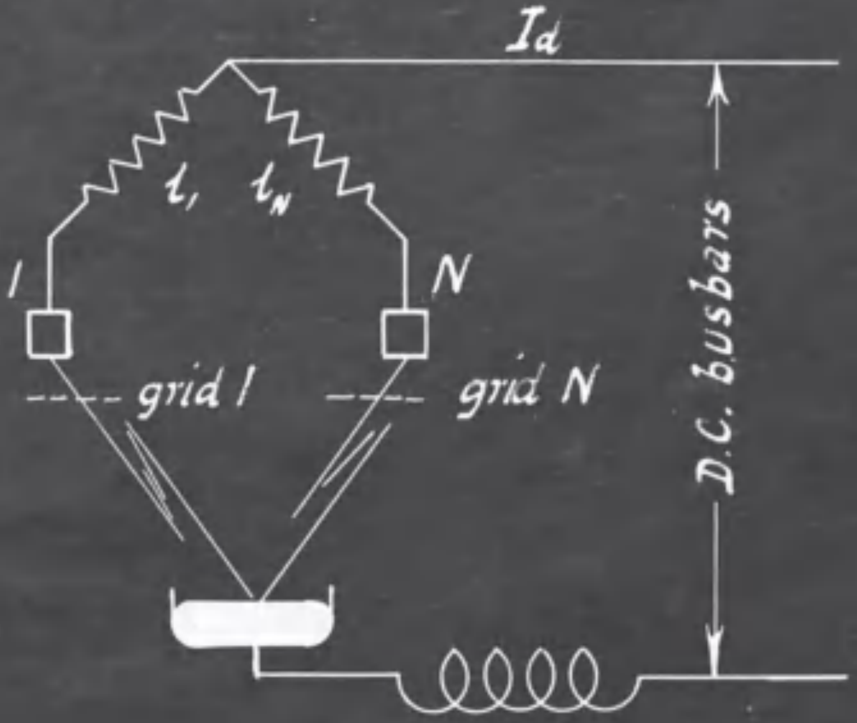

Id
i1
iN
1
N
grid 1
grid N
D.C. busbars

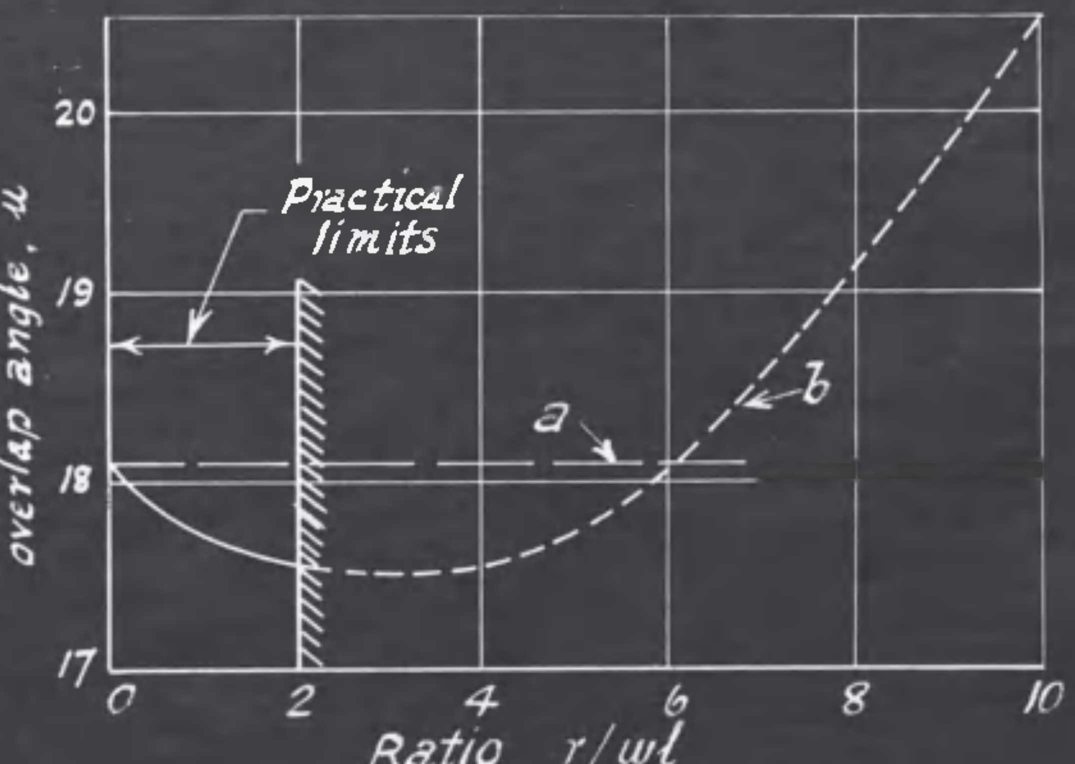

overlap angle, u
17
18
19
20
Practical limits
a
b
0
2
4
6
8
10
Ratio r/ωl

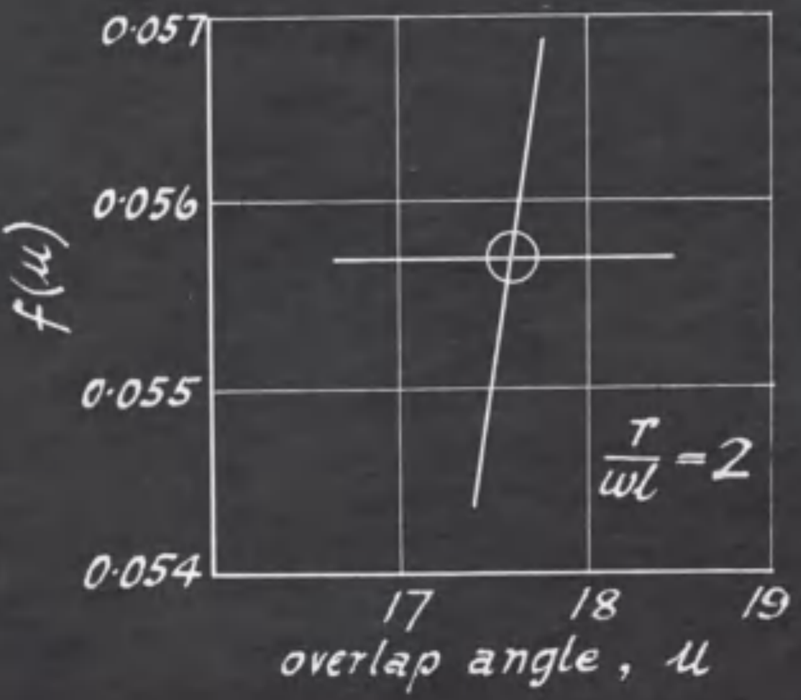

f(u)
0·057
0·056
0·055
0·054
r/ωl = 2
17
18
19
overlap angle, u

Fig. 45. Induction regulator used as phase shifting transformer.

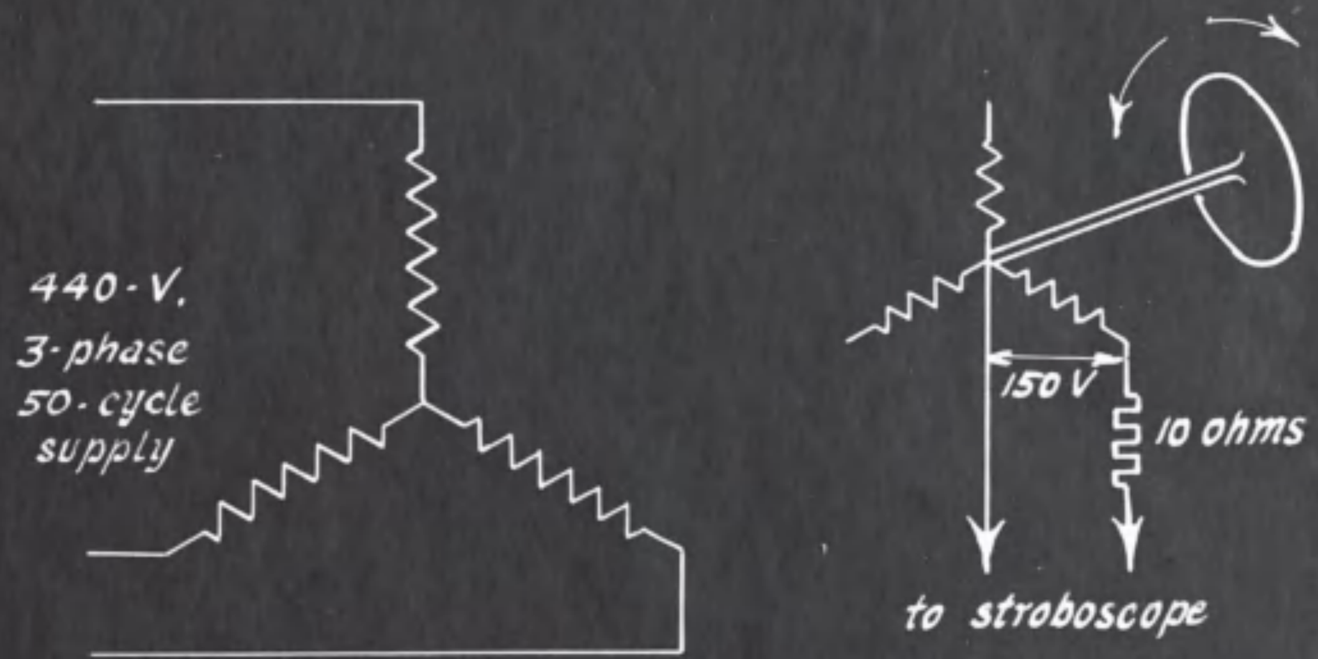
440-V,
3-phase
50-cycle
supply
150 V
10 ohms
to stroboscope

Fig. 46. Pertaining to the measurement of u by the stroboscope.

Fig. 47. The stroboscope circuit diagram.

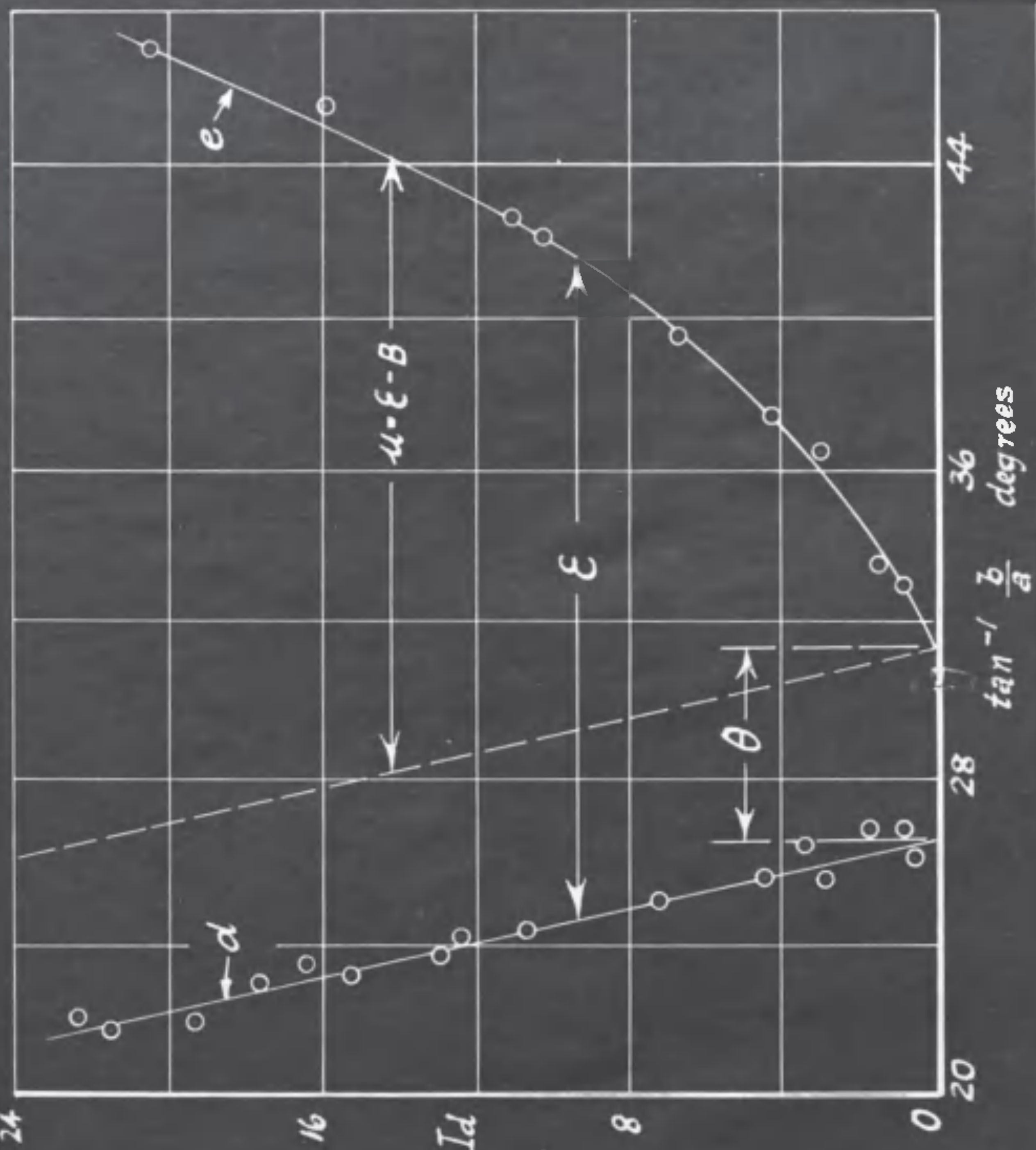
24
16
Id
8
0
20
28
36
44
tan⁻¹ b/a degrees
e
u-ε-B
ε
θ
α

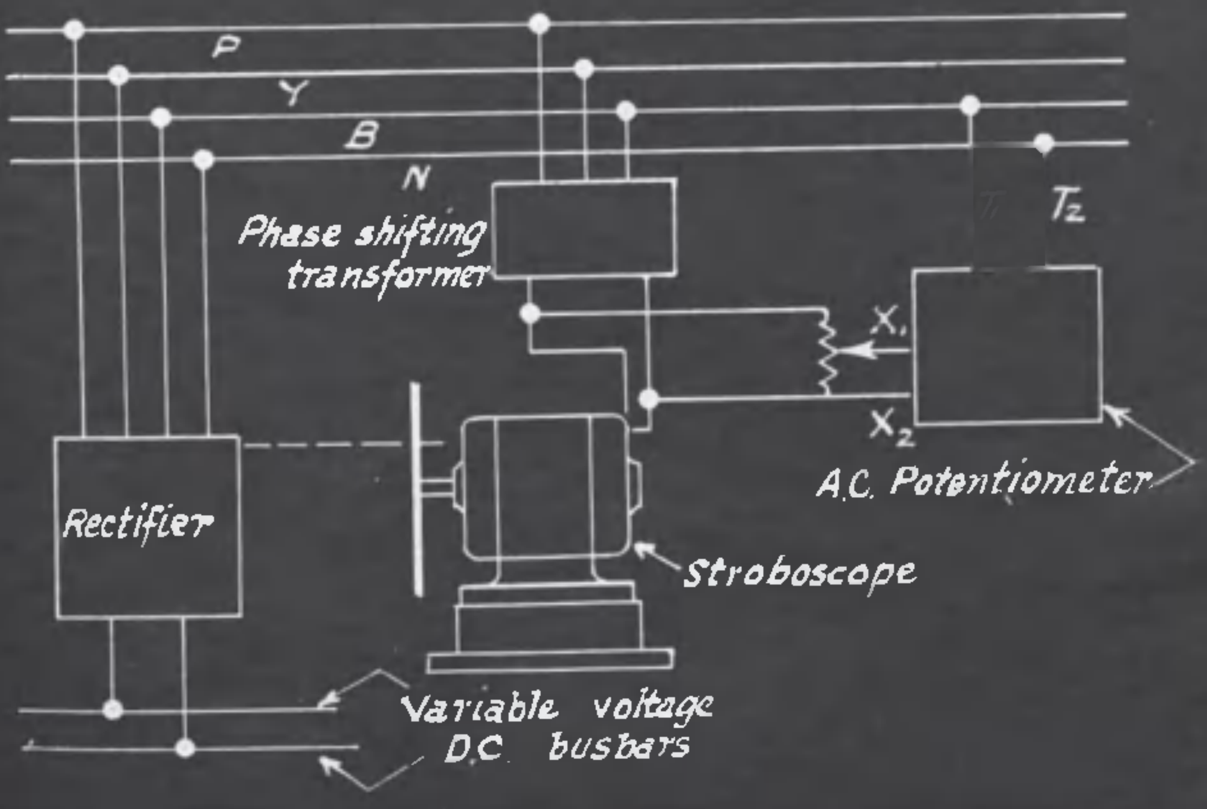
P
Y
B
N
Phase shifting transformer
T₂
X₁
X₂
A.C. Potentiometer
Rectifier
Stroboscope
Variable voltage D.C. busbars

Fig. 48. Pertaining to interphase transformer design. Anode currents.

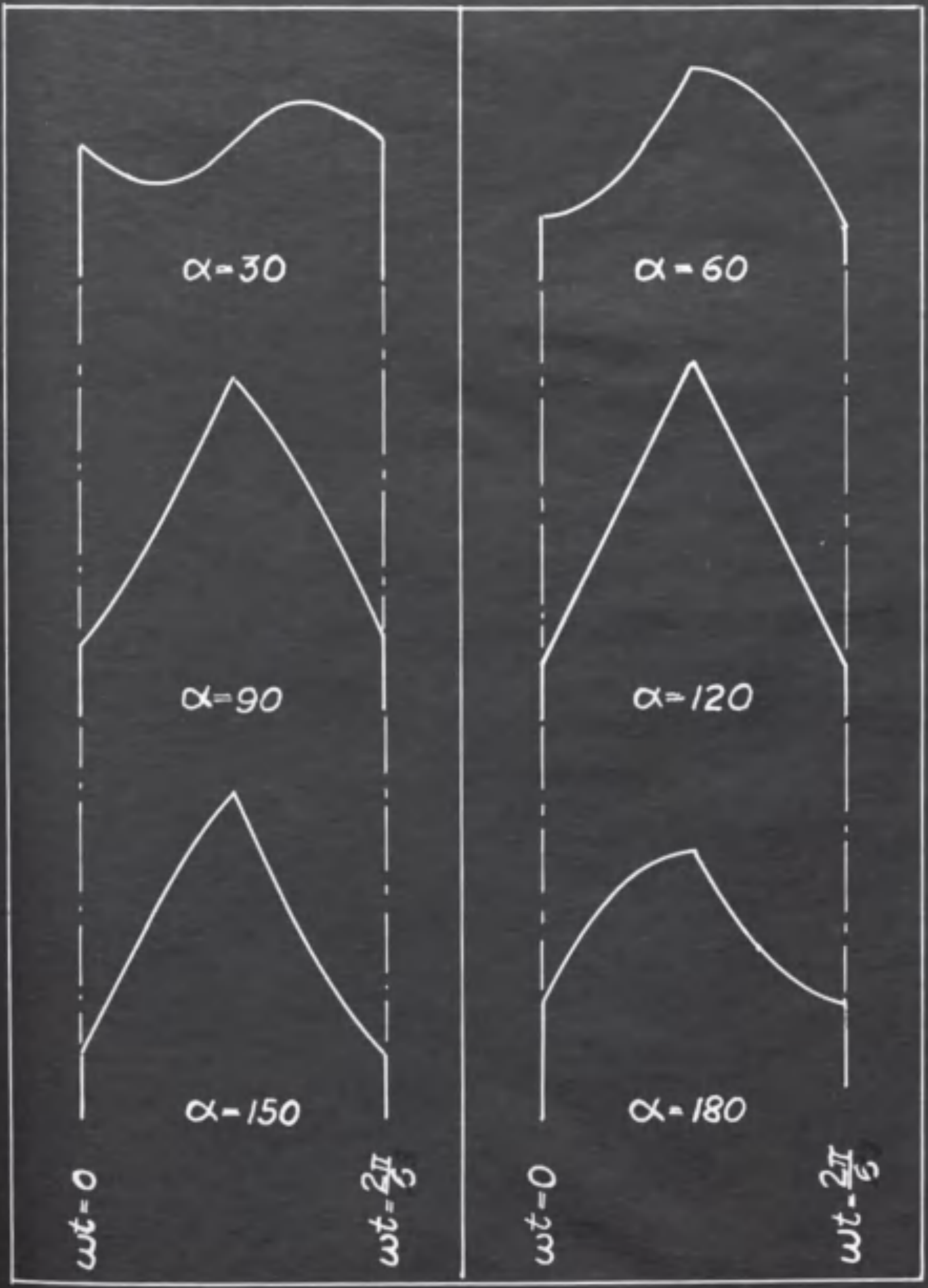
α=30
α=60
α=90
α=120
α=150
α=180
ωt=0
ωt=2π/3
ωt=0
ωt=2π/3

Fig. 49. Pertaining to interphase transformer design. Voltage across the winding.

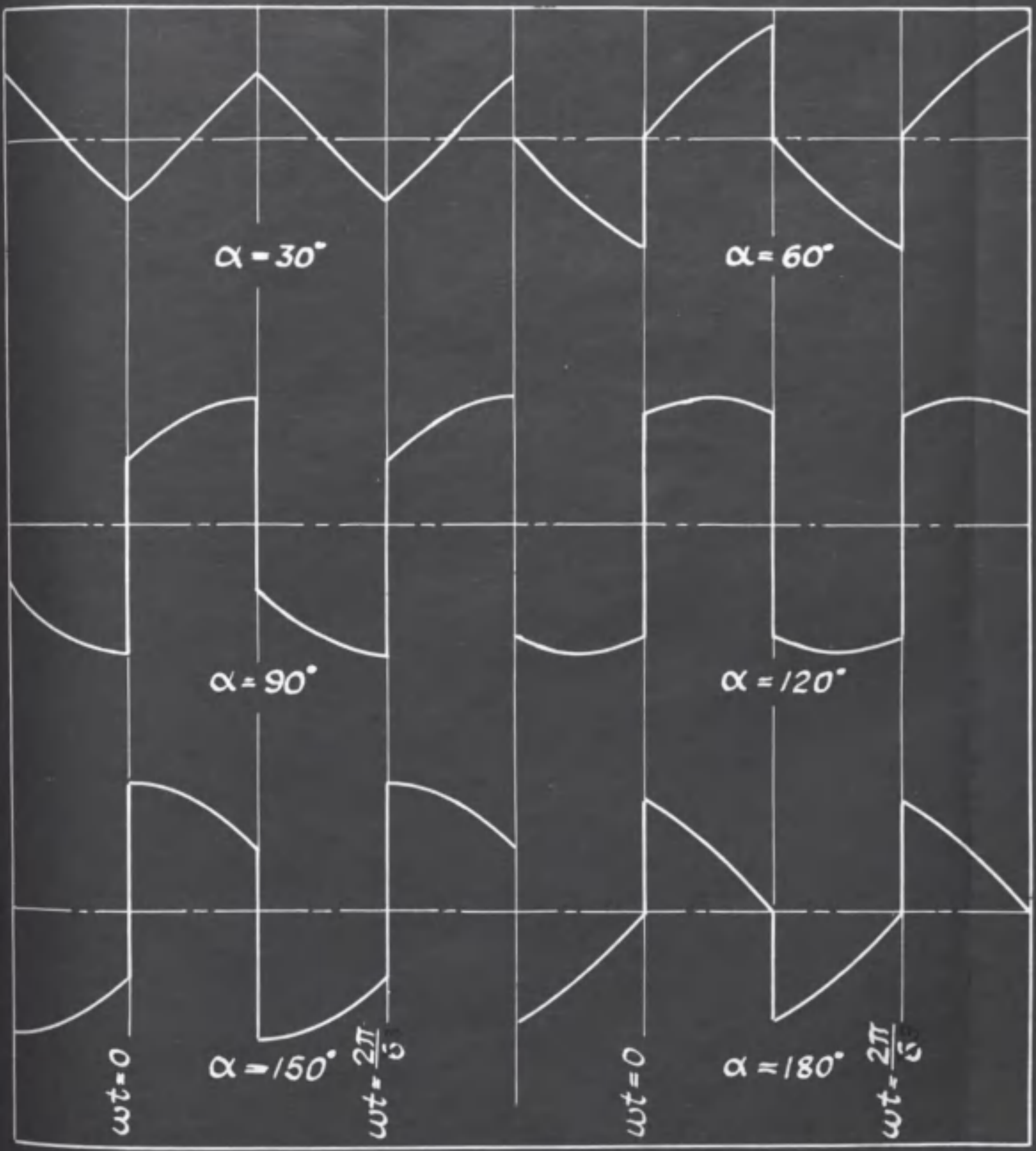
α = 30°
α = 60°
α = 90°
α = 120°
α = 150°
α = 180°
ωt = 0
ωt = 2π/3
ωt = 0
ωt = 2π/3

Fig. 50. Pertaining to interphase transformer design.

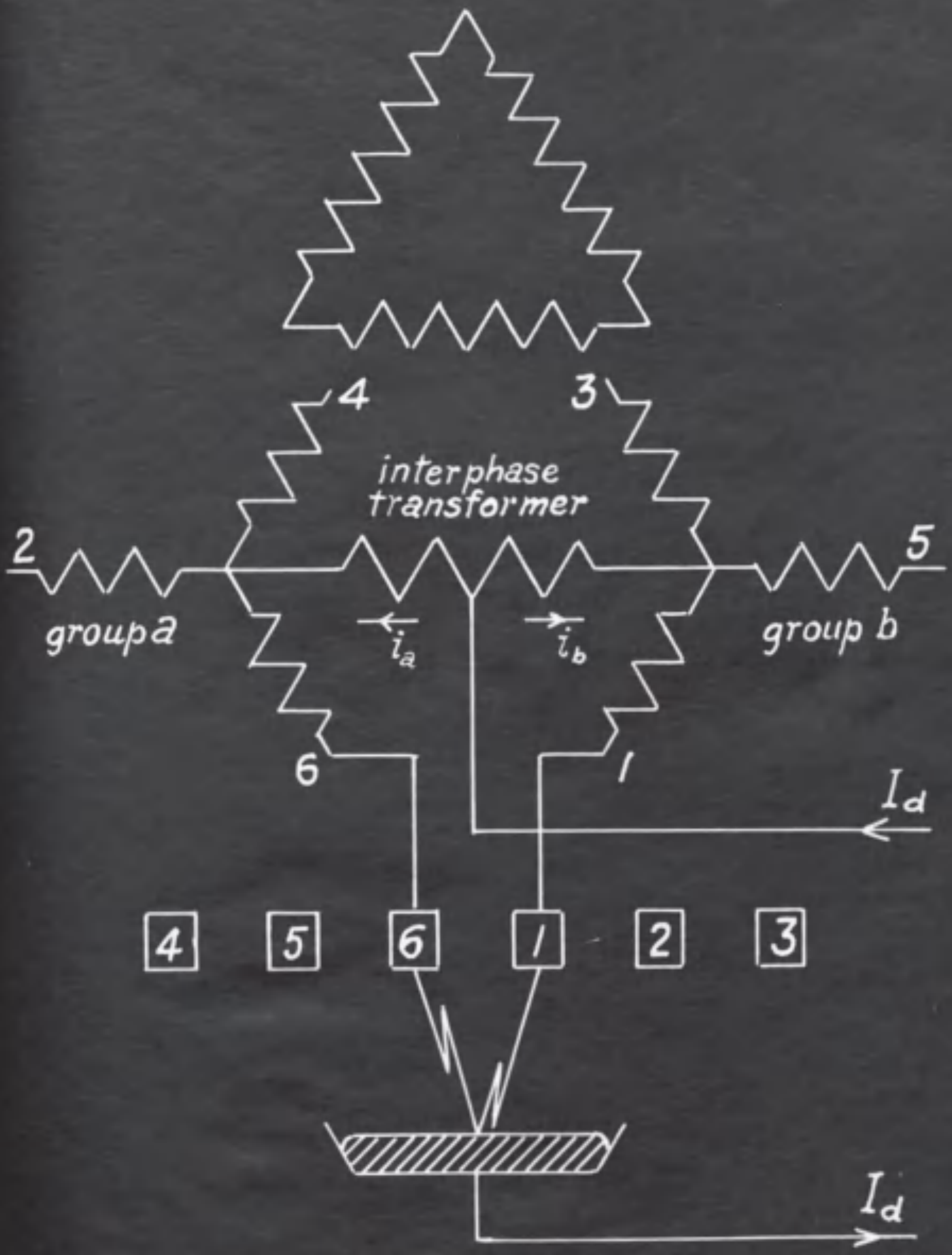
interphase transformer
group a
group b
i_a
i_b
I_d
I_d

Fig. 51. Pertaining to the construction of the wave-form of the interphase transformer voltage.

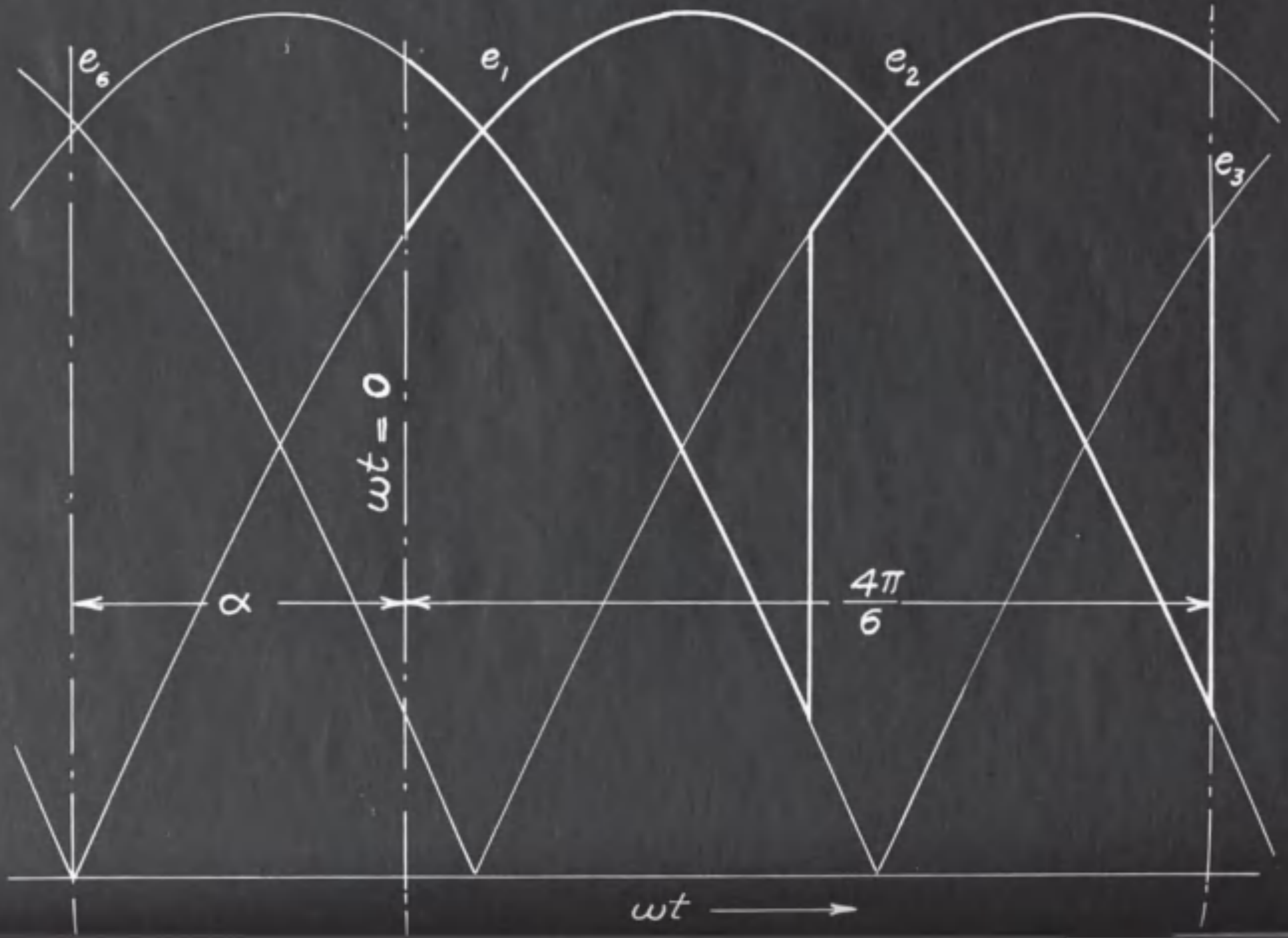
e_6
e_1
e_2
e_3
$\omega t = 0$
α
$\frac{4\pi}{6}$
$\omega t \longrightarrow$

Fig. 52. Pertaining to interphase transformer design.

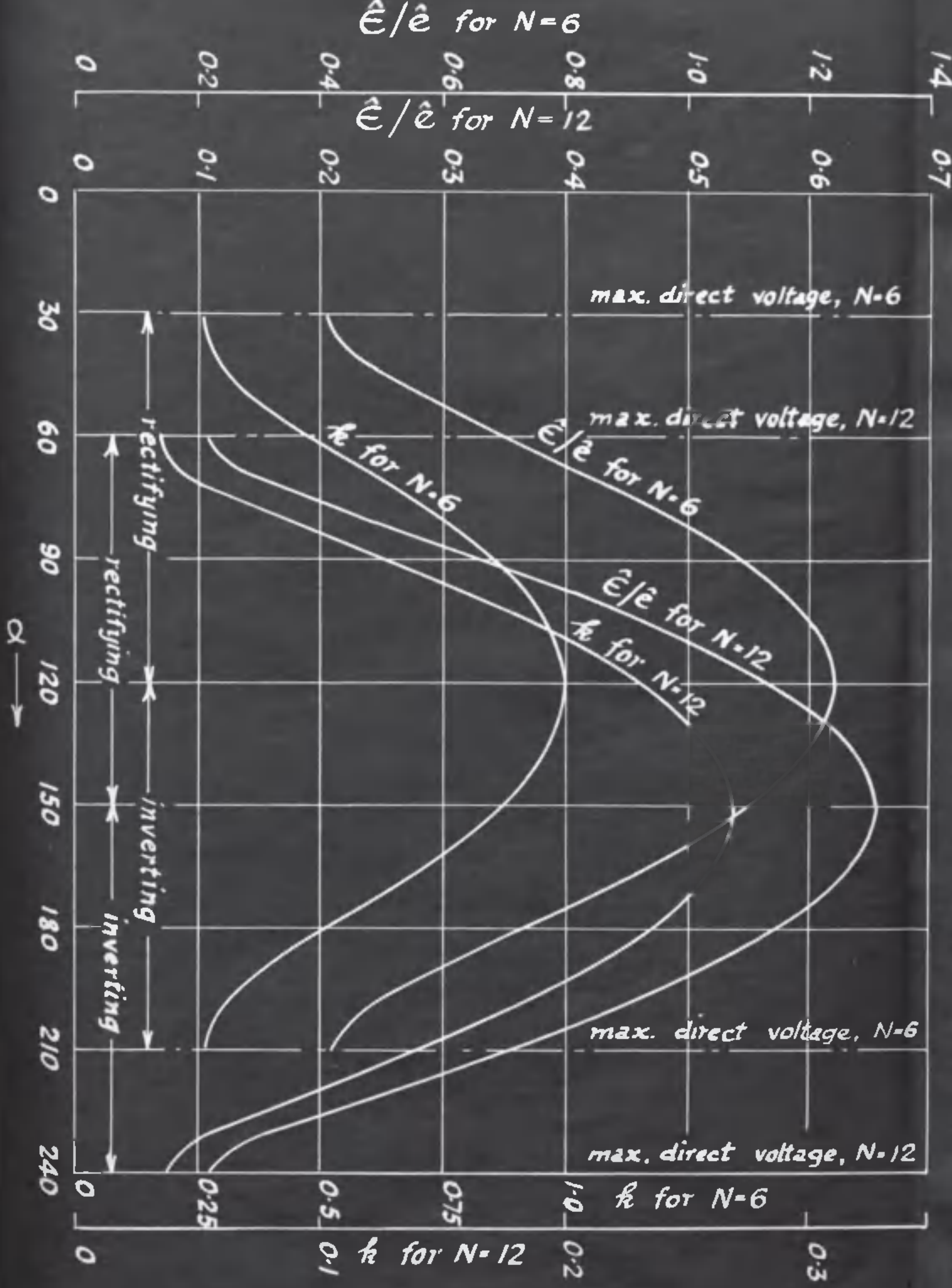

Ê/ê for N=6
0
0·2
0·4
0·6
0·8
1·0
1·2
1·4
Ê/ê for N=12
0
0·1
0·2
0·3
0·4
0·5
0·6
0·7
0
30
60
90
120
150
180
210
240
α
max. direct voltage, N-6
max. direct voltage, N=12
max. direct voltage, N-6
max. direct voltage, N=12
k for N-6
Ê/ê for N-6
Ê/ê for N=12
k for N=12
rectifying
rectifying
inverting
inverting
0
0·25
0·5
0·75
1·0
k for N=6
0
0·1
0·2
0·3
k for N=12

Fig. 53. Iron loss curves for Stalloy laminations 0·014" thick (supplied by the courtesy of Messrs Sankeys, Ltd.)

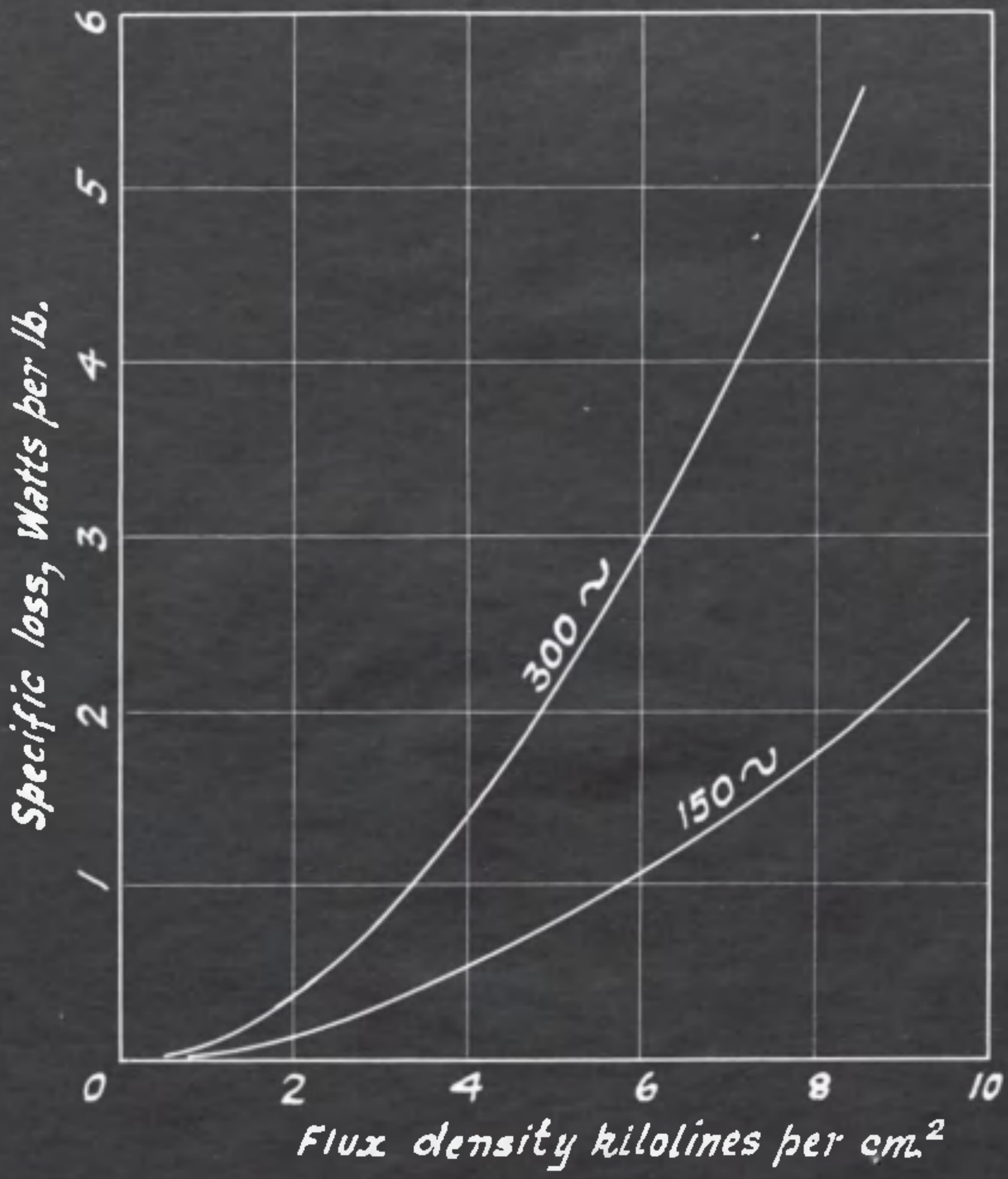
Specific loss, Watts per lb.
0
1
2
3
4
5
6
2
4
6
8
10
Flux density kilolines per cm.²
300 ~
150 ~

Fig. 54. Pertaining to interphase transformer design.

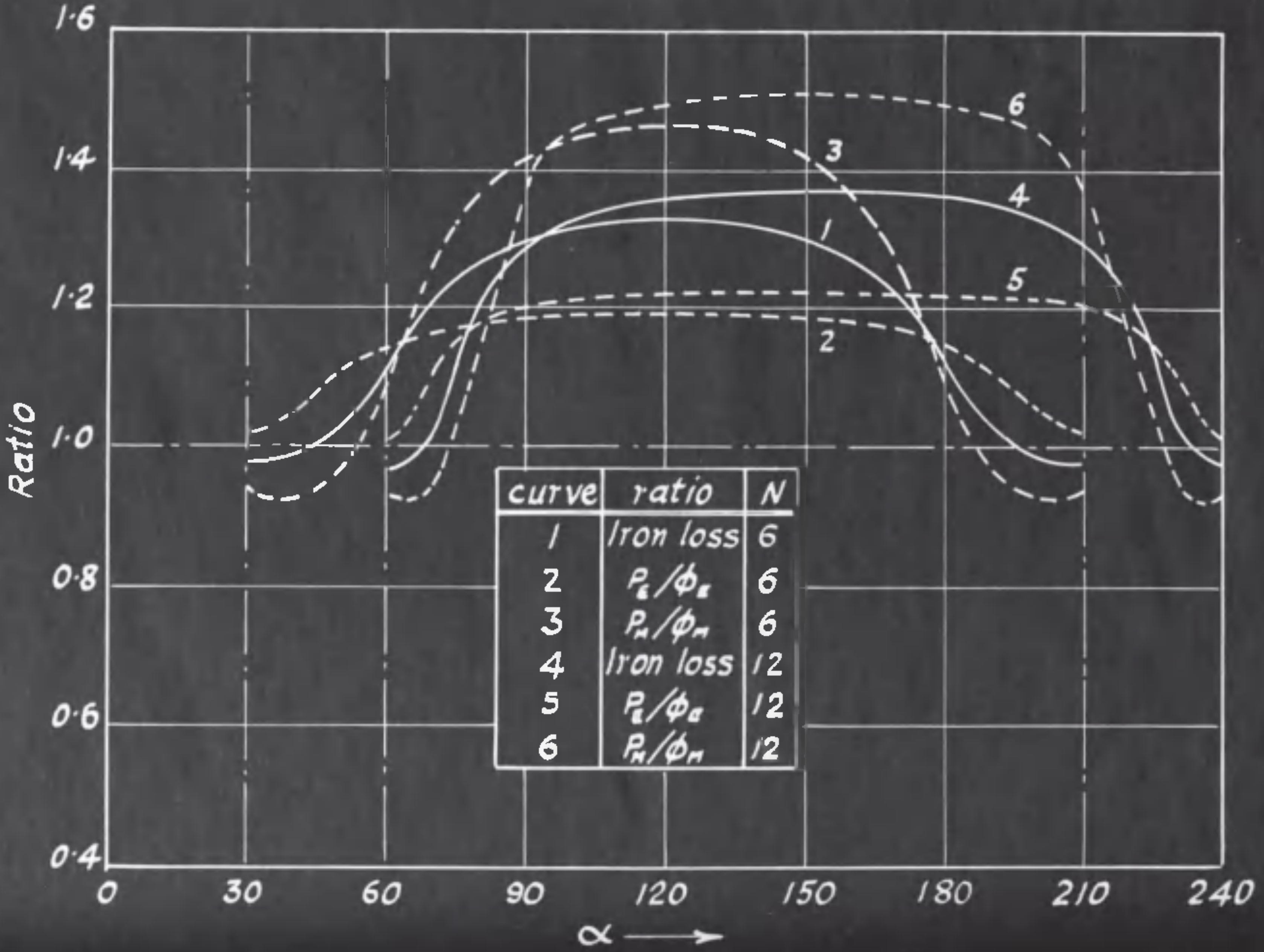
Ratio
1·6
1·4
1·2
1·0
0·8
0·6
0·4
0
30
60
90
120
150
180
210
240
α ⟶
1
2
3
4
5
6
curve | ratio | N
1 | Iron loss | 6
2 | P_E/ϕ_E | 6
3 | P_M/ϕ_M | 6
4 | Iron loss | 12
5 | P_E/ϕ_E | 12
6 | P_M/ϕ_M | 12

Fig. 55. Pertaining to interphase transformer design.

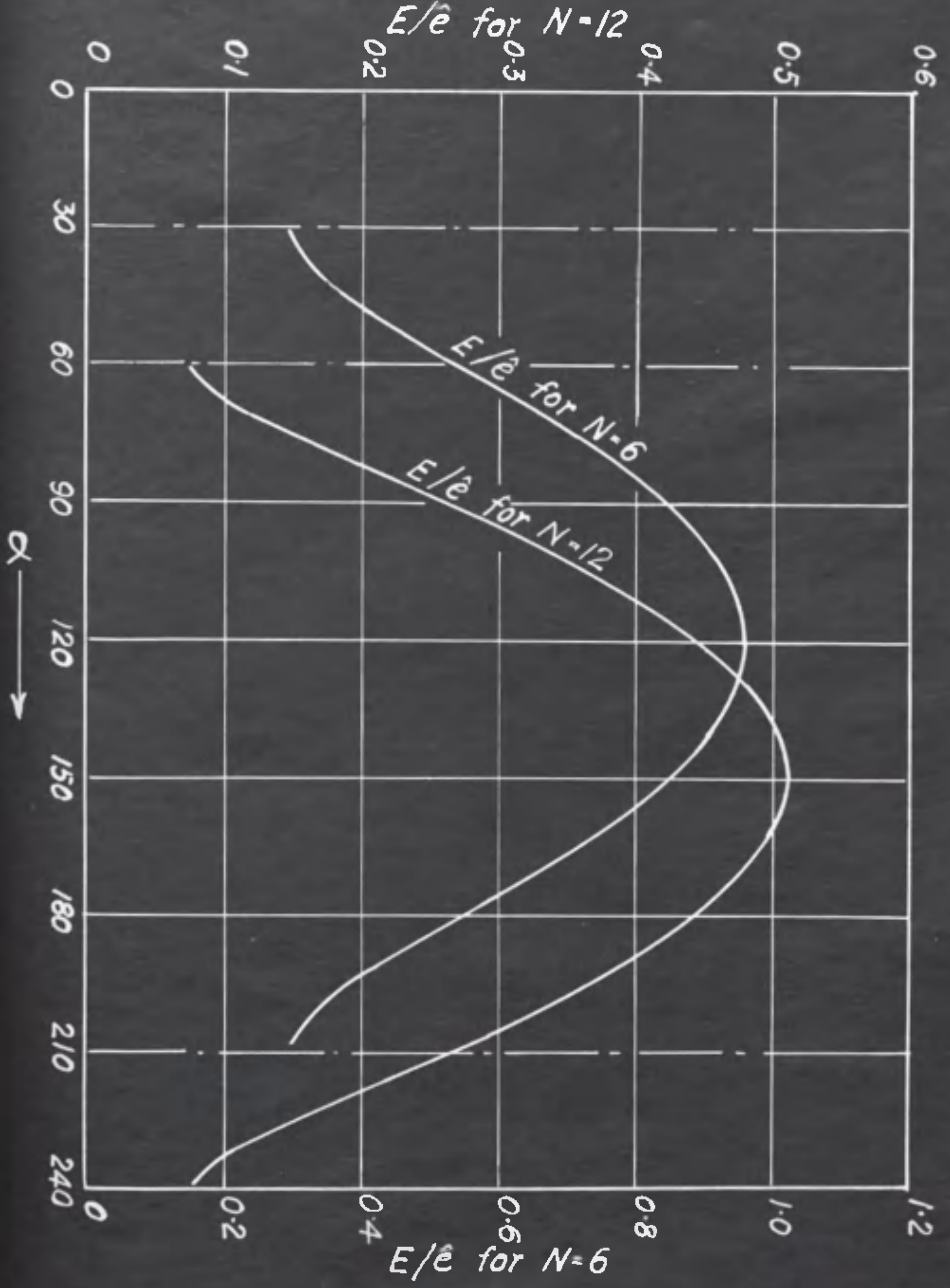
E/ê for N=12
0
0·1
0·2
0·3
0·4
0·5
0·6
0
30
60
90
120
150
180
210
240
α
E/ê for N=6
E/ê for N=12
0
0·2
0·4
0·6
0·8
1·0
1·2
E/ê for N=6

Fig. 56. Magnetisation curve for Stalloy laminations.

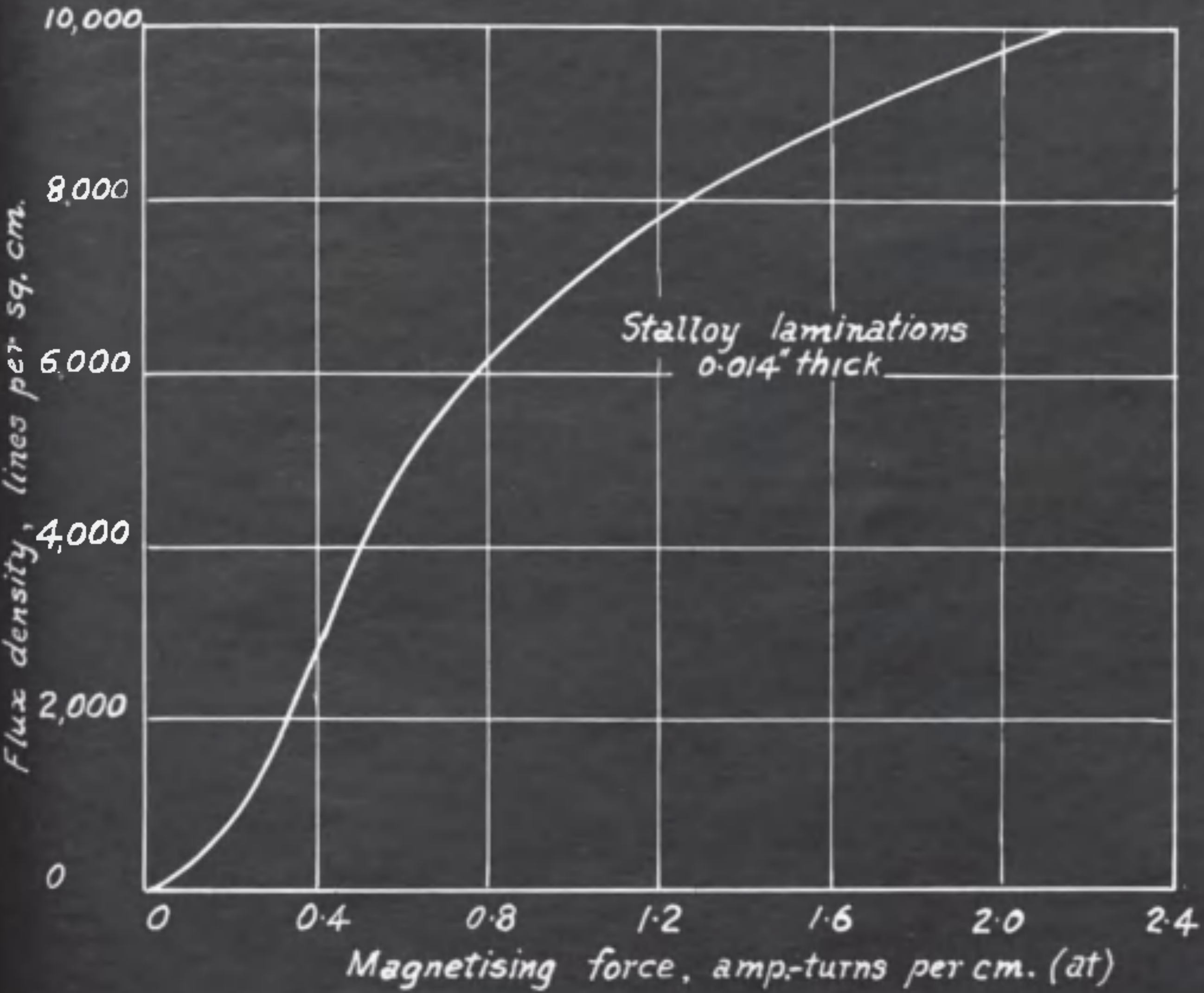
10,000
8,000
6,000
4,000
2,000
0
Flux density, lines per sq. cm.
0
0·4
0·8
1·2
1·6
2·0
2·4
Magnetising force, amp.-turns per cm. (at)
Stalloy laminations
0·014" thick

Fig. 57. 12-phase connection with three interphase transformers.

Fig. 58. Pertaining to the design of interphase transformer C .

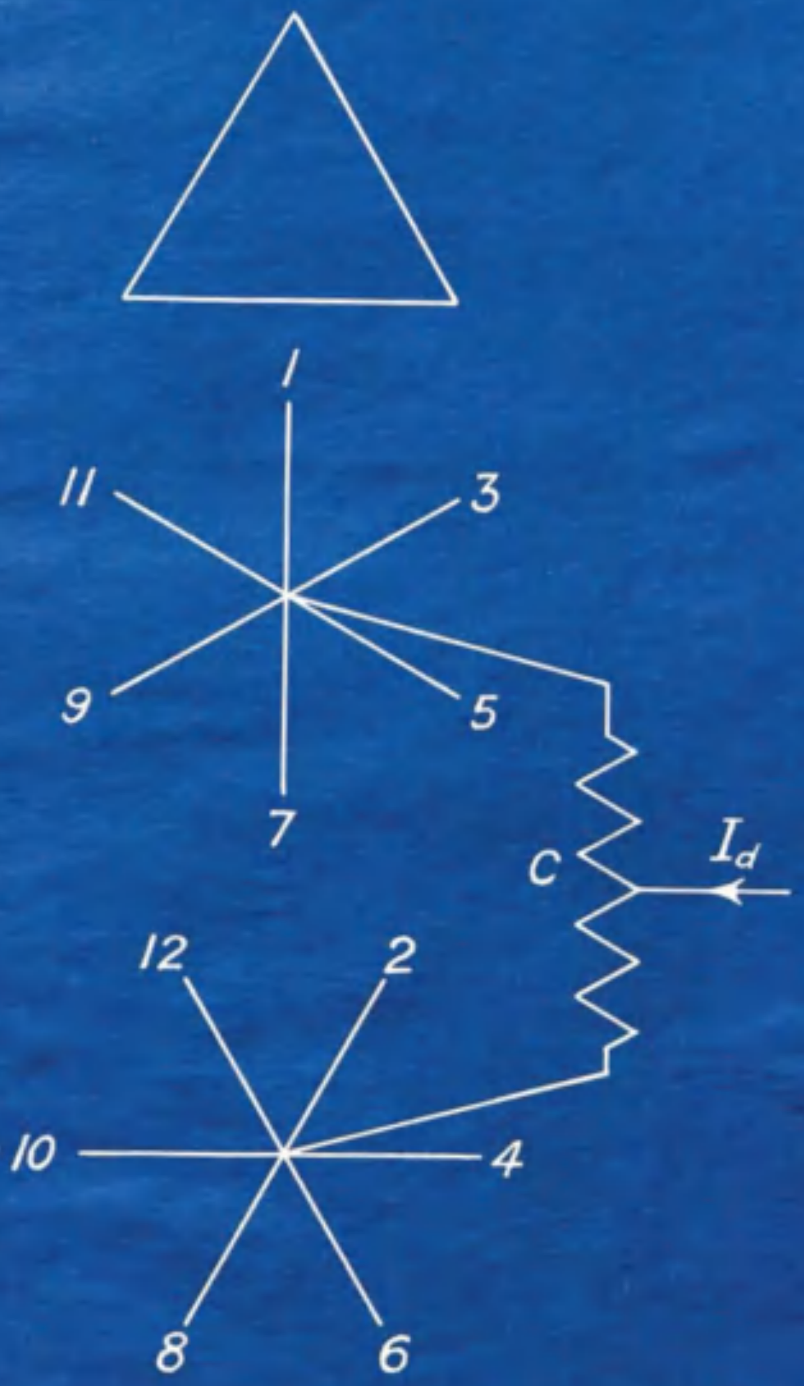
C
I_d

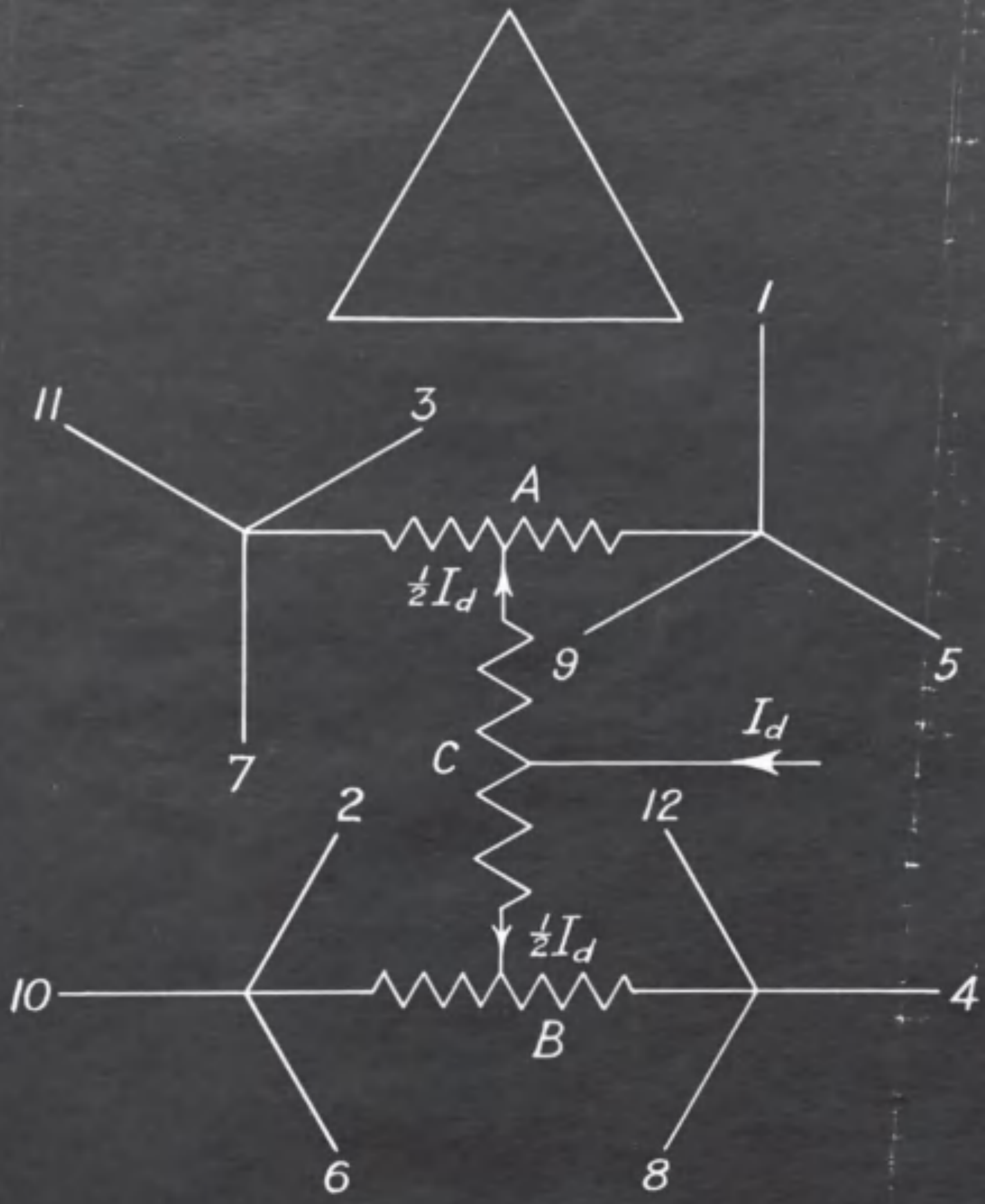
A
$\frac{1}{2}I_d$
I_d
C
$\frac{1}{2}I_d$
B

Fig. 59. Pertaining to the calculation of the direct voltage.

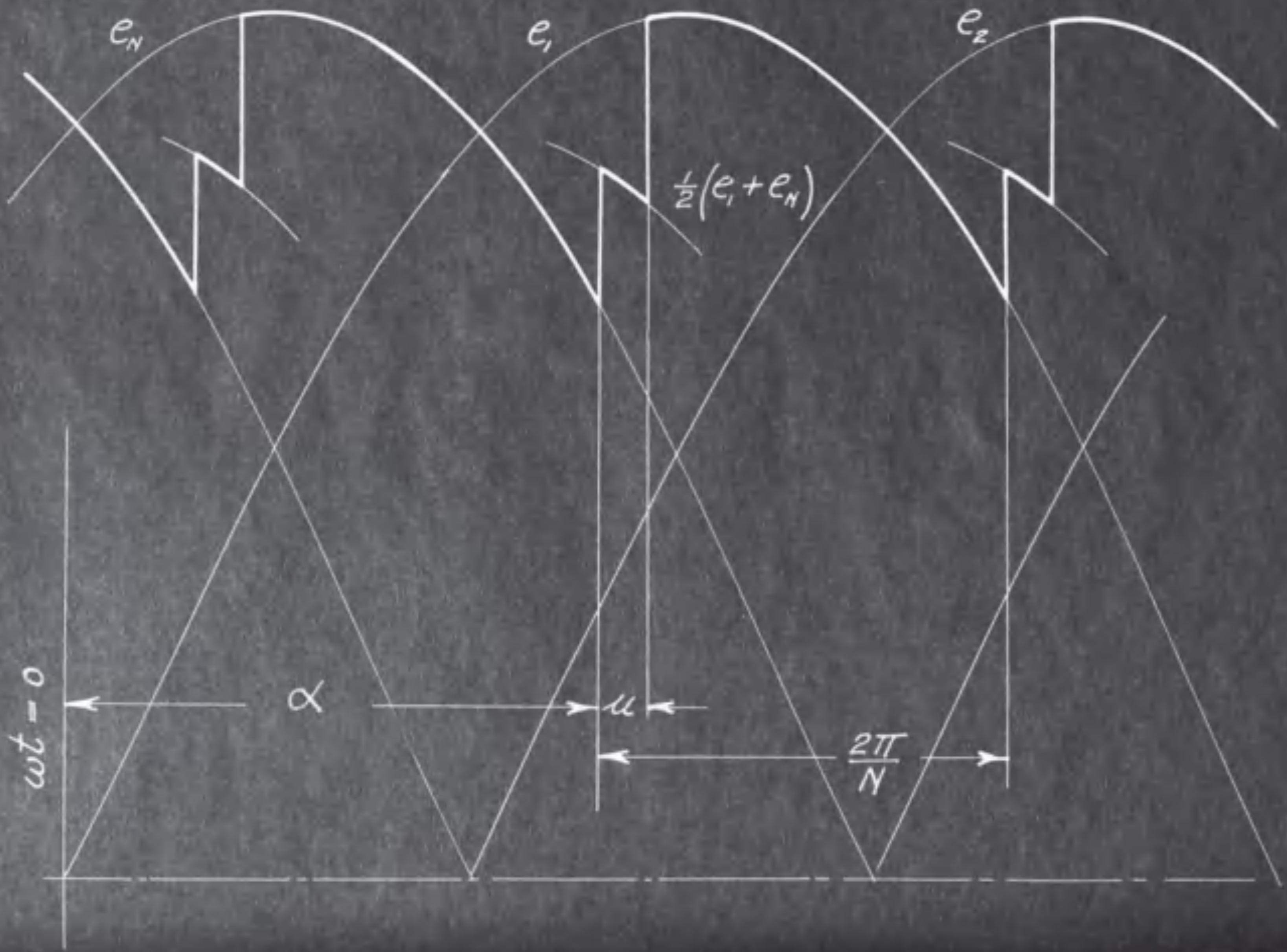
e_N
e_1
e_2
$\frac{1}{2}(e_1+e_N)$
$\omega t = 0$
α
u
$\frac{2\pi}{N}$

Fig. 60. Pertaining to the construction of the line and neutral currents.

Fig. 61. The construction of the line and neutral currents.

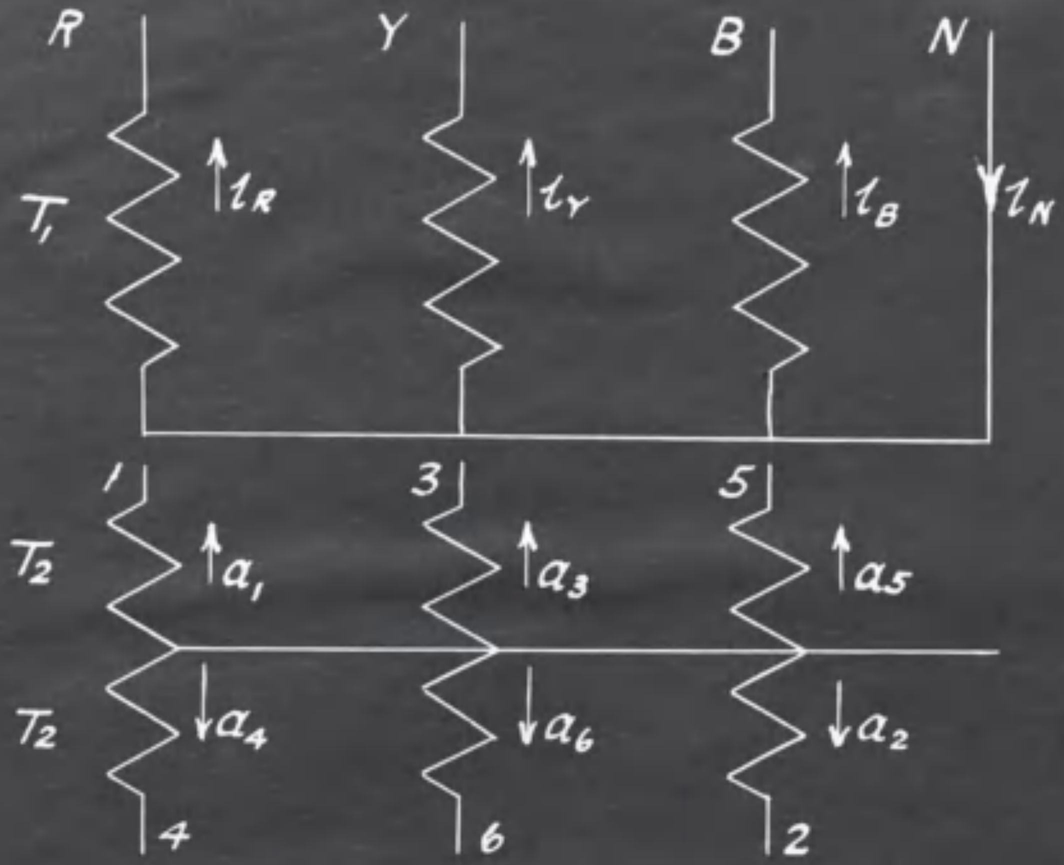
R
Y
B
N
T1
iR
iY
iB
iN
1
3
5
T2
a1
a3
a5
T2
a4
a6
a2
4
6
2

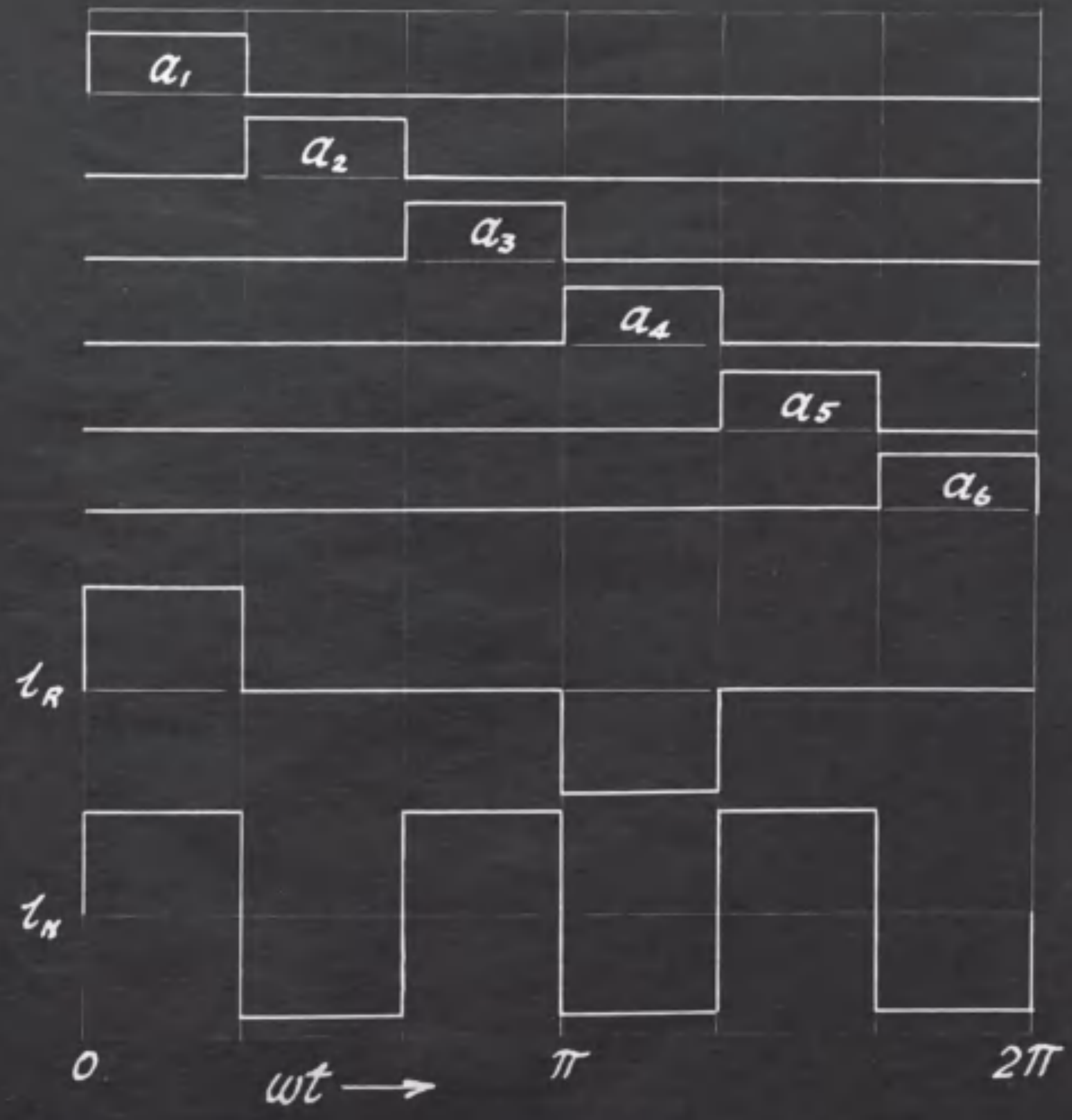
a1
a2
a3
a4
a5
a6
iR
iN
0
ωt →
π
2π

Fig. 62.   The excitation circuit diagram.

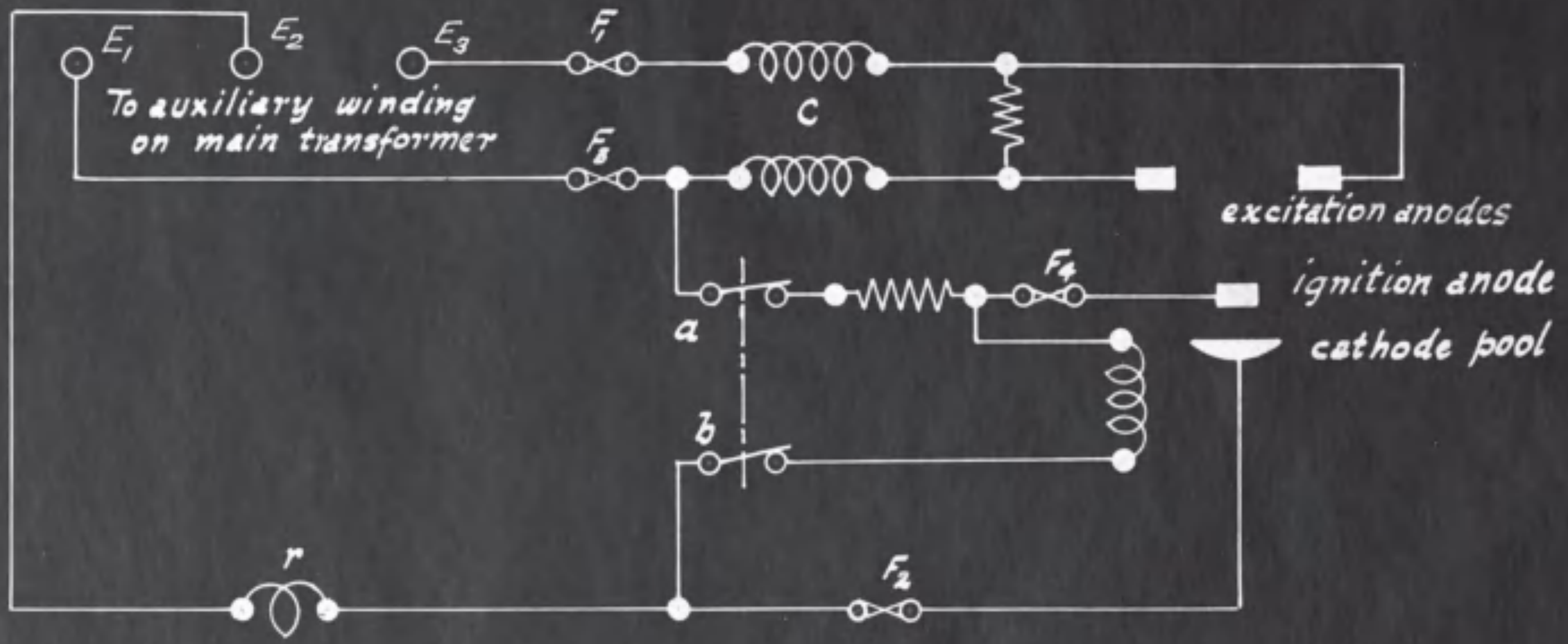
E1
E2
E3
To auxiliary winding on main transformer
F1
F3
C
F4
F2
a
b
r
excitation anodes
ignition anode
cathode pool

Fig. 63. The grid circuit diagram.

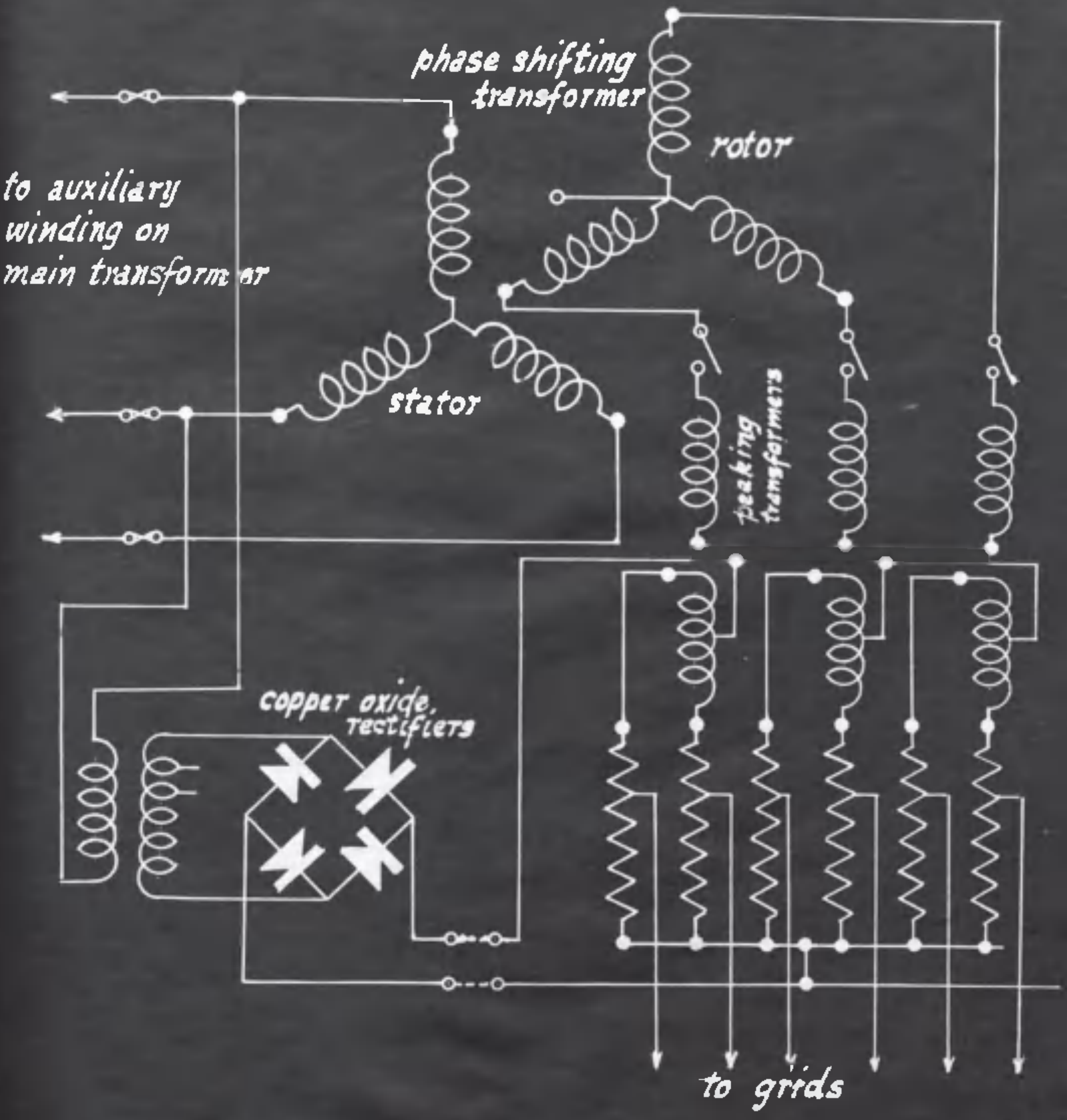
phase shifting transformer
rotor
to auxiliary winding on main transformer
stator
peaking transformers
copper oxide rectifiers
to grids

Fig. 64. The tube unit circuit diagram.

r_1 ... 0·8-ohm, 1-W resistor.

r_2 ... 0·5-megohm variable potentiometer.

r_4 r_5 ... 2·0-megohm, 2-W variable potentiometer.

r_3 r_6 ... 1·0-megohm, 1-W resistors.

r_7 ... 3·0-megohm, 3-W resistor.

r_8 r_9 r_{10} r_{11} ... 5·0-megohm, 1-W resistors.

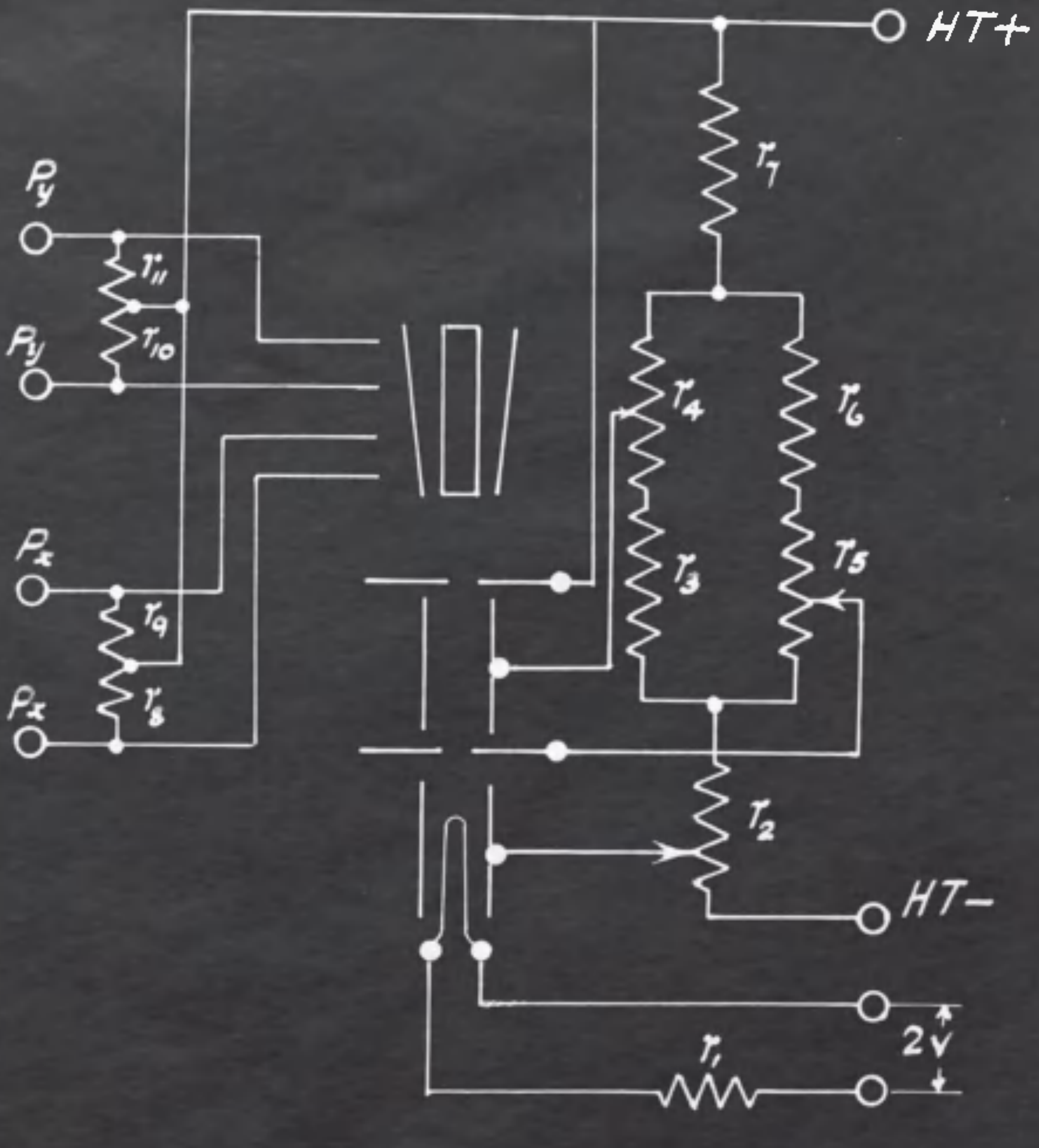
HT+
r_7
P_y
r_{11}
r_{10}
P_y
r_4
r_6
P_x
r_3
r_5
r_9
P_x
r_8
r_2
HT−
r_1
2V

Fig. 65. The rectifier unit circuit diagram.

$r_1 r_2$ .... 100,000-ohm, 1-W resistors.
$C_1 C_2$ ... 0·5 μF, 4,000-V condensers.
V . . . $\frac{1}{2}$-wave rectifying valve.
T . . . 1-phase, 250/3,999-V, 50-W transformer.

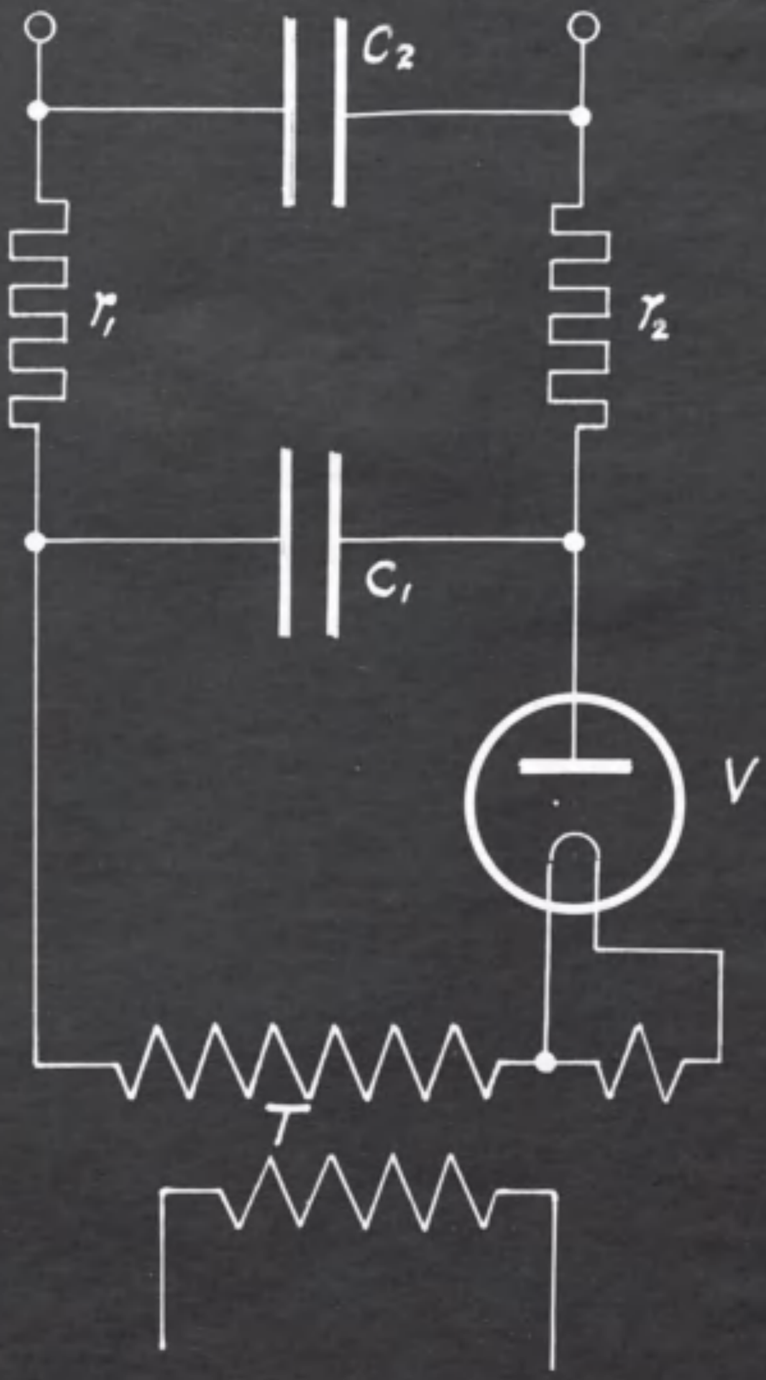
C_2
r_1
r_2
C_1
V
T